Dissecting the role of dopamine in brain stimulation reward: neuroeconomic, pharmacological, and optogenetic studies

Ivan Trujillo-Pisanty

A Thesis

In the Department

of

Psychology

Presented in Partial Fulfillment of the Requirements
For the Degree of Doctor of Philosophy at
Concordia University
Montreal. Quebec, Canada
June 2016

Examining Committee:

Dr. Joanne Tumbull (Chemestry & Biochemestry), Chair _____

Dr. Peter Shizgal (Psychology), Supervisor_____

Dr. Christopher Brett (Biology)_____

Dr. Andreas Arvanitogiannis (Psychology)_____

Dr. Wayne Brake (Psychology)_____

Dr. Geoff Schoenbaum (University of Maryland School of Medicine), External examiner_____

ABSTRACT

Dissecting the role of dopamine in brain stimulation reward: neuroeconomic, pharmacological, and optogenetic studies.

Ivan Trujillo-Pisanty
Concordia University, 2016

Dopamine (DA) is critical for reward-seeking. However, its specific role in reward has remained elusive. In the Intracranial Self-Stimulation (ICSS) paradigms, animals are trained to perform operant tasks to deliver trains of electrical or optical pulses to reward-related brain regions. The tight experimental control attainable by these paradigms makes them suitable for psychophysical and computational studies aiming at understanding how specific neural circuits and signals mediate reward seeking. However, common measurement methods in ICSS studies fail to distinguish between effects arising at different stages of reward processing. The *reward-mountain model* links the effects of experimental manipulations to specific stages of neural processing.

I used *the reward-mountain model* to distinguish between variables affecting the integration of reward intensity and other factors that influence ICSS. I administered a DA reuptake blocker or a DA receptor antagonist to animals working for electrical stimulation of the Medial Forebrain Bundle (MFB). The results show that DA signaling affects ICSS at a stage beyond the computation of reward intensity by modulating reward gain, costs, or the value of competing activities.

Optogenetics allows for direct optical stimulation of specific neural subtypes with tight temporal control. I present a technical development that proved critical in running long experimental sessions with rats. I used optogenetics to bypass the inputs to midbrain-DA neurons. I adapted the *reward-mountain paradigm* to rats working for optical stimulation of midbrain-DA neurons, allowing me to further dissect the role of DA in reward seeking. In these animals, DA reuptake blockade affected the integration of reward intensity. This contrasts with the effects produced by the same drug in rats working for electrical ICSS (eICSS). The drug also affected reward gain, cost, or the value of competing activities.

Overall, the results show that elCSS and optical lCSS (olCSS) recruit the reward system at different stages of neural processing. In elCSS, DA signaling affects reward-seeking at a stage beyond the computation of reward intensity, whereas in olCSS of midbrain-DA neurons, reward intensity is determined by a second reward-integrator downstream from the one that determines the reward intensity in elCSS.

ACKNOWLEDGMENTS

First of all I would like to thank my supervisor, Dr. Peter Shizgal, for guiding me throughout this wonderful process. His intelligence, insight, patience, and unique approach to doing high quality science will forever remain a strong influence in my scientific endeavor. Thank you for everything Peter!

Throughout my graduate studies, I had the privilege of working closely with Dr. Kent Conover. His unique way of approaching science and his admirable quantitative skills have inspired me deeply and were crucial in all of the studies presented here (and the many more that will be published shortly). The way I see neuroscience has been transformed by working with you Kent.

I am also grateful to Dr. Ilana Witten and Dr. Karl Deisseroth for their generous contribution and guidance. Not only did the TH::Cre rats we received from them made Chapter 4 possible, but their collaborative attitude towards science has thought me that scientific progress can greatly benefit from open interinstitutional teaching and sharing. Indeed the openness of the optogenetic community in general, and the Deisseroth lab in particular, have been critical to this scientific revolution. Bravo!

I would like to thank the members of my committee for reading this thesis and for helping me improve it. I am specially thankful to Dr. Christopher Brett for making it possible to have robust microscopy in this thesis (and to acquire my confocal microscopy skills), to Dr. Andreas Arvanitogiannis for providing valuable professional and personal support during my graduate studies, and to Dr. Wayne Brake for his enduring interest and enthusiasm in my scientific development.

None of my studies would have been possible without the wonderful support of CSBN members and staff. I am particularly grateful to Dave Munroe and Steve Cabilio for keeping the equipment up to their excellence standards, and for helping us push our hardware and software to its limits (even at odd hours!). Isabelle Bouvier was indispensable in running the show from behind the stage and in providing immeasurable personal support. Heshmat

Rahabi was my second backbone throughout my graduate studies. Aileen Murray was always supportive and sympathetic, my experimental subjects were almost as lucky as I was to have her in charge of the ACF. I am incredibly fortunate to have worked with all of you and to have your support and encouragement!

I would also like to thank all of my colleagues from the Shizgal lab. Dr. Giovanni Hernandez was a role model throughout my masters and PhD. Dr. Rebecca Solomon was an example of perseverance, thoroughness, and high scientific standards. Dr. Yannick Breton always offered a novel perspective and valuable MATLAB code that influenced my science and made it possible. Brian Dunn was an inspirational figure at the lab whose endless knowledge and novel points of view kept my mind open. Marie Pierre-Cossette was with me on each step of the way, we faced many of the challenges of our field shoulder to shoulder, and she shared her vast skills and knowledge with me: I could have not asked for a better person to climb this steep hill with.

I was fortunate enough to work closely with a vast number of talented undergraduate students and volunteers in the lab. Nothing teaches you more than teaching. Ian Moreau-Debord will forever be the one and only *undergrad*. Daniel Palacios always supported me and contributed greatly to a number of experiments, his enthusiasm for science was contagious. Chafic LaRochelle's sense of humor and manual skills helped us see the light at the end of the tunnel. Alison Martel's curiosity, creativity and perseverance were admirable. Diana Sarghi was an example of commitment and practicality. Alex Yacksich's curiosity and animal ethics standards greatly improved the quality of our surgeries and of our experiments. Pavel Solis went from a casual stranger in the 105 bus to a committed neuroscientist with serious interdisciplinary skills, it would have been impossible to run so many experiments simultaneously without his valuable contributions. I am looking forward to seeing what you will all accomplish in the years to come. I thank you all for your trust, patience, hard work, and for making everyday at the lab something to look forward to. Most of all, I am grateful for your friendship.

The interdisciplinary nature of this thesis was a fertile ground for learning several techniques and their underlying theory. I was fortunate enough to count on the support and guidance of

several experts. Immunostaining was possible thanks to the help from Dr. Natalina Salmaso, Dr. Cecilia Flores, Dr. Elizabeth Steinberg, and Dr. Flora Vaccarino. I learned the basics of viral transfection from Dr. Antoine Adamantidis, Dr. Sonia Jego, and Dr. Stephen Glasgow. Building and working with optical components was facilitated by Dr. Nadia Chaudhri, Dr. Dennis Sparta, and Dr. Garret Stuber. The basics of breeding were though to me by Dr. Mayte Parada. Our genotyping protocol was established by Tricia John and Marie-Pierre Cossette. Confocal microscopy and image analysis using Imaris were made possible with the support from Dr. Chloe van Oostende, Melina Jaramillo, Dr. Christopher Brett, and Dr. Alisa Piekny from the Center for Microscopy at Concordia University (CMAC).

Teamwork has been fundamental throughout my studies. The most important member in my team has always been my wife, Denisse Horcasitas-Ruiz. Her love, incomparable support, encouragement, and understanding makes my every day possible (inside and outside of the lab). ¡Te amo chonita!

I would like to thank my parents for teaching me to be passionate about my work, to enjoy learning and to pursue my goals. The unconditional support from them and my brother has kept my afloat throughout my life and professional development.

I also want to thank all my friends from Mexico, Canada, and elsewhere for their support and patience: this is what I was up to whenever I was not spending time with you!

Learning is a cumulative and sequential spiral. I would like to thank my teachers and friends from UNAM who set the foundations for my graduate studies. Gracias Olga Rojas, gracias Hugo Sanchez, gracias David Velazquez, gracias Cesar Casasola, gracias Oscar Zamora, gracias Florencio Miranda.

Last but not least, I would like to thank Dr. Jane Stewart for talking to a complete stranger at a bus stop in Tübingen, and seeing a future doctor of philosophy in that strange young man. Thank you for everything Jane!

This thesis was supported by scholarships to Ivan Trujillo-Pisanty from the FRQS-MELS-PBEEE 1M program (#149498), CONACYT (209314/309126), and the Concordia University Graduate fellowship. Peter Shizgal received funding from the Canadian Institutes of Health Research (#MOP–74577), a group grant from the “Fonds de recherche Québec—santé” to the “Groupe de Recherche en Neurobiologie Comportementale”/Center for Studies in Behavioural Neurobiology (Shimon Amir, p.i.), the Concordia University Research Chairs program and an NSERC grant (#RGPIN308-11).

CONTRIBUTION OF AUTHORS

This is a manuscript based thesis, the contribution of the authors to each manuscript is listed below.

Chapter 1:

- I contributed to the experimental design of the second set of behavioral experiments, conducted the surgeries for those subjects, and conducted the behavioral testing. I also contributed to the analysis strategy, data analysis, and in writing all versions of the manuscript.
- Giovanni Hernandez designed the neurochemical and behavioral experiments, performed the neurochemical experiments and the first set of behavioral experiments, contributed to the analysis strategy, analyzed data. He wrote the first draft of the paper and contributed to subsequent versions.
- Marie-Pierre Cossette performed the neurochemical experiments.
- Kent Conover led the analysis strategy and analyzed data.
- Peter Shizgal contributed to the experimental designs, contributed to the analysis strategy, analyzed data, and contributed in writing all versions of the manuscript.

Chapter 2:

- I designed and conducted the experiments. I also performed preliminary daily analysis of the data, and contributed to the analysis strategy. I wrote the first draft of the manuscript and contributed to subsequent versions.
- Kent Conover developed the analysis strategy and the MATLAB code to analyze the data and generate some of the figures.
- Peter Shizgal contributed to the design of the experiments and the analysis strategy. He also contributed in writing all versions of the manuscript.

Chapter 3:

- I developed and tested the prototype and subsequent versions of the patch-cord. I wrote the first draft of the paper and contributed with subsequent versions. I also constructed the patch cord for the figures.

• Christian Sanio contributed to the testing of the patch-cord and provided insights to their improvement.

• Nadia Chaudhri assisted with the construction of the first version of the patch cord and contributed in writing all versions of the paper.

• Peter Shizgal provided insights in improving the patch cord and contributed in writing all versions of the paper.

Chapter 4 (*unpublished manuscript*):

• I designed and conducted all phases of the experiments. Built optical implants and patch cords. Adapted the mountain-model methodology to optical self-stimulation, contributed to the data-analysis strategy and wrote the first draft of the chapter and contributed to all subsequent versions. I was also responsible for developing and maintaining the colony of TH::Cre rats.

• Pavel Solis contributed to the behavioral testing using the reward-mountain model, built some of the optical implants and cords, and provided assistance during surgery.

• Daniel Palacios contributed in developing successful optogenetic surgeries and implants.

• Dayane Karkouti contributed to the histology.

• Kent Conover led the data-analysis strategy and developed the MATLAB code to analyze the results and produce some of the figures.

• Marie-Pierre Cossette contributed in developing optical methods in our lab, and was responsible for genotyping.

• Ilana Witten developed the TH:Cre rats and donated the first three sires to establish the transgenic rat colony, as well as valuable advice to conduct optogenetic studies with these animals.

• Karl Deisseroth developed the TH::Cre rats and donated the first three sires to establish the transgenic rat colony, develop the viral vectors and made them available to us, and provided valuable guidance in conducting optogenetic studies using TH::Cre rats.

• Peter Shizgal contributed to the experimental design, analysis strategy, and in writing all versions of the chapter.

TABLE OF CONTENTS

LIST OF FIGURES

LIST OF TABLES

GENERAL INTRODUCTION

Measure what is measurable, and make measurable what is not so.

Galileo Galilei

Electrical Intracranial Self Stimulation and Brain Stimulation reward

In 1954, Olds & Milner reported a serendipitous finding that would forever change the study of reward and addiction (Olds & Milner, 1954): *electrical Intracranial Self-Stimulation* (eICSS). The phenomenon consists of instrumental behaviors, such as lever pressing or running down an alleyway, performed to trigger the delivery of trains of electrical pulses to specific brain regions and pathways. Not only was eICSS of interest in its own right, but it was soon recognized as a powerful paradigm to study the brain substrates responsible for reward and addiction. eICSS offers unparalleled control over the rewarding stimulus and stable behavioral performance over time; unlike natural reinforcers, brain stimulation reward is not susceptible to satiety effects (McSweeney & Roll, 1993; Olds, 1958).

The phenomenon was further exploited to study the neural substrate of reward by incorporating pharmacological manipulations. Animals were trained to emit instrumental responses to trigger the intracranial delivery of a fixed number of electrical pulses. If a given pharmacological manipulation increased eICSS (as assessed by changes in response rate), the neurotransmission systems that the drug acted upon (or mimicked) were inferred to participate in reward processing. When rats working for eICSS were administered cocaine (a blocker of the noradrenergic, dopaminergic, and serotonergic transporters), the response rate for eICSS increased abruptly suggesting a facilitatory effect of the drug on reward and a potential role for noradrenaline, dopamine (DA), and/or serotonin in reward processing (Crow, 1970). The suspicion that DA is involved in reward was further strengthened by the finding that the effects on response rate for eICSS were bidierectional: DA agonists increased response rate, whereas DA antagonists decreased it (Liebman & Butcher, 1973). However, this relatively simple behavioral measurement had important caveats. Response rate can vary as a

consequence of changes in psychomotor capacity independently of changes in the subjective intensity of the electrical reward. Moreover, assessing eICSS with a fixed electrical pulse-frequency prevents accurate quantitative characterization of the psychological processes underlying performance for the electrical reward and its modification by drugs (Shizgal & Hernandez, 2015).

The behavioral task and analysis strategy were eventually modified so as to support the quantitative study of eICSS and the underlying psychological processes. A first step in this direction was provided by the introduction of the *curve-shift method* (Campbell, Evans, & Gallistel, 1985; Carlezon & Chartoff, 2007; Edmonds & Gallistel, 1974; Gallistel & Freyd, 1987; Gallistel, Shizgal, & Yeomans, 1981; Miliaressis, Rompre, Laviolette, Philippe, & Coulombe, 1986b), which provides robust and replicable observations of how a given manipulation (such as administering a drug or lesioning a brain region) affects eICSS performance. In this method, animals are trained to perform an operant response in order to receive the rewarding stimulation. The magnitude of the reinforcer is systematically manipulated across experimental trials by varying the pulse frequency or the current of the rewarding electrical stimulation. The dependent variable is the vigor of the operant response (commonly response rate). The curve-shift method allows for parametric analysis of reward: the behavioral effectiveness of the electrical reward can be inferred from behavior and modeled quantitatively in a manner that is analogous to dose-response curves in pharmacology. The curve-shift method was regarded as a major breakthrough because it appeared to differentiate changes in performance capacity and reward effectiveness: if a given experimental manipulation produced a horizontal displacement of the curve, then reward effectiveness was thought to be affected. Specifically, manipulations that enhance reward would shift the curve leftwards: lower pulse-frequencies would be required to attain a given reward effectiveness, and manipulations that dampen reward would shift the curve rightwards: higher pulse-frequencies would be necessary to produce the same behavioral effect. Conversely, effects on performance capacity would be reflected by vertical shifts of the curve (Edmonds & Gallistel, 1974; Miliaressis, Rompre, Laviolette, Philippe, & Coulombe, 1986b).

The curve-shift method allowed for the development of quantitative models to account for the observed behavioral effects. One model of particular relevance for this thesis is *the spike-counter model* (Gallistel, 1978; Gallistel et al., 1981; Simmons & Gallistel, 1994; Yeomans, 1975). The number of reward-relevant fibers recruited by the electrical stimulation is dependent on the current (which determines the radius of excitation by the electrical impulse), whereas the number of action potentials triggered by the stimulation depends on the pulse-frequency of the electrical train (Gallistel, 1978; Gallistel et al., 1981). When the train duration is held constant, rats working for electrical stimulation of the Medial Forebrain Bundle (MFB) at the level of the Lateral Hypothalamus (LH) show equivalent responses to a train of high frequency and low current, or a train of low frequency and high current (Gallistel, 1978; Gallistel et al., 1981; Simmons & Gallistel, 1994; Yeomans, 1975). This observation suggests that the volley of action potentials produced by the rewarding stimulation is integrated spatially and temporally to yield a neural signal that is translated ultimately into the subjective value of the reward. In other words: the number of action potentials produced within and between reward-relevant fibers is summed to determine the intensity of the reward. Similarly to how higher concentrations of sucrose increase the subjective experience of sweetness, higher electrical pulse-frequencies or currents increase the subjective intensity of the reward.

The contribution of the output from the spike-counter to reward intensity was explored by means of operant-choice experiments: rats were allowed to choose between two different manipulanda which triggered electrical stimulation of different pulse-frequencies and currents that were systematically manipulated (Gallistel & Leon, 1991; Gallistel, Leon, Waraczynski, & Hanau, 1991; Leon & Gallistel, 1992; Simmons & Gallistel, 1994). This dual-lever strategy provides an elegant way to asses which combinations of pulse-frequencies and currents yield similar subjective reward intensities (i.e. by determining which combinations of currents and frequencies are equally preferred by the rat) while overcoming potential performance confounds associated with simple response-rate measurements (e.g. a ceiling effect in the rate of lever pressing). Moreover, it provided the means to relate the output of the spike-

counter to the intensity of the reward and to asses this relationship quantitatively. The sum of reward-relevant spikes is mapped (i.e. integrated) into a logistic function (Sonnenschein, Conover, & Shizgal, 2003) that describes the relationship between the intensity of the stimulation and the intensity of the reward (the *reward-growth function*): the intensity of the reward increases steeply as the number of induced action potentials increases, but eventually it plateaus and further increments in pulse-frequency or current no longer impact the subjective reward-strength.

Dopamine and the substrate of brain stimulation reward

Understanding the neural basis of eICSS has been a major goal in behavioral neuroscience. Early behavioral pharmacology studies using the curve-shift method implicated DA as a critical player in eICSS. Specifically, DA agonists consistently shifted the rate-frequency curves leftwards (i.e. lower pulse-frequencies were required to produce equivalent performance), suggesting a facilitatory effect on reward (Bauco & Wise, 1997; Colle & Wise, 1988; Gallistel & Karras, 1984; Gilliss, Pieper, & Carlezon, 2002; Hernandez, Haines, & Shizgal, 2008a; Ranaldi, Bauco, & Wise, 1997; Wise & Rompré, 1989). Conversely, DA antagonists shifted the curve towards the right (i.e. higher pulse-frequencies were necessary to attain a given level of performance), dampening the rewarding effectiveness of the electrical stimulation (Atalay & Wise, 1983; Carlezon & Chartoff, 2007; Davis & Smith, 1975; Fouriezos, Hansson, & Wise, 1978; Gallistel & Davis, 1983; Gallistel & Karras, 1984; Miliaressis, Malette, & Coulombe, 1986a; Spiller et al., 2007; Wasserman, Gomita, & Gallistel, 1982; Wise, 1996). These findings were complemented by neurochemical assays showing increased DA concentrations in the DA terminal region, the nucleus accumbens, following eICSS (Blaha & Phillips, 1990; Garris et al., 1999; Hernandez & Shizgal, 2009; Hernandez et al., 2006; Hernandez, Rajabi, Stewart, Arvanitogiannis, & Shizgal, 2008).

Even though midbrain DA has been shown to be critical for eICSS, several lines of evidence argue that the rewarding effects produced by the stimulation are not due primarily to the direct stimulation of midbrain DA neurons. The axons of DA neurons are unmyelinated and very fine; their threshold for activation by extracellular currents is very

high (Bielajew & Shizgal, 1982; Yeomans, Maidment, & Bunney, 1988). The refractory periods of the directly stimulated substrate in eICSS has been characterized (Bielajew, Lapointe, Kiss, & Shizgal, 1982; Murray & Shizgal, 1996b; Rompré & Miliaressis, 1987; Rompré & Shizgal, 1986; Shizgal, Bielajew, & Rompre, 1988; Yeomans, 1975; 1979) and they range between 0.5 and 1.2 ms, in sharp contrast to the longer refractory periods of DA axons which range between 1.2 and 2.5 ms (Anderson, Fatigati, & Rompré, 1996; Yeomans et al., 1988). In addition, the conduction velocities of DA neurons ranges between 0.3-0.9 m/s while the conduction velocities of the reward-relevant fibers is much faster: 2.2-7.2 m/s (Bielajew et al., 1982; Bielajew & Shizgal, 1982; 1986; Murray & Shizgal, 1994; 1996a; 1996b; Shizgal, Bielajew, Corbett, Skelton, & Yeomans, 1980). Moreover, it has been shown that the behaviorally-relevant direction of conduction in at least some of the directly stimulated fibers subserving the rewarding effect is rostro-caudal (Bielajew & Shizgal, 1986), whereas DA neurons project caudal-rostrally (Iversen & Iversen, 2007). These findings strongly suggest that the recruitment of midbrain-DA neurons by electrical stimulation of the MFB is not through direct stimulation, but rather, through transsynaptic activation. Considering these findings, two main questions are left unanswered: 1) which neuronal subtypes constitute the directly stimulated substrate for eICSS of the MFB? and 2) what is the precise role of DA in eICSS? In this manuscript-based thesis, I present a set of experiments using groundbreaking behavioral, pharmacological, and optogenetic strategies to address question 2.

The reward mountain model

Despite the major contributions to the study of eICSS achieved using the curve-shift method, the paradigm suffers from important limitations. When an animal is in an operant chamber, it faces the choice between working for eICSS or investing its time on other activities such as grooming, resting, or exploring (Shizgal, 2012). Working for eICSS imposes an opportunity cost for the animal: the time invested in harvesting the electrical reward is also time that was not used to pursue other forms of reward that could be available in the operant chamber (such as resting, grooming, or exploring). In addition, the animal must expend physical effort to perform the instrumental response.

Thus, the amount of trial time the animal spends working for eICSS depends not only on the intensity of the reward, but also on the opportunity and effort costs entailed in harvesting the electrical stimulation. In the *reward mountain model*, the subjective reward intensity (which results from the spatio-temporal integration of the output from the directly stimulated fibers), is translated into an intensity-growth function which varies as a function of the duration and strength of the stimulation (Sonnenschein, Conover, & Shizgal, 2003). Reward *sensitivity* is determined by the spike count required to attain a reward of a given intensity (Figure 1A$_1$). The resulting reward intensity is scaled by the reward *gain* (which determines the maximal reward attainable, Figure 1A$_2$). The resulting rescaled reward intensity is weighed against the cost of the reward to compute the payoff (Figure 1A$_3$) from the electrical stimulation (Arvanitogiannis & Shizgal, 2008; Hernandez, Breton, Conover, & Shizgal, 2010). This value is then compared to the payoff from other competing activities (such as resting, grooming, or exploring) in order to determine how much the animal should invest working for eICSS (Fig. 1A$_4$).

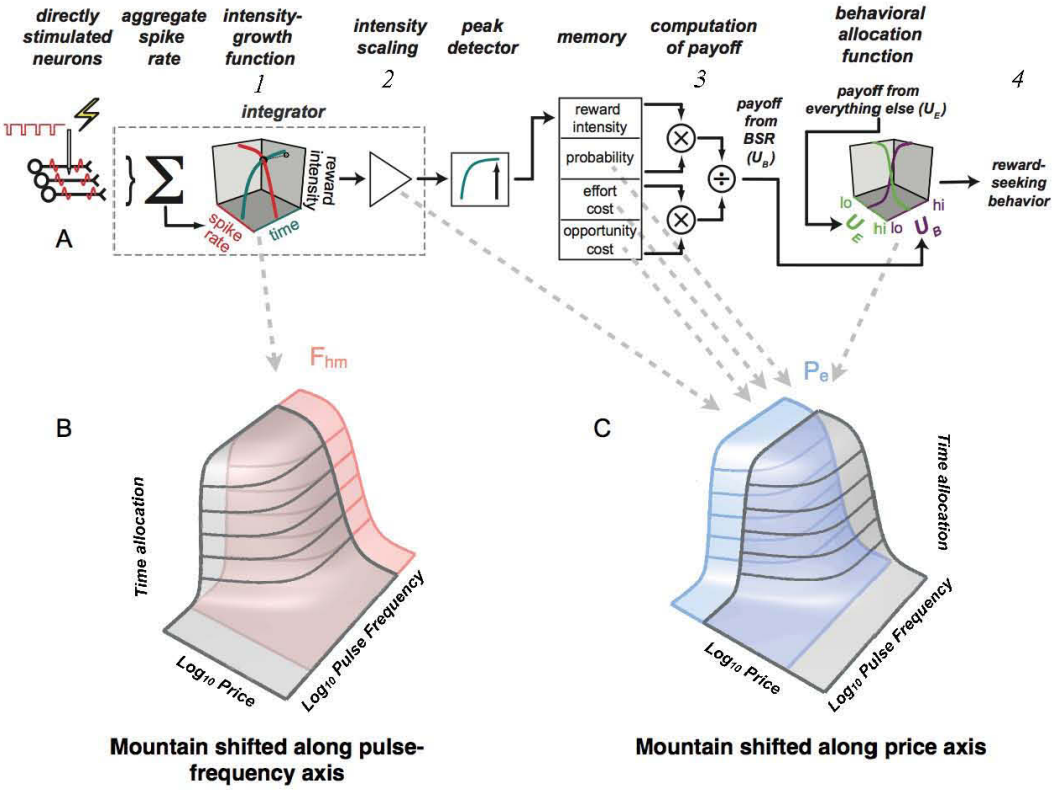

Figure1: **A** Graphical representation of the reward mountain model. The number of reward-relevant action potentials induced by the electrical stimulation in the directly stimulated neurons is summed by a spike counter. *1* The intensity-growth function is derived form the spatio-temporal integration of the spikes from the directly stimulated substrate. *2* The function can be rescaled by multiplying all values by a constant (i.e. a change in gain). *3* weighing reward intensity by reward costs yields a payoff. *4* Reward seeking is determined by the payoff from electrical stimulation and the payoff of competing activities. **B** Manipulations affecting reward seeking prior or at the output of the intensity-growth function shift the mountain along the frequency axis (change in F_{hm}). **C** Manipulations affecting reward downstream from the output of the intensity-growth function shift the mountain along the price axis (change in P_e).

The distinctions between reward strength and cost and between reward sensitivity and gain are inaccessible to the curve shift-method: traditionally, curve-shifts have been interpreted as changes in reward sensitivity. However, similar shifts could also be produced by variations in reward gain or subjective reward costs that are induced by experimental manipulation (Fouriezos, Bielajew, & Pagotto, 1990; Frank & Williams, 1985). Specifically, the curve-shift paradigm cannot differentiate between variables affecting the reward intensity or other aspects of reward-seeking, such as the effort or opportunity costs of the reward. Thus, the curve-shift method is ambiguous in that it cannot distinguish manipulations affecting reward seeking upstream and downstream from the reward integrator (Fig. 1 and Fig. 2). This ambiguity greatly limits our understanding of how specific environmental and physiological variables, neurotransmitter systems, and neural populations contribute to or modulate reward-seeking behavior. The reward mountain model was developed to address this limitation and to further refine formal explanations of reward and decision-making processes. The model readily predicts the time that the animal will spend working for eICSS as a function of both reward strength and cost (Arvanitogiannis & Shizgal, 2008; Breton,

Conover, & Shizgal, 2014; Breton, Mullett, Conover, & Shizgal, 2013; Hernandez et al., 2010).

The first validation of the mountain model was published by Arvanitogiannis and Shizgal (2008) shortly before I started conducting the research that encompassed my masters thesis in the Shizgal lab. During my graduate studies, further validation experiments and formal refinements were conducted by Dr. Yannick Breton and Dr. Rebecca Salomon as part of their Ph.D. dissertations (Breton et al., 2013; 2014; Solomon, Trujillo-Pisanty, Conover, & Shizgal, 2015). Pharmacological studies using the model have been performed by Dr. Giovanni Hernandez and myself as part of our graduate work in the Shizgal lab, and have also provided further validation of the model (Hernandez et al., 2010; Hernandez, Trujillo Pisanty, Cossette, Conover, & Shizgal, 2012; Trujillo-Pisanty et al., 2013; 2011).

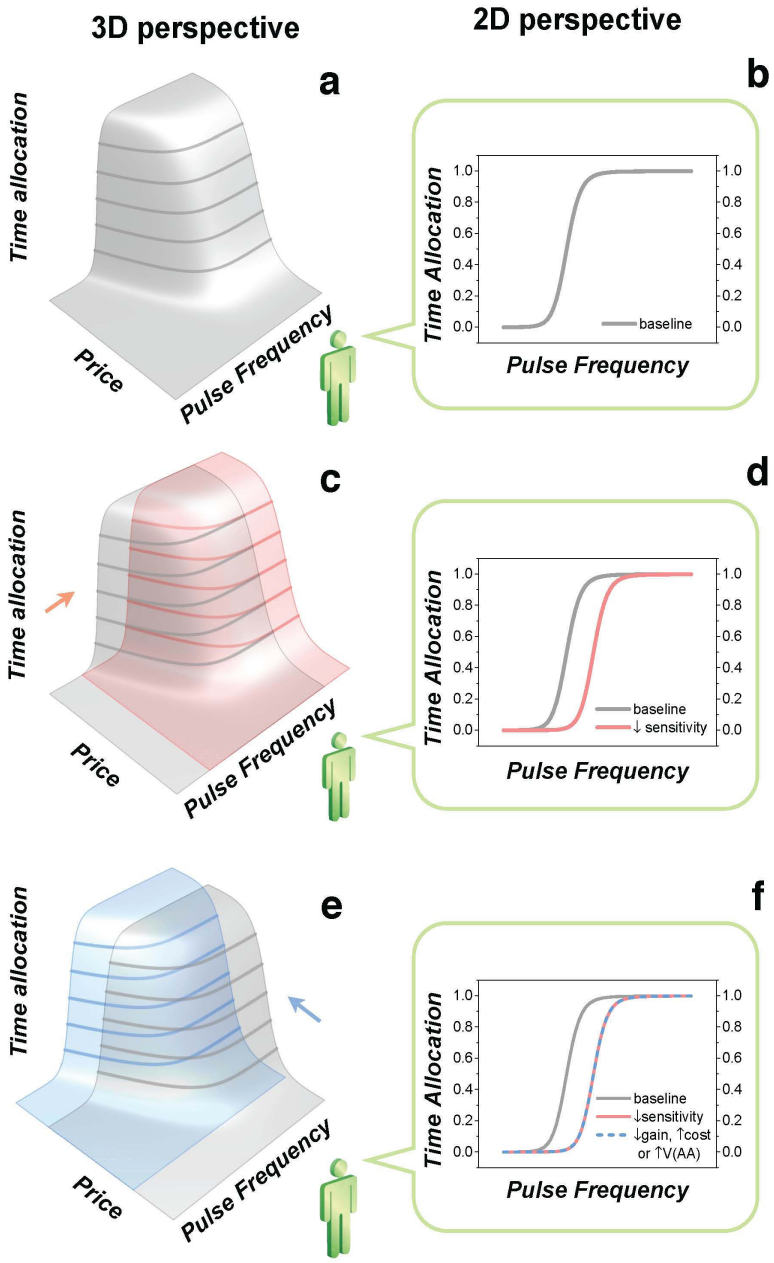

Figure 2: Ambiguity of 2D curve shifts. The grey surface (a) represents the reward mountain in the baseline condition. Decreases in the sensitivity of the reward circuitry shift the mountain rightwards along the pulse-frequency axis (c), whereas decreases in reward-circuit gain, increases in subjective effort costs, or increases in the value of alternate activities (V(AA)) shift the mountain leftwards along the price axis (e). An observer views the silhouette of the reward mountain in 2D against a "screen" consisting of an opaque vertical plane (not shown) that cuts through the mountain at a particular price. The perspective of the observer

is the same as that of an experimenter who employs the curve-shift method, and the silhouettes the observer sees (b,d,f) are analogous to rate-frequency curves. Such an observer cannot determine whether the 3D structure has moved along the pulse-frequency (c,d) or price (e,f) axis. The same silhouette can be produced by displacement of the 3D structure along either of the two axes (f). (Adapted from Hernandez et al., 2010, reproduced from Trujillo-Pisanty, Conover, & Shizgal, 2013).

The behavioral data required to fit the mountain model are obtained by systematic manipulation of two independent variables: reward strength and cost. Rats are trained to hold down a lever for a given cumulative time in order to obtain a reward. The pulse-frequency (the stimulation strength that determines subjective reward intensity) and the amount of time the animal must hold down the lever in order to harvest the reward (i.e. the opportunity cost ("price")) are systematically manipulated across test trials. The dependent variable is termed *Time Allocation* (TA): the proportion of trial time the animal spends working for the electrical reward. The animal's behavior can be represented graphically by a curved surface along which TA is mapped as a function of both stimulation strength and costs. The three-dimensional fit of the model to single-subject data allows for the prediction of TA for any combination of strengths and costs. The position of the mountain along the frequency axis is determined by the stimulation strength required to produce half-maximal reward intensity (the F_{hm} parameter), whereas the location of the surface along the price axis is determined by the price that produces half-maximal time allocation (the P_e parameter) to pursuit of a maximal reward. If a manipulation (such as changing the electrical current or train duration) affects eICSS at a stage of neural processing prior to the output of the intensity-growth function, the structure shifts along the pulse-frequency axis (a change in F_{hm}, Fig 1B); in contrast, if a manipulation affects eICSS beyond the output of the intensity-growth function (such as a change in subjective reward cost), the structure shifts along the price axis (a change in P_e, Fig 1C).

The second published mountain-model study introduced a pharmacological manipulation. Dr. Giovanni Hernandez et al. (2010) tested the effects of cocaine on reward-seeking behavior. They found that cocaine produced a rightward shift along the price axis (an increase in P_e). This finding challenges the traditional view that DA neurotransmission is involved in the computation of reward sensitivity and suggests that it affects eICSS downstream from the output of the reward-growth function. Even in the face of substantial price increases, the rats were able to maintain TA to a reward of a given strength while under the influence of the drug. In contrast, the effect of the drug on reward sensitivity was inconsistent and small in the cases in which it could be discerned at all. This suggests that DA affects eICSS primarily by altering reward gain, probability or costs. However, the lack of specificity of cocaine for the DA transporter made it hard to determine to what degree the observed effects were due to the changes in DA signaling or to the increases in serotonin and/or noradrenaline also induced by the drug. Overall, the experiment provides insight into the potential usefulness of the mountain paradigm in understanding the specific role of DA in eICSS, and contributes to the validation of the model. On the practical front, it also served as a foundation for further refinement of the reward-mountain methodology (especially when working with pharmacological manipulations), and it was an important step forward in understanding how useful the model could be in understanding the role of different neurotransmitter systems in reward. Soon after the cocaine study, Dr. Hernandez began a follow-up experiment to test the effect of the selective DA transporter blocker GBR12909 on the position of the mountain (Hernandez et al., 2012).

For my master's dissertation, we used the mountain model to address an ongoing controversy: the effect of cannabinoid antagonists on eICSS (Trujillo-Pisanty et al., 2011). Previous studies using the curve-shift method had yielded inconsistent results: despite inducing clear and consistent devaluation of food and drug reward, a systemic injection of a cannabinoid 1 receptor (CB1) antagonist produced either no reliable effects on eICSS, or only small rightward shifts (Solinas, Goldberg, & Piomelli, 2008). We demonstrated that these inconsistencies were due to the implicit limitations of the traditional curve-shift method. When the three-dimensional approach (implemented in

the mountain model) was used to test the effects of cannabinoid antagonist on reward-seeking behavior, we found a consistent leftward shift along the price axis that would have been undetectable using the more-common, two-dimensional approach. Moreover, Marie-Pierre Cossette, Ian Moreau-Debord (the first undergraduate student I supervised at Concordia) and I obtained evidence using microdialysis suggesting that this effect could be mediated by a decrease in DA release in the NAc induced by the CB1 antagonist. This result provides correlational evidence that DA could be modulating eICSS by affecting stages downstream from the output of the reward integrator, which complements the findings from the cocaine study. Importantly, the effect is in the opposite direction (i.e. decreasing P_{θ}), as would be expected if the cocaine effects are indeed due to an increase of DA signaling in the NAc. This finding provided further support for the role of DA beyond the computation of the reward-growth function, and led us to continue our efforts in seeking to understand the role of DA in eICSS.

The nature of the shifts in the position of the mountain produced by CB1 blockade made testing slightly simpler than in the case of DA-reuptake blockers. The experimental procedure used for the mountain model entails numerous trials, which requires very long, repeated experimental sessions that extend over several weeks or months, even after the animals have been trained on the task. These are important challenges due to the possibility that food and water deprivation during prolonged test sessions could act as an extraneous variable, and drift in the state of the preparation over many weeks of testing could inflate the error variance. The cannabinoid antagonist reduces the time the animals work for the reward, which reduces testing time when the rats are under the influence of the drug. This allowed me to collect two complete datasets per session while keeping testing sessions under six hours. The CB1 experiment thus helped me better grasp the most efficient and effective ways to conduct pharmacological studies using the three-dimensional methodology.

Blockade of DA reuptake transforms the virtue of the cannabinoid antagonist into a vice: the animals were willing to work so much for the electrical stimulation that the drug sessions were often several hours longer than the vehicle counterparts. Hernandez and

Shizgal had tested several different strategies to deal with the difficulties imposed by these long sessions, one of which was to collect the necessary data for a single mountain across more than one session; they collected data from six rats that way. Although initially, this strategy seemed sound, it resulted in some undesirable inconsistencies across sessions, which also limited the resampling strategy that could be used when fitting the mountain model to the datasets so obtained. These were still early days for the mountain model, and we were still learning what was the optimal method to conduct these studies. Having finished the cannabinoid experiment at that point, I joined Hernandez's efforts on the GBR12909 experiment. Our specific goal at the time was to capitalize on my newly acquired skills working with the model by running a set of rats without spreading acquisition of a dataset across sessions. Our new strategy involved collecting only one complete dataset per drug session (instead of the two I could obtain during the cannabinoid study). The new approach paid off: the datasets were indeed cleaner than those from the first six rats, they were consistent within and between subjects, and were amenable to different resampling strategies. These data proved important in confirming the effects that had been initially found by Hernandez. GBR12909 produced consistent and reliable increases in P_e without affecting F_{hm}, once again arguing that DA modulates eICSS downstream from the reward-growth function. The initial experiment was complemented by neurochemical findings obtained through microdialysis by Marie-Pierre Cossette and allowed us to understand differences in effect size between GBR12909 and cocaine. This study was later published in *The Journal of Neuroscience* (Hernandez et al., 2012), and its design has been adapted for this thesis in Chapter 1.

Following our success using the mountain model to clarify the role of DA in eICSS, and having begun to confirm how this approach surpasses the curve-shift paradigm, we decided to conduct a complementary behavioral pharmacology experiment. The microdialysis data we obtained in the cannabinoid study suggested that decreasing dopamine signaling, would decrease P_e. However, our evidence at that point was strictly correlational. The reliable increase in P_e we observed with the DA reuptake blocker encouraged us to obtain causal evidence of the effect produced by attenuating DA

signaling. We decided to address this question by blocking DA receptors with the DA antagonist, *pimozide*, which had been traditionally used to study the role of DA signalling in eICSS (Gallistel & Karras, 1984; Gomita & Gallistel, 1982; Miliaressis, Malette, & Coulombe, 1986a). Pimozide was challenging to work with because even moderate doses completely suppress lever pressing (Atalay & Wise, 1983), which would prevent us from performing the behavioral measurements necessary for the mountain model. However, after conducting a couple of pilot studies, we found a dose that was compatible with previous studies (Fouriezos et al., 1978; Gallistel & Karras, 1984; Gomita & Gallistel, 1982; Wasserman et al., 1982) and which was effective enough to answer our question. As expected, pimozide produced shifts in the opposite direction to that observed under the influence of DA reuptake blockers: it decreased P_e without affecting F_{hm}. This study was published in *Psychopharmacology* (Trujillo-Pisanty et al., 2013) and has been adapted for this thesis in Chapter 2.

The optogenetic revolution and the study of reward

Having a model that allowed for the behavioral dissection of different stages of reward processing made us eager to selectively manipulate each of these stages with physiologically relevant temporal resolution. In 2008, when I began my pharmacological experiments using the mountain model, the selective activation and inactivation of neuronal subtypes with physiologically relevant temporal resolution was a prevailing ambition shared by many neuroscientists. Importantly, the first steps that would make that objective possible had been taken only three years earlier by Ed Boyden, Feng Zhang, Ernst Bamberg, Georg Nagel, and Karl Deisseroth (Boyden, Zhang, Bamberg, Nagel, & Deisseroth, 2005), at Stanford University.

Francis Crick, had suggested that in order to understand the brain, neuroscientists needed a way to control one type of cell at a time while leaving the others unaltered (Deisseroth, 2010). This would allow investigators to turn neurons “on” and “off” at will in order to understand their function. Unfortunately, the technology that was available to neuroscientists before 2005 was ineffective at manipulating neural activity with such precision: electrical stimulation of the brain only allowed for the activation of neurons

that surround the tip of the electrode. Although the effects sometimes reassemble physiologically-relevant signals (Conover & Shizgal, 1994a), the electrical current nonetheless activates many neurons in addition to those of interest. Pharmacological manipulations are more selective to cells expressing specific receptors or transporters, yet the half-life of the drugs tends to be orders of magnitude longer than the speed at which neurons commonly communicate. Moreover, the limited specificity of most pharmacological agents and the difficulty of restricting the effects of the drugs to specific brain areas can make it difficult to draw solid conclusions. Lesions and ablations were also commonly used. Although some selectivity in lesioning can be achieved by neurotoxins, the ensuing neuroplastic changes make the behavioral effects difficult to interpret. Moreover, most lesion methods produce irreversible changes, which further complicate interpretation of the effects. Looking back, it is astonishing that we were able to make so much progress in our understanding of the brain and behavior in the past century with such limited strategies.

In their groundbreaking work, Boyden *et al.* (2005) made use of cutting-edge molecular and genetic tools to bring neural activity under optical control. They made use of channelrhodopsin-2 (ChR2), a light-sensitive cation channel naturally expressed by the unicellular alga *chlamydomonas reinhardtii*. Boyden et al. succeeded in expressing this channel in mammalian hippocampal neurons and demonstrated that pulses of blue light could reliably and selectively depolarize these transfected cultured cells. In the following years, different wavelengths of light would be used as the stimulus to activate or inactivate neuronal cell bodies or projections at will. The many natural and artificial variants of microbial opsins would become the *on* and *off* switches of choice (Airan, Thompson, Fenno, Bernstein, & Deisseroth, 2009; Berndt, Lee, Ramakrishnan, & Deisseroth, 2014; Berndt et al., 2016; 2011; Berndt, Yizhar, Gunaydin, Hegemann, & Deisseroth, 2009; Chow et al., 2010; Chuong et al., 2014; Deisseroth, 2011; Deisseroth et al., 2006; Fiala, Suska, & Schlüter, 2010; Govorunova, Spudich, Lane, Sineshchekov, & Spudich, 2011; Gradinaru, Thompson, & Deisseroth, 2008; Gradinaru et al., 2010; Gunaydin et al., 2010; Han & Boyden, 2007; Klapoetke et al., 2014; Liu & Tonegawa, 2010; Wietek et al., 2014; Zhang, Aravanis, Adamantidis, de Lecea, & Deisseroth,

2007a; Zhang et al., 2010; 2007b), and transgenic organisms and viral vectors would allow for the selective targeting of these effectors to specific cell types (Atasoy, Aponte, Su, & Sternson, 2008; Beier et al., 2015; Gong et al., 2007; Gradinaru et al., 2010; Kuhlman & Huang, 2008; Lammel et al., 2012; Marshall, Allison, Templeton, & Foote, 2004; Miyoshi & Fishell, 2006; Nagel et al., 2003; Ramirez et al., 2013; Shimano et al., 2012; Witten et al., 2011; Yang & Gong, 2005; Zhao et al., 2011). This made it possible to control the behavior of mammals through the intracranial delivery of light to neuronal populations expressing light-sensitive channels and pumps (Jennings et al., 2013b; 2015; Nieh et al., 2015; Sparta et al., 2014; Stamatakis & Stuber, 2012; Stamatakis et al., 2013; Stuber, 2010; Stuber & Wise, 2016; Stuber, Hnasko, Britt, Edwards, & Bonci, 2010; Tan et al., 2012; Tsai et al., 2009; Tye et al., 2013; 2011; Warden et al., 2012). The field of optogenetics was born, and neuroscience research would be drastically transformed!

Optogenetic methods were soon incorporated into the study of reward-seeking behavior with the aim of understanding the circuitry responsible for goal-oriented behavior and addiction. The Ventral Tegmental Area (VTA) is of particular interest as its DA output to the NAc has been considered an important component of the neurobiological substrates for natural and artificial reward seeking (Aston-Jones, Smith, Moorman, & Richardson, 2009; Aston-Jones et al., 2010; Carlezon & Thomas, 2009; Conover & Shizgal, 1994b; 1994a; Gutierrez, Lobo, Zhang, & de Lecea, 2011; Ikemoto, 2007; Salamone, Cousins, & Snyder, 1997; Schultz, 1997; Shizgal, Fulton, & Woodside, 2001; Wise, 1998; 2006; 2008).

The VTA is one of the main sources of DA projections in the brain; it has been shown to be necessary for motivated behavior and in the rewarding effects of eICSS, natural rewards, and drugs of abuse (Dietrich & Horvath, 2009; Figlewicz & Sipols, 2010; Gutierrez et al., 2011; Iversen & Iversen, 2007; Wise, 1998; Wise & Rompré, 1989). The VTA is comprised of dopaminergic, GABAergic and glutamatergic neurons (Fields, Hjelmstad, Margolis, & Nicola, 2007; Morales & Root, 2014; Root et al., 2014; Swanson, 1982). DA neurons in the VTA receive several monosynaptic inputs from the striatum,

the pallidum, amygdala, hippocampus, the medial preoptic area (MPA), lateral preoptic area (LPO), the lateral habenula (LHB), paraventricular hypothalamic nucleus, the LH, the zona incerta, the parasubthalamic nucleus, the reticular formation, retrorubral field, the dorsal raphe nucleus (DR), and the parabrachial nucleus (PB), among others (Watabe-Uchida, Zhu, Ogawa, Vamanrao, & al, 2012). The main glutamatergic inputs to the VTA include the medial prefrontal cortex (mPFC), prelimbic cortex (PrL), MPA, LPO, LH, LHB, DR and PB (Geisler, Derst, Veh, & Zahm, 2007). The Bed Nucleus of the Stria Terminalis (BNST) sends both GABAergic and glutamatergic projections to the VTA. Other VTA inhibitory inputs have been identified from the Rostro-Medial Tegmental nucleus (RMTg) (Jhou, Fields, Baxter, Saper, & Holland, 2009), the LH (Nieh et al., 2015), and the NAc. In turn, the VTA sends dopaminergic projections to the NAc, the BLA, and the mPFC. The heterogeneity of this region and the complex distribution of its afferents and efferents have made it difficult to establish causal relationships between specific VTA neuronal subtypes, their inputs, and their outputs by means of traditional neurochemical, electrophysiological and behavioral techniques. Optogenetics has provided the technology to dissect the specific role of each of these neuronal subtypes and projections in reward and drug abuse. Some of these findings are summarized below.

Optogenetic studies of the contribution of VTA cell bodies to reward: Selective optogenetic activation of VTA DA neurons is sufficient to support conditioned place preference (Tsai et al., 2009) and also supports optical Intracranial Self Stimulation (oICSS) (Adamantidis et al., 2011; Ilango et al., 2014; Witten et al., 2011). Conversely, selective activation of GABA interneurons in the VTA alters natural reward seeking and decreases DA release in the NAc (van Zessen, Phillips, Budygin, & Stuber, 2012). Overall, these findings suggest that VTA DA neurons are necessary and sufficient for reward seeking.

In another study entailing optogenetic activation of VTA DA neurons, AMPA receptor redistribution induced by a single administration of cocaine, morphine or nicotine was mimicked by selective optical stimulation of these cells (Brown et al., 2010). This

suggests that activation of DA VTA neurons is sufficient to induce at least some of the neuroplastic changes that have been linked to addiction (Lüscher & Malenka, 2011; Montague, Dayan, & al, 1996; Nugent, Hwong, Udaka, & Kauer, 2008).

Optogenetic studies of the contribution of VTA inputs to reward: Optical stimulation of LH inputs to the VTA supports oICSS, an effect that was blocked by NMDA and neurotensin 1 receptor antagonism (Kempadoo et al., 2013); importantly, this suggests that NMDA receptors are necessary for the rewarding effects produced by activation of this pathway, but it does not provide sufficient evidence to confirm that glutamate release from the stimulated LH terminals is responsible for that effect. In fact, a number of studies suggest that GABA projections from the LH to the VTA are particularly important for reward. Selective stimulation of LH neurons expressing the vesicular GABA transporter (Vgat) were shown to support oICSS and to induce feeding (Jennings et al., 2015), these effects resemble those obtained by LH electrical stimulation (Gratton & Wise, 1988a; 1988b; Hoebel & Teitelbaum, 1962; Margules & Olds, 1962). Conversely, selective stimulation of LH neurons expressing the type 2 vesicular glutamatergic transporter (Vglut2) produces aversion and decreases food consumption (Jennings, Rizzi, Stamatakis, Ung, & Stuber, 2013a). LH projections expressing vesicular GABAergic and glutamatergic transporters (Vgat and Vglut2) synapse on VTA DA and GABA neurons, and selective stimulation of the inhibitory projections preferentially induces feeding and oICSS (Nieh et al., 2015). Overall, these findings highlight the role of LH-VTA inputs in reward and suggest that Vgat and Vglut LH neurons are responsible for bidirectional signaling, which is conveyed directly and indirectly to VTA DA neurons (Stuber & Wise, 2016); disinhinibition of VTA-DA neurons through inhibitory projections to VTA GABA neurons seems particularly relevant for reward seeking. Selective optical stimulation of the excitatory input to the VTA from the BNST produces aversion, whereas stimulating the GABAergic input supports conditioned place preference; both types of projections synapse onto GABAergic VTA interneurons, further suggesting that the rewarding effects could arise from disinhibition of DA neurons, and that the anxiogenic effects could result from excessive inhibition of these cells (Jennings et al., 2013b).

Optical stimulation of excitatory inputs from the lateral habenula to the VTA produces conditioned place avoidance, an effect due to the excitatory synapses between this nucleus and GABAergic neurons in the VTA and the RMTg (Stamatakis & Stuber, 2012). The lateral habenula also receives excitatory inputs from the LH; these projections in turn excite GABAergic neurons that project to the VTA. Selective optogenetic inhibition of LH-lateral habenula excitatory projections produces place preference and increased food consumption, whereas selective stimulation of this pathway decreases feeding behavior and is aversive. These latter effects are likely mediated through indirect inhibition and dishinibition of VTA DA neurons (Stamatakis et al., 2016).

Selective optogenetic stimulation of non-serotonergic neurons of the Dorsal Raphe Nucleus (DRN) is sufficient to support oICSS; this effect is DA-dependant, and is due to the activation of VTA DA neurons by non-serotonergic, glutamatergic projections from the DRN (McDevitt et al., 2014). However, it has also been shown that serotonergic and glutamatatergic DRN-VTA and DRN-NAc projections could differentially contribute to reward signaling. Genetic deletion of the vesicular glutamate transporter (Vglut3) attenuated oICSS of serotonergic projections to the VTA in mice working on a continuous reinforcement (CRF) schedule. However, in mice lacking tryptophan hydroxylase 2 (the rate-limiting enzyme in serotonin synthesis), performance on a CRF schedule appeared normal but was attenuated when the mice work on a fixed ratio 8 schedule (Liu et al., 2014).

Optogenetic studies of the contribution to reward of VTA outputs and inputs to NAc medium spiny neurons: The DAergic projection to the NAc has been postulated as a particularly important pathway in goal-oriented behaviors and drug abuse (Berridge & Kringelbach, 2008). Selective optogenetic stimulation of the terminals of VTA DA neurons produce co-release of DA and glutamate in the NAc, but not in the dorsal striatum (Stuber et al., 2010; Tecuapetla et al., 2010). Interestingly, activation of medium spiny neurons (the main neuronal type in the NAc, MSN) as well as their glutamatergic

inputs from the basolateral amygdala (BLA), the ventral hippocampus, and the prefrontal cortex, is sufficient to support intracranial self stimulation, an effect that also requires D1 receptor activation (Britt et al., 2012; Stuber, Britt, & Bonci, 2012). This suggests that reinforcement can occur by a strong excitatory drive to the MSNs, which is modulated by DA release in the NAc. In line with this suggestion, disinhibition of MSNs by selective optogenetic inhibition of cholinergic interneurons in the NAc is sufficient to prevent cocaine-induced conditioned place preference (Witten et al., 2010).

Optogenetics and formal explanations in Psychology

The introduction of optogenetics to the study of the neural basis of reward has greatly increased our understanding of brain reward circuitry, and it promises to push this field even further in the years to come. However, the behavioral assays that have been commonly employed to characterize the role of each neuronal subtype have been limited. Identifying whether silencing or activating a specific neuronal population promotes reward (e.g. by supporting place preference, or oICSS) or induces aversion (e.g. by supporting place avoidance or escape) does not provide sufficient information to make inferences concerning the specific psychological processes responsible for these behaviors. The fact that many different types of neurons and projections similarly support reward-related behaviors (and that these resemble eICSS) does not necessarily mean that all the behaviors in question are maintained by the same psychological processes.

Formal explanations are necessary to understand the psychological causes of behavior (Killeen, 2001). This type of explanation relies on quantitative approaches such as psychophysics. The development of quantitative models that reflect the relationship between a variable and a given behavior and that predict the changes of behavior across time, are a common goal of formal explanations in psychology. However, most behavioral optogenetic papers published to this date have employed simple measurements of the vigor of behavior. Such measurements do not provide a sufficient foundation for formal psychological and computational explanations.

We strove to understand how VTA DA signaling affects reward seeking by incorporating optogenetic strategies in the reward-mountain methodology; the theoretical and formal strengths of the model combined with the unparalleled specificity and temporal resolution of optogenetics provide us with the means to behaviorally dissect the circuitry in an unprecedented way. We used optogenetics as a means to bypass the traditionally stimulated MFB substrate in eICSS by activating midbrain DA neurons directly in TH::Cre rats. This allowed us to behaviorally interrogate the role of DA neurons from a decision-making perspective, enhancing our ability to make formal psychological and computational inferences about their potential role in reward. The first results of this approach will be submitted for publication shortly, and are presented in Chapter 4 of this thesis.

Incorporation of optogenetic methods into the reward-mountain methodology poses several challenges. This required major modifications to the workflow and infrastructure in our lab, which included acquiring new skills, multidisciplinary knowledge, and new techniques. Chapter 3 of this thesis is an example of the many methodological obstacles we faced and how we overcame them: In order to run the long sessions that are commonly required by the mountain model, we had to design robust optical-fiber cables suitable to connect the laser output to optical-fibers chronically implanted in the brains of large, vigorously behaving rats. This design proved critical to the success of our experiments. Exchanges with other researchers conducting optogenetic research with rats revealed that our patch-cord design could help other teams overcome similar obstacles. We published the protocol in *Methods X* (Trujillo Pisanty, Sanio, Chaudhri, & Shizgal, 2015), a peer reviewed open-access journal specializing in methodological advances. This report has been adapted to thesis format and it is presented in Chapter 3 of this thesis.

Hypotheses and overview of this thesis

In chapter 1, we explored the stage of reward processing at which DA signaling affects operant performance for electrical stimulation of the MFB at the level of the LH. If DA

neurons subserve the electrically induced reward signal at a stage of processing prior to the output of the reward-growth function, preventing DA reuptake by administering GBR12909 should shift the mountain along the frequency axis (i.e. F_{hm} should decrease). However, if DA signaling contributes to reward seeking after the initial integration of reward strength, then this pharmacological manipulation should shift the mountain along the price axis (i.e. P_e should increase). We found consistent increases in P_e without significant changes in F_{hm}, suggesting that DA is recruited in eICSS beyond the integration of the effects produced by the volley of action potentials directly induced by the electrical stimulation. DA may modulate eICSS by affecting the computation of reward gain, payoff, or costs.

If DA participates in reward seeking beyond the computation of the MFB-eICSS reward-growth function, then DA receptor blockade should decrease P_e. We tested this hypothesis by administering the DA receptor antagonist *pimozide*. Chapter 2 reports consistent drug-induced decreases on P_e without significant changes in F_{hm}. These results confirm the involvement of DA signaling in reward seeking at a secondary stage of neural processing and further suggests that DA may modulate eICSS by affecting the computation of reward gain, payoff, or costs.

In chapter 3, I present one of my technical contributions to the application of optogenetics in behavioral experiments carried out in rats. The optical patch-cord design was critical for running long experimental sessions with rats. This advance allowed us to run the experiments presented in chapter 4.

Optogenetic stimulation of midbrain DA neurons bypasses the traditionally stimulated substrate in eICSS, making it possible to test the contribution of these neurons in reward-seeking by stimulating them directly. The results from chapters 1 and 2 suggest that these neurons could code for reward gain, payoff, or costs. In the mountain model, payoff is determined by the relative weights of reward intensity and reward costs (Figure $1A_3$). If midbrain-DA neurons are responsible for the computation of payoff, than optical stimulation should bypass the computation of reward cost, making animals insensitive to

increments in the price of the reward. This insensitivity would prevent the decline of the reward-mountain surface along the price axis in animals working for direct optogenetic activation of midbrain DA neurons. In chapter 4, I show that optical mountains similar in shape to those obtained in the eICSS paradigm can be obtained in the oICSS paradigm as well, casting doubt on the view that phasic DA signaling represents payoff. Moreover, if DA signaling contributes to the computation of reward strength in oICSS, then DA reuptake blockade should boost the output from the directly stimulated neurons, thereby decreasing F_{hm}. I tested this hypothesis by administering GBR12909 and observed the expected decreases in F_{hm}, along with consistent increases in P_e. The contrasting effects on F_{hm} of DA-reuptake blockade in eICSS and oICSS demonstrate that eICSS and oICSS activate different neural populations directly. Finally, I show evidence for spatio-temporal integration of optical-reward intensity in DA neurons.

Taken together, the results from chapters 1, 2 and 4 suggest that the neural circuit responsible for the integration of the output from midbrain DA neurons differs from, and lies downstream of the circuit that integrates the output of the directly stimulated neurons subserving eICSS. The interaction between the two integrators could be related to the rescaling process of the reward-intensity signal. Moreover, the consistent drug-induced increases in P_e observed both in studies of eICSS and oICSS suggest that DA signaling may play more than one role in reward seeking: it is responsible for the computation of reward intensity in oICSS (as reflected by the increase in F_{hm}), but it may also play a role in computing reward costs (as reflected by the increase in P_e). This dual role may be related to the distinction between phasic vs tonic DA signaling.

CHAPTER I

Role of dopamine tone in the pursuit of brain stimulation reward

Giovanni Hernandez, Ivan Trujillo-Pisanty, Marie-Pierre Cossete, Kent Conover, and Peter Shizgal.

Hernandez, G., Trujillo Pisanty, I., Cossette, M.-P., Conover, K., & Shizgal, P. (2012). Role of dopamine tone in the pursuit of brain stimulation reward. *Journal of Neuroscience, 32*(32), 11032–11041. http://doi.org/10.1523/JNEUROSCI.1051-12.2012

Abstract

Dopaminergic neurons contribute to intracranial self-stimulation (ICSS) and other reward-seeking behaviors, but it is not yet known where dopaminergic neurons intervene in the neural circuitry underlying reward pursuit or which psychological processes are involved. In rats working for electrical stimulation of the medial forebrain bundle, we assessed the effect of GBR-12909, a specific blocker of the dopamine transporter. Operant performance was measured as a function of the strength and cost of electrical stimulation. GBR-12909 increased the opportunity cost most subjects were willing to pay for a reward of a given intensity. However, this effect was smaller than that produced by a regimen of cocaine administration that drove similar increases in nucleus accumbens (NAc) dopamine levels in unstimulated rats. Delivery of rewarding stimulation to drug-treated rats caused an additional increase in dopamine concentration in the NAc shell in cocaine-treated, but not GBR-treated, rats. These behavioral and neurochemical differences may reflect blockade of the norepinephrine transporter by cocaine but not by GBR-12909. Whereas the effect of psychomotor stimulants on ICSS has long been attributed to dopaminergic action at early stages of the reward pathway, the results reported here imply that increased dopamine tone boosts reward pursuit by acting at or beyond the output of the circuitry that temporally and spatially summates the output of the directly stimulated neurons underlying ICSS. The observed enhancement of reward seeking could be due to a decrease in the value of competing behaviors, a decrease in subjective effort costs, or an increase in reward-system gain.

Introduction

Intracranial self-stimulation (ICSS) was the subject of the very first experiment on the role of dopamine in reward seeking (Crow, 1970) and has continued to contribute heavily to the study of brain reward circuitry. ICSS is typically measured in the curve-shift (Edmonds & Gallistel, 1974; 1977; Miliaressis, Rompre, Laviolette, Philippe, & Coulombe, 1986b) or progressive-ratio paradigm (Hodos, 1961). It has been

demonstrated recently (Arvanitogiannis & Shizgal, 2008; Hernandez et al., 2010; Trujillo-Pisanty et al., 2011) that neither method provides sufficient isolation of the different process underlying reward seeking to distinguish between competing hypotheses concerning the variables to which dopamine neurons contribute, which include the sensitivity and gain of brain reward circuitry (Hernandez et al., 2010) and subjective effort cost (Niv, Daw, Joel, & Dayan, 2006; Salamone, Correa, Mingote, & Weber, 2005).

The ambiguity inherent in curve-shift and progressive ratio measures is reduced by measuring ICSS as a function of both the strength and cost of reward (Arvanitogiannis & Shizgal, 2008; Hernandez et al., 2010). This method, which produces a three-dimensional (3D) structure called the "reward mountain," can distinguish between changes in the sensitivity of the reward circuitry and changes in a diverse set of variables that includes reward-circuit gain, subjective effort cost, and the value of alternate activities, such as grooming, exploring, and resting. Sensitivity of the ICSS substrate is indexed by the pulse frequency required to produce a reward of half-maximal subjective intensity; it is analogous to the affinity of a drug for a receptor. Gain indexes the maximum rewarding effect achievable; it is analogous to the relationship between the number of available receptors and the magnitude of a drug effect.

Application of the 3D measurement method has challenged the long-standing hypothesis that psychomotor stimulants, such as cocaine, increase the sensitivity of the ICSS substrate (Crow, 1970; Esposito, Motola, & Kornetsky, 1978; Wise, 1980). By measuring displacement of the reward mountain by cocaine, Hernandez et al. (2010) showed that some combination of changes in gain, subjective effort costs, and the value of alternate activities is responsible for the drug-induced enhancement of ICSS performance. Although that experiment achieves greater specificity at the behavioral level than prior studies employing two-dimensional measurement methods, the results are ambiguous at the neurochemical level because cocaine blocks the transporters for dopamine, norepinephrine, and serotonin (Iversen, 2000).

In the present study, we isolated the contribution of dopamine tone by measuring displacement of the reward mountain in response to GBR-12909, a drug that blocks the dopamine transporter (DAT) with high specificity (Andersen, 1989). In parallel, we used in-vivo microdialysis to measure the effect on dopamine tone in the nucleus accumbens of GBR-12909, cocaine, and their interaction with rewarding brain stimulation. The behavioral and neurochemical effects of GBR-12909 mimic some, but not all, of the effects of cocaine, thus implicating increased dopamine tone in the enhancement of reward pursuit by psychomotor stimulants and suggesting synergistic roles for dopamine and norepinephrine in the neurochemical and behavioral effects of cocaine.

Materials and Methods

Microdialysis experiments

Subjects: 24 male Long-Evans rats (Charles River, St. Constant, Quebec, Canada) weighting between 350-400 grams at the moment of surgery served as subjects for the microdialysis experiments. The rats were housed individually in hanging cages and maintained on a 12-hr reverse light– dark cycle (lights off from 0800 to 2000), with ad libitum access to water and food (Purina Rat Chow).

Surgery

Atropine sulfate (0.5 mg/kg sc) was administered to reduce bronchial secretions prior to induction of anaesthesia with a ketamine (10mg/kg, i.p.) / xylazine (100 mg/kg, i.p.) mixture. The topical anaesthetic, Xylocaine, was applied prophylactically to the external auditory meatus to reduce discomfort that could arise from the ear bars after the rat was mounted in the stereotaxic frame. Isoflurane was used to maintain anaesthesia. A 20-gauge guide cannula (Plastics One, Roanoke, VA) for microdialysis was aimed stereotaxically at the nucleus accumbens septi (1.5 AP, ±2.8 ML, and –5.4 DV from skull at a 10° angle).

GBR-12909 blocks the DAT with a much longer half-life than cocaine (Menacherry & Justice, 1990). To bring the time courses of the effects produced by the two drugs into closer concordance, cocaine was administered continuously. A route for continuous administration was establish by implanting perforated Tygon® tubing subcutaneously, as

described elsewhere (Hernandez et al., 2008). In 13 of these subjects, a monopolar stimulating electrode was aimed at the lateral hypothalamus (LH; –2.8 AP, 1.7 ML, and –8.8 DV from skull) ipsilateral to the cannula. The electrode was made of stainless-steel wire (0.25 mm diameter) and insulated with Formvar except for the region extending 0.5 mm from the tip. The anode consisted of two stainless-steel screws fixed in the skull, around which the return wire was wrapped. The electrode and the cannula were secured with dental acrylic and skull-screw anchors. At the end of the surgery the rats were injected with buprenorphine (0.05 mg/kg s.c.), to reduce pain, and with a sterile saline solution (1 ml/kg s.c.), to provide fluid replacement. The rats were allowed to recuperate for 5 to 7 days post surgery before any experimental manipulation.

Self-stimulation training

Each of the rats implanted with stimulating electrodes was shaped to lever press for a 0.5-s train of cathodal, rectangular, constant-current pulses, 0.1 ms in duration. Shaping took place in a Plexiglas operant chamber (30 cm long x 21 cm wide x 51 cm high) equipped with a retractable lever located on the right wall of the box and a cue light positioned 1.5 cm above the lever. A continuous reinforcement schedule was in force. The self-stimulation training was carried out as in previous experiments (Hernandez et al., 2006; 2007). Once the rat pressed the lever consistently for currents between 125 and 400 µA, a time-allocation versus pulse-frequency curve was obtained by varying the stimulation frequency across trials over a range that drove the number of rewards earned from maximal to minimal levels; the stimulation frequency was decreased from trial to trial by 0.08 $\log_{10}$ units. The series of trials conducted to obtain a time-allocation versus pulse-frequency curve is called a "frequency sweep." The frequency used during the subsequent microdialysis sampling was one $\log_{10}$ unit greater than the lowest frequency that supported a maximal response rate, as determined from the time allocation-frequency curve.

In vivo microdialysis

Testing was conducted in similar operant chambers to the ones used during training, but with the levers removed. Each testing chamber was housed in a dark Styrofoam-lined enclosure with a small opening at the top. All testing took place during the dark phase of

the circadian schedule. The methodology for microdialysis sampling has been described in detail elsewhere (Hernandez et al., 2006; 2008). Dialysate samples were collected every 20 min and immediately analyzed. Baseline was defined as a series of three consecutive microdialysis samples in which the dopamine concentration fluctuated by ≤5%. After the baseline was determined, a single i.p. injection of GBR-12909 (10 mg/kg, i.p.) was given or the subcutaneous infusion of cocaine began (1.75 mg/kg/hr). For the rats that were not implanted with electrodes, dialysate samples were collected for an additional 360 minutes. In the cocaine- and GBR-treated rats, samples were collected for an additional 200 or 120 minutes, respectively, before stimulation commenced. Following the onset of the stimulation, sampling continued for 140 or 240 minutes, respectively.

Stimulation during microdialysis sessions

During the microdialysis sessions, stimulation trains were delivered according to a variable time, twelve-second (VT-12) schedule of reinforcement. The schedules were programmed using LabVIEW software (National Instruments, Austin, TX) installed on an IBM laptop computer. The intervals constituting the VT schedule were drawn from lagged exponential distributions with a mean of 11 seconds; a fixed lag of 1 second was added to each interval in order to prevent the stimulation trains from overlapping in time or occurring at very short temporal offsets. The stimulation was delivered by a Master 8 pulse generator (A.M.P.I., Jerusalem, Israel), which drove a constant-current amplifier (Mundl, 1980). The stimulation current was monitored with an oscilloscope (Tektronix TDS2014), which read the voltage drop across a 1-kΩ resistor (1% precision) in series with the electrode.

Analytical chemistry

A description of the procedures for analytic chemistry can be found in Hernandez et al. (2006).

Histology

After completion of the experiment, a lethal dose of sodium pentobarbital was administered. If a stimulation electrode had been implanted, iron was deposited at the

site of the electrode tip by passing a 1 mA current for 15 s, with the electrode as the anode and the skull screws as the cathode. The animals were then perfused intracardially with 0.9% sodium chloride followed by 10% formalin; if electrodes were implanted, a formalin-Prussian Blue solution (10% formalin, 3% potassium ferricyanide, 3% potassium ferrocyanide, and 0.5% trichloroacetic acid) was used in lieu of 10% formalin. The latter solution forms a blue precipitate from the iron particles deposited at the electrode tip. After perfusion the animals were decapitated and the brains were removed from the skulls and fixed with 10 % formalin solution for at least 7 days. Coronal sections, 40 μm thick, were cut with a cryostat (Thermo Scientific). The probe and electrode-tip locations were determined microscopically at low magnification with reference to the stereotaxic atlas of (Paxinos & Watson, 2007). Histological reconstructions show that the probe tips were located within the shell region of the nucleus accumbens NAc (Figure 3, 4a), and the electrode tips were located in the LH (Figure 4b).

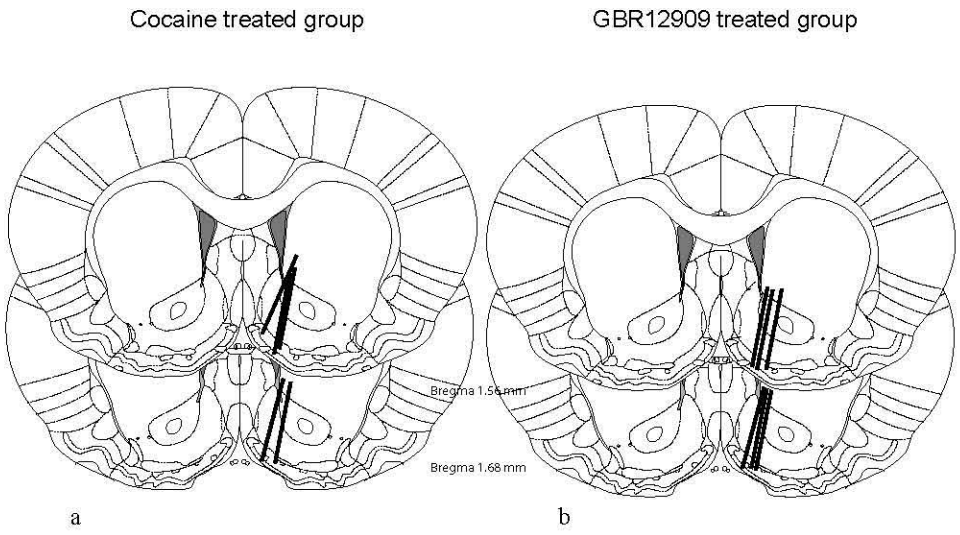

Figure 3: Location of microdialysis probes in the cocaine- (1.1a) and GBR-12909-treated rats (1.1b). The tips of all the probes are located within the NAc shell, as determined with respect to the Paxinos and Watson (2007) atlas.

Behavioural experiment

Subjects were 10 male Long-Evans rats (Charles River, St. Constant, Quebec, Canada) weighting between 350-400 grams at the time of surgery. They were housed and fed as described above.

Surgery

The subjects were prepared for surgery as described above, with the exceptions that stimulating electrodes were aimed bilaterally at the LH (-2.8 AP, 1.7 ML, and -8.8 DV from skull), and no cannula was implanted. The monopolar stainless-steel electrodes were constructed as described above. A 5- to 7-day period was provided for post-surgical recuperation before the self-stimulation training began.

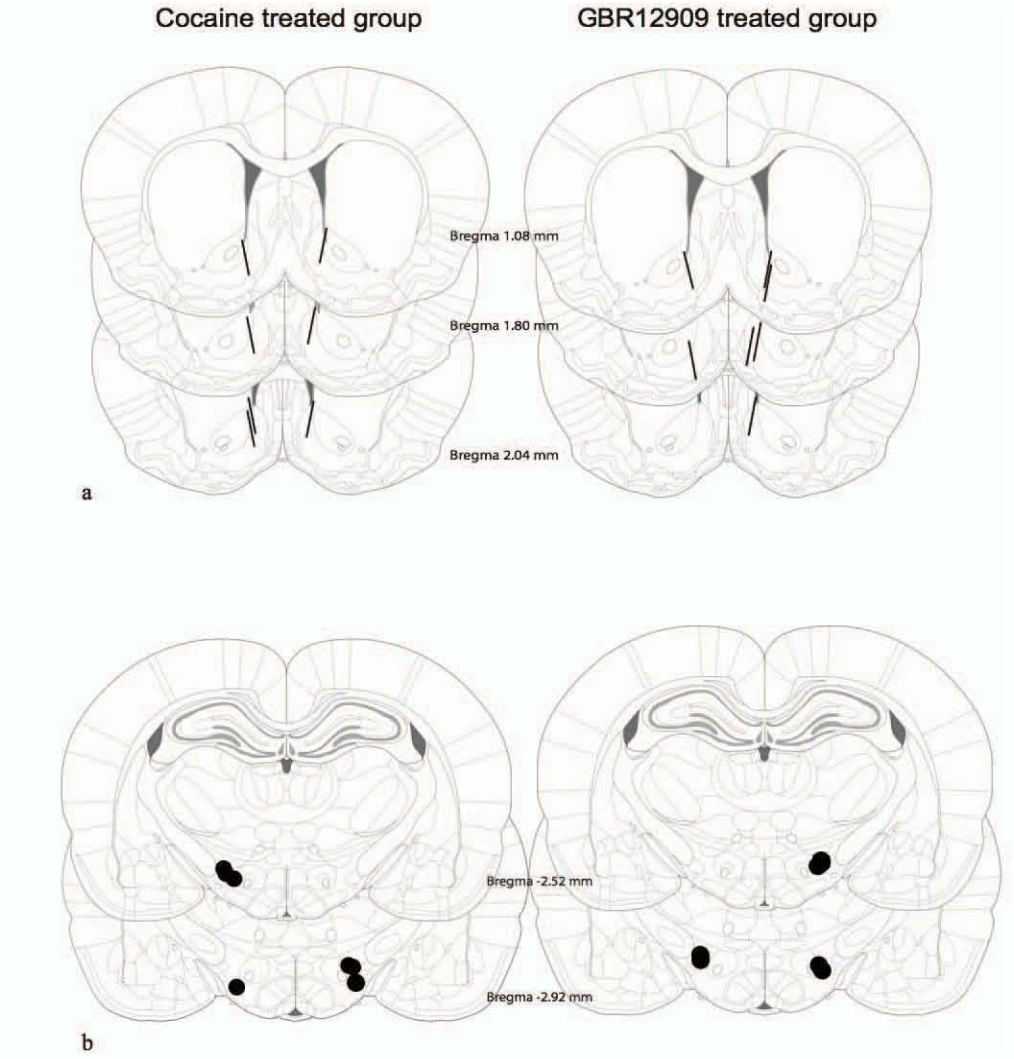

Figure 4: Location of microdialysis probes and electrode tips in the cocaine- and GBR-12909- treated rats. The tips of all the microdialysis probes (4a) are located within the NAc shell, and the electrode tips (4b) fell within the boundaries of the MFB, at the level of the LH as determined with respect to the Paxinos and Watson (2007) atlas.

Self-stimulation training and stabilization

Self-stimulation of both LH sites was assessed, and the electrode that supported the most vigorous lever pressing in the absence of motor side effects was chosen for further testing. Shaping was done as described above. A cumulative handling time schedule of reinforcement (Breton, Marcus, & Shizgal, 2009) controlled the delivery of rewarding

stimulation. Under this schedule, a reward is delivered when the cumulative time that the lever has been depressed reaches a value set by the experimenter (the "price" of the reward). Depression of the lever was accompanied by illumination of the neighboring cue light. As soon as the rat satisfied the response criterion, the lever was retracted, and a stimulation train was delivered. After a 2-second delay, the lever was re-introduced into the cage, the cumulative timer was reset to zero, and the rat could resume working to obtain another reward.

Each trial consisted of a fixed time during which the price and pulse frequency parameters were held constant. The duration of each trial was sufficient to allow a rat that allocated all of its time to lever pressing to harvest 20 rewards. At the end of each trial and prior to the start of the next one, the lever retracted for 10 s, and the house light flashed. Two priming trains were delivered during the final 2 seconds of the inter-trial interval. The priming stimulation was held constant across trials and was delivered at a pulse frequency that previously had been shown to support vigorous responding; the remaining parameters were the same as those used during the test trials.
During the initial training, the price of the reward was increased from 1 second of cumulative lever depression to 4 seconds, the value that would be used during the frequency sweeps throughout the saline condition of the experiment. This price (i.e., opportunity cost) was selected because at this and greater values, objective and subjective prices have been shown to correspond closely (Solomon, 2014). Once performance stabilized across successive frequency sweeps, "price-sweep" testing commenced. During price sweeps, the pulse frequency was set to the maximum value used during the frequency sweeps, and the price of the reward was increased successively from trial to trial. Once performance stabilized across successive price sweeps, "radial-sweep" testing commenced. At each step along a radial sweep, the pulse frequency is decreased and the price is increased.

Two sweeps of each type were run during every stabilization session. We use the term "survey" to refer to the combination of a frequency sweep, a price sweep, and a radial sweep; these provide the minimal dataset required to fit the mountain model. The sequence of sweeps was random within session for subjects GBR2-GBR8 and random

within survey for GBR11-GBR14. These two randomization approaches differ in terms of the condition for repeating a particular sweep. In the survey method, a sweep could be repeated only when a set, consisting of one instance of each sweep type, had been completed. In the session method, a given sweep type might be tested twice before one or both of the others had been tested in that session. The survey approach makes it possible to fit two mountains to the data from a single session whereas the session method allows only one to be fit. Thus, the survey approach was introduced to increase the power of the resampling-based surface-fitting approach.

Self-stimulation testing

The pharmacological treatment began after stable performance was achieved in stabilization sessions that included all three sweep types. GBR-12909 was dissolved in sterile saline at a concentration of 10 mg/ml, and adjusted to a pH of 5 ± 0.1 by means of the addition of 0.1M NaOH. The drug solution was injected i.p. at a dose of 10 mg/kg, and the vehicle solution, also injected i.p., consisted of sterile physiological saline (0.9%).

Vehicle sessions were run on Mondays and Thursdays and were composed of two sets of frequency, price, and radial sweeps. The order of the sweeps was randomized in the same manner as in the stabilization sessions.

Drug sessions were run on Tuesdays and Fridays. Due to the effect of the drug on the position of the mountain, it was necessary to structure these sessions in a different manner than the vehicle sessions. As described below, the drug generally shifted the mountain rightward along the price axis. For ease of comparison between the two data sets, one frequency sweep was run at the same price as that used in the vehicle sessions, and a second frequency sweep was added at a higher price estimated to offset the shift produced by the drug. The shift necessitated testing higher prices, and the additional time involved, coupled with the addition of the second frequency sweep, made it unfeasible to collect two complete sets of sweeps in a single session. In the case of rats GBR2-8, multiple sessions were required to obtain a single survey of the mountain under the influence of GBR-12909; in the case of rats GBR11-14, each drug

session provided one complete survey (one sweep of each type). In the price sweeps carried out with rat GBR6, there was no drug-induced shift to offset and thus it was not possible to generate a high-price frequency sweep for this rat. Thus, in this subject only, a complete survey of the mountain in the drug condition consisted of only three sweeps.

The self-stimulation tests began 2 hours after the GBR or saline injection. The first determination of the time-allocation-versus-frequency curve was considered a warm-up and was not included in the analysis. The collection of the behavioral data was restricted to the period when the GBR elevation in dopamine concentration had been shown to be stable by means of the microdialysis data reported below. After the first week of experimentation, a preliminary fit of the mountain model to the data was performed and the results were used to adjust the tested values of pulse frequency and price so as to optimize sampling. The new values were selected to accommodate the drug-induced displacement of the 3D structure and to select the price for the high-price frequency sweep that was included in the drug condition. The price in question was chosen to offset the effect of the drug so that in the plot representing time-allocation as function of pulse frequency, the high-price frequency sweep carried out in the GBR condition would overlap the plot obtained at the lower price employed in the saline condition. Thus, the price employed for the high-price frequency sweep exceeded the price employed for the frequency sweep in the vehicle condition by an amount equal to the estimated drug-induced shift of the 3D structure along the price axis.

Statistical treatment of behavioural data

The 3D model was fit separately to the data from the vehicle and drug sessions using the non-linear least-squares routine in the MATLAB Optimization Toolbox (The Mathworks, Natick, MA). The fitting approach is described in detail elsewhere (Hernandez et al., 2010). The objective was to obtain unbiased estimates of the parameters of the reward-mountain surface and their dispersions without making unrealistic assumptions about normality and lack of correlation between parameter values. Our approach is based on resampling (Efron & Tibshirani, 1994). Multiple datasets (1000) are generated by randomly sampling the TA values with replacement. The mountain model is fit to each dataset or to each of its component surveys, and

descriptive statistics (means and 95% confidence intervals) are generated for each parameter.

The mountain model has two location parameters (Arvanitogiannis & Shizgal, 2008; Hernandez et al., 2010), which set the position of the 3D structure along the pulse-frequency and prices axes. The pulse frequency at which reward intensity is half-maximal is designated F_{hm} whereas P_e designates the price at which the proportion of time allocated to pursuit of a maximal reward falls half way between the base and summit of the mountain. The 3D structure is considered to have shifted when zero falls outside the 95% confidence interval about the difference between the estimates for a location parameter obtained in the drug and vehicle conditions.

The resampling method employed depended on how the drug sessions were structured. In the cases of rats GBR11-14, each drug session included a complete survey of the mountain. In these cases, the data were resampled by survey (Hernandez et al., 2010; Trujillo-Pisanty et al., 2011). For example, ten drug sessions were run with rat GBR11. One thousand datasets, consisting of ten sessions each, were generated by random resampling with replacement. One such dataset might consist of data from sessions 2,3,3,4,5,5,7,8,10,10, and another might consist of data from sessions 1,2,3,4,4,6,6,7,8,9. To construct surveys for rats GBR2-8, we followed the same procedure employed by Hernandez et al., (2010). Three pools were constructed, consisting of all sweeps of a given type. Surveys were built by drawing one sweep randomly from each of the pools. The number of surveys in each of the resampled datasets was equal to the number of sessions run in the drug condition.

Two different versions of the mountain model were fit to the data. One has 6 parameters (2 location parameters, 2 slope parameters, and 2 scale parameters (maximum and minimum TA) whereas the other includes a seventh parameter that can be interpreted to represent the conditioned value of reward-related stimuli or reward-seeking actions (Hernandez et al., 2010). Each of these models was fit in two different ways. The "location-specific" method entails estimating location-parameter values for each individual survey. This method defends the location-parameter estimates against the bias introduced by within-condition shifts of the mountain. The "all-common" method estimates a single set of location parameters for each dataset, thus minimizing the

number of parameter values estimated.

Prior to resampling, both versions of the mountain model were fit to the data using both the location-specific and all-common methods. The Akaike Information Criterion (AIC) (Akaike, 1974) was then measured, and its value was used to select the best model and fitting method. The subsequent resampling made it possible to refine the parameter estimates and to measure their dispersion.

Inferential statistics and graphs were based on the surfaces defined by the mean parameter estimates and 95% confidence intervals derived from the resampling procedure for the model and fitting method deemed best by the AIC. Graphs were plotted using Origin (OriginLab Corporation, Northhampton, MA).

Histology

The histological procedure was carried out as described above. The electrode tips were located in the LH (Figure 5).

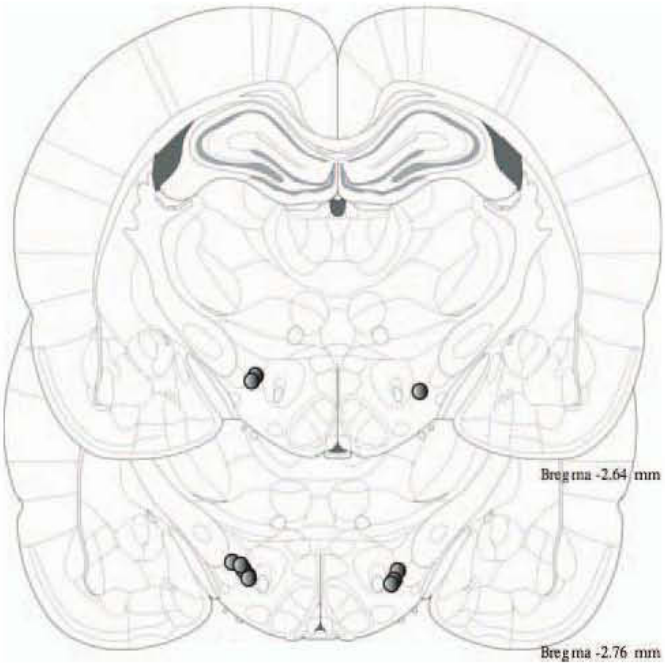

Figure 5: Location of electrode tips in the subjects of the reward-mountain experiment. Each electrode tip fell within the boundaries of the MFB, at the level of the LH as determined with respect to the Paxinos and Watson (2007) atlas.

Results

Microdialysis experiments

The goal of the first experiment was to ascertain whether the changes in extracellular dopamine produced by a single i.p. injection of GBR-12909 (10mg/kg) resemble those produced by the lowest effective dose of continuous, subcutaneously administered cocaine (Hernandez et al., 2010). In addition, we wanted to replicate previous studies that suggest that a single injection of GBR-12909 is sufficient to produce a long lasting and stable increase in extracellular dopamine (Budygin, Kilpatrick, Gainetdinov, & Wightman, 2000; Gagnaire & Micillino, 2006; Rothman et al., 1991), a necessary condition for running the mountain experiment.

As shown in Figure 6a, both a single i.p. injection of GBR-12909 (10 mg/kg, n=6) and continuous subcutaneous infusion of cocaine (1.75 mg/kg/hr, n=5) increased dopamine levels in the NAc shell. In the case of the behavioral results described below, data acquisition began 120 minutes following administration of GBR-12909. In the microdialysis data shown in Figure 6a, dopamine levels had approached asymptote by that time point in response to both drug treatments and remained quite stable for an additional 4 hours. The two drug-administration regimens appear fairly well matched in terms of the asymptotic concentration of dopamine in the dialysate, which were 210% and 190% of baseline for GBR-12909 and cocaine, respectively (means of observations obtained 120-360 minutes following onset of drug treatment).

Figure 6b depicts the time course of changes in dopamine concentration observed during delivery of MFB stimulation in two additional groups of drug-treated subjects (GBR: n=6; cocaine: n=7). In prior behavioural testing, the rats had worked vigorously for identical stimulation trains, indicating that these trains were rewarding. Conditions prior to stimulation onset were the same as those in force when the data in Figure 6a were obtained, and reasonably similar results were observed. Again, the two drug-administration regimens appear fairly well matched in terms of their effects on the asymptotic level of dopamine in the dialysate, which were 246% and 232% of baseline values for GBR and cocaine, respectively (means of observations obtained 60-120

minutes and 120-200 minutes following onset of GBR and cocaine treatment, respectively). After these plateaus in dopamine levels were observed, delivery of MFB stimulation commenced (GBR: light-blue background, cocaine: light-red background). Whereas the MFB stimulation failed to further boost dopamine levels in the GBR-treated rats (blue time course), it markedly increased dopamine concentration in the cocaine-treated rats (red time course), reaching a second plateau at 439% of the baseline values (mean of last 4 observations). A repeated-measures ANOVA was carried out by means of Statistica (Statsoft, Inc., Tulsa, OK) on the dopamine concentrations measured during the time when which BSR was delivered to both groups (220 – 340 minutes following the onset of drug treatment). The across-group difference in dopamine levels meets the criterion for statistical significance ($F_{(1,11)} = 5.85$, $p = 0.03$) as does the interaction between the sample time and drug treatment ($F_{(6,66)} = 2.53$, $p = 0.02$).

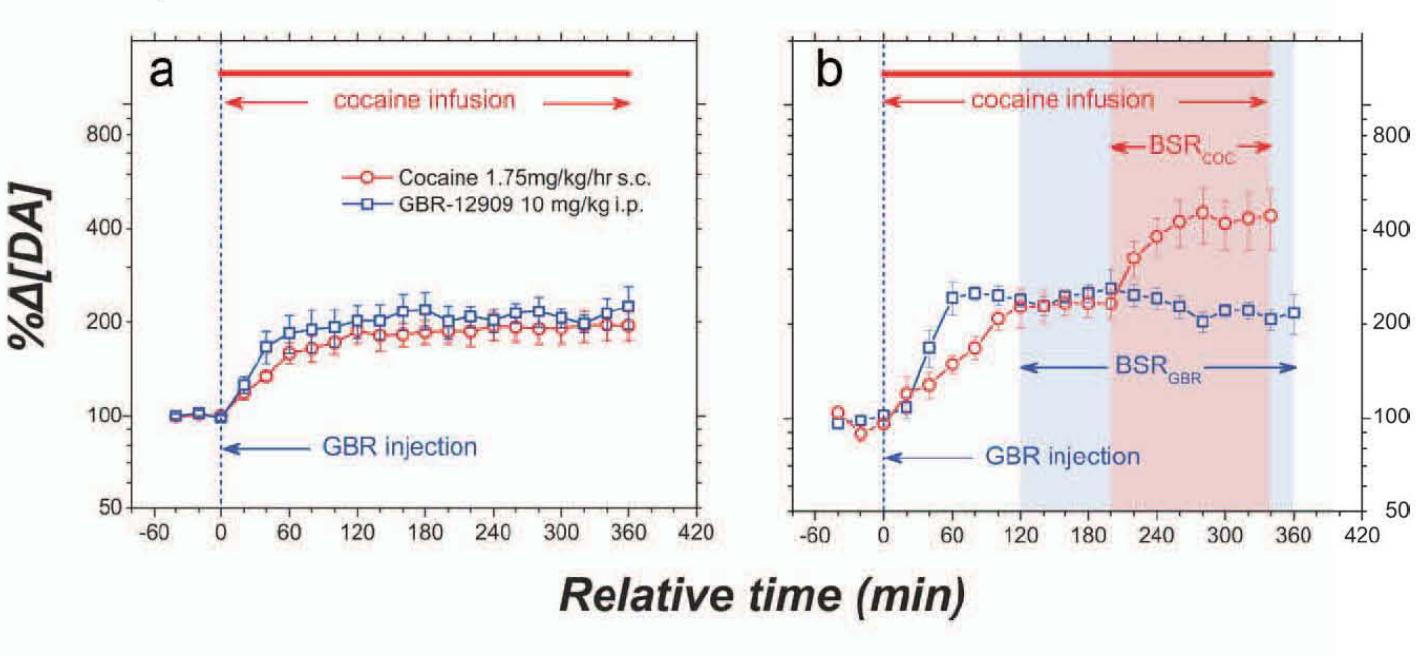

Figure 6: a, Dopamine levels in the NAc shell produced by continuous subcutaneous infusion of cocaine [1.75 mg • kg^{-1} • h^{-1}, the most common drug dosage used in a previous experiment (Hernandez et al., 2010)] and by a single intraperitoneal injection of GBR (10 mg/kg). The plateau levels of dopamine were quite well matched in the two groups of rats: ~200% above baseline level for the GBR-treated rats and ~190% above baseline level for the cocaine-treated rats. b,

Effect of delivering rewarding MFB stimulation to rats treated withGBR(blue) or cocaine (red). Before the onset of the electrical stimulation, the two drug treatments produced similar increases in NAc dopamine levels. In contrast, the stimulation further boosted dopamine levels in the cocaine-treated rats but not in the GBR-treated rats.

Behavioral experiment

Surface fitting

Table 1 shows the AIC values for the fits to 6-parameter and 7-parameter models carried out using the "all-common" or "location-specific" approaches. In the vehicle condition, the 7-parameter model proved best in 6/10 cases, despite the penalty imposed by the AIC for additional parameters. The location-specific method, which better defends the estimates of the slope parameters against the bias introduced by within-condition shifts, proved superior in 8/10 cases. In the drug condition, the 7-parameter model provided the best fit in only 3/10 cases, and the location-specific method fared best in 9/10 cases. The adjusted R^2 for the best-fitting surfaces for the vehicle mountain ranged from .954 to .988 and from .930 to .970 for the GBR mountain surface. These values suggest that the 3D surfaces fit the time-allocation data well.

Two-dimensional representation

Figure 7 shows two-dimensional (2D) projections of the fitted surface and the behavioral data for rat 12. We show these 2D projections to facilitate comparison with the results of prior studies employing curve-shift or progressive-ratio scaling. However, previous papers describing the mountain model and its application (Arvanitogiannis & Shizgal, 2008; Hernandez et al., 2010) demonstrate that a 3D surface must be fit to the data in order to determine how the mountain has been displaced by experimental treatments such as drug administration. This point is made with particular clarity in the movie referenced in the note below. Displacement of the mountain cannot be discerned unambiguously by means of visual inspection of 2D projections (Arvanitogiannis & Shizgal, 2008; Hernandez et al., 2010).

Table 1. Surface-fitting parameters by sampling strategy and model

Rat	Resampling	VEH 6 parameter AIC common	VEH 6 parameter AIC specific	VEH 7 parameter AIC common	VEH 7 parameter AIC specific	VEH R^2 best fit	DRG 6 parameter AIC common	DRG 6 parameter AIC specific	DRG 7 parameter AIC common	DRG 7 parameter AIC specific	DRG R^2 best fit
GBR2	Sweep	−1108	−1259.968*	−1111.165	−1249.491	0.973	−1317.872	−1321.099	−1315.771	−1312.01	0.958
GBR3	Sweep	−1154.156	−1304.628	−1167.8	−1369.9*	0.987	−1191.311	−1224.819	−1199.9	−1230.4*	0.951
GBR4	Sweep	−1015.962	−999.618	−1068.432*	−1043.609	0.954	−1351.774	−1326.227	−1482.425	−1482.458*	0.93
GBR6	Sweep	−1888.927	−1913.297	−1901.265	1930.925*	0.976	−1535.432	−1515.956	−1612.515*	−1582.794	0.956
GBR7	Sweep	−1894.27	−2032.806	−1899.394	−2043.902*	0.988	−1763.8	1793.8*	−1765.6	−1785.2	0.985
GBR8	Sweep	−2046.717	−2109.947*	−1726.9	−1702.1	0.959	−2056.207	−2098.483*	−1741.6	−1819.2	0.952
GBR11	Survey	−1857.709	−1844.276	−1867.3*	−1854	0.965	−1991.445	−2028.68*	−1412.3	−1445.446	0.957
GBR12	Survey	−1887.373	−2011.911	−1919.9342	−2067.14*	0.979	−2073.095	−2356.08*	−2085.089	−2348.925	0.958
GBR13	Survey	−1879.429	−1969.469*	−1878.633	−1939	0.973	−2399.623	−2440.2426*	−2397.873	−2414.279	0.959
GBR14	Survey	−1674.503	−2039.026*	−1674.239	−2031.694	0.973	−2111.744	−2653.042*	−2111.294	−2644.428	0.969
Minimum						0.954					0.93
Maximum						0.988					0.985

Values of the AIC for the six- and seven-parameter models and for both fitting strategies (all common or location specific). Asterisks indicate best (most negative) values. Also shown are goodness-of-fit (adjusted R^2) values, which indicate that the fitted surfaces describe the time-allocation data well. VEH, Vehicle; DRG, drug.

Table 1: Values of the Akaike Information Criterion for the 6- and 7-paramter models and for both fitting strategies ("all common" or "location-specific"). Best (most negative) values are denoted by asterisks. Also shown are goodness-of-fit (adjusted-R^2) values, which indicate that the fitted surfaces describe the time-allocation data well.

To obtain the data shown in Figure 7, the pulse frequency was decreased and/or the price was increased from trial to trial sequentially ("swept"). Panel *a* shows the frequency-sweep curves obtained, at a price of 4 seconds, for the vehicle (red) and GBR (pink) conditions. This panel represents the data in the same manner as in conventional curve-shift studies. The data points obtained in the GBR condition (pink) are displaced to the left of those obtained in the vehicle condition (red), as would be expected on the basis of previous studies (Maldonado-Irizarry, Stellar, & Kelley, 1994; Melnick, Maldonado-Vlaar, Stellar, & Trzcińska, 2001). However, when the price at which the mountain is sectioned is increased, the two sets of data points overlap closely, as shown in Panel *b*. In panel *c*, price-sweep data are shown in lighter blue for the vehicle condition and in darker blue for the GBR condition. GBR produced a rightward displacement of the price-sweep curves. The radial-sweep data from the vehicle (light green), and GBR (dark green) conditions are plotted against the pulse-frequency axis in panel *d* and against the price axis in panel *e*.

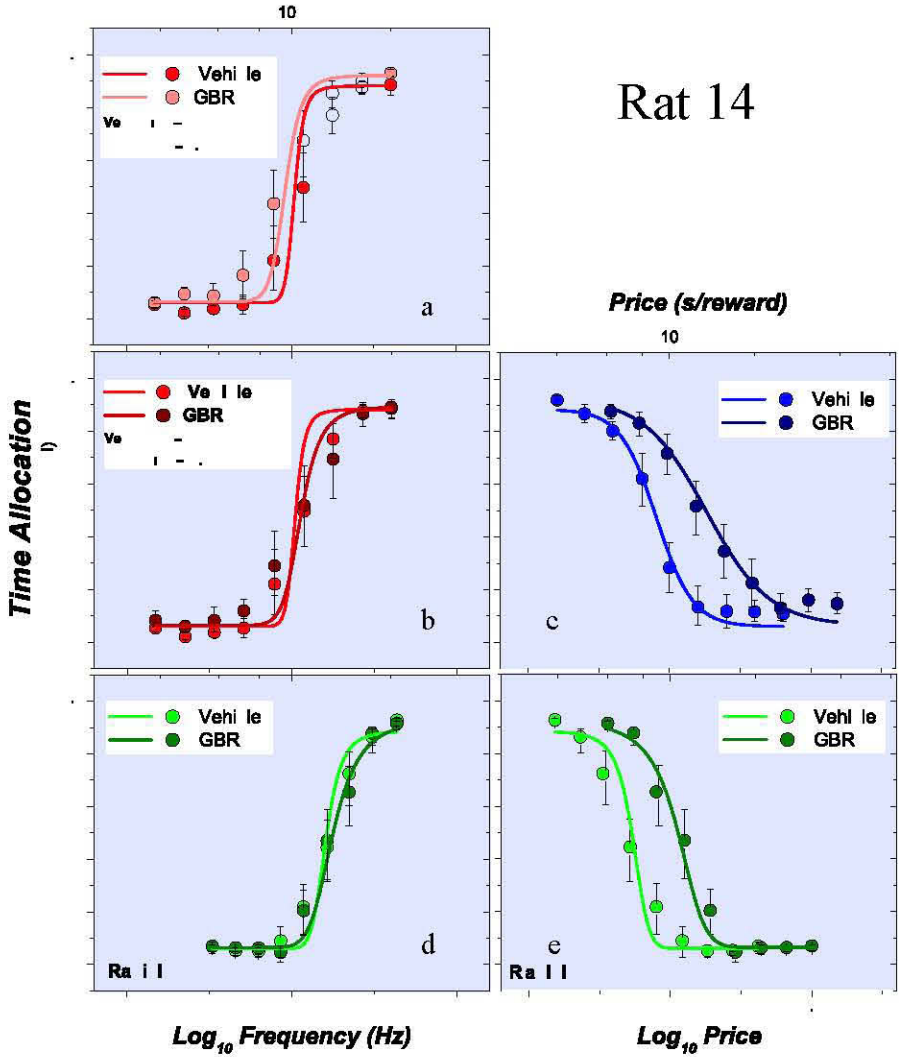

Figure 7: Time-allocation data from rat 12 from the vehicle and GBR conditions. Panel *a* shows the frequency-sweep data obtained at a 4-second price (vehicle: red; GBR-12909: light red). The data for the GBR condition is displaced leftward. When the price is adjusted to offset the displacement of the 3D structure along the price axis, the data points overlap, as shown in panel *b* (vehicle: red; GBR-12909: dark red). Panel *c* shows price-sweep data (vehicle: light blue; GBR-12909: dark blue). The drug produced a rightward displacement. Panels *d,e* show the radial-sweep plotted against the pulse frequency and price axis, respectively (vehicle: light green; GBR-12909: dark green).

Three-dimensional representation

Our 3D analysis of performance for BSR (Arvanitogiannis & Shizgal, 2008; Hernandez et al., 2010) reveals that 2D depictions, such as those in Figure 7, are fundamentally ambiguous with regards to the direction in which a drug treatment has shifted the mountain. At pulse frequencies that produce sub-maximal rewarding effects, the surface of the mountain is oriented diagonally. Thus, displacement of a 2D section, such as the curves in Figure 7, could arise from a shift in the mountain along the depicted x-axis, a shift along the unseen, orthogonal, independent-variable axis, or both. This ambiguity is resolved by plotting the data in a 3D space, as shown in Figure 8, which shows the data from Figure 7 in this new perspective. Mean time allocation is represented by the spherical symbols; the wire-mesh depicts the surface obtained by fitting the reward mountain model to the vehicle data (panel *a*) and to the GBR data (panel *b*). Figure 9 shows the same data replotted as contour graphs constructed by plotting on a plane the cross-sections obtained by horizontally slicing the fitted surface at fixed intervals representing 10% changes in time allocation. To facilitate comparison with the contour graph and data from the GBR condition (panel *b*), the contour graph and data from the vehicle condition are shown twice (panels *a* & *a'*). The pulse frequencies and prices sampled along the pulse-frequency, price, and radial sweeps are indicated by the circular symbols. The price sweep constrains the position of the mountain along the price axis whereas the frequency sweep constrains the position along the pulse-frequency axis. The radial sweep determines the curvature of the contour lines while providing additional positioning information, which is most precise when the radial sweep passes through the point defined by the two location parameters (F_{hm}, P_e).

The superimposed solid lines in Figure 9 represent the location parameters (F_{hm}, red; P_e, blue) whereas the dashed lines represent the 95% confidence interval around each of the parameter estimates. As indicated by the blue arrow, GBR-12909 moved the structure rightward along the price axis by 0.125 $\log_{10}$ units (thus, increasing P_e to 1.33 times the value obtained in the vehicle condition) but moved it downward along the pulse-frequency axis by only 0.009 $\log_{10}$ units (to .98 of the value obtained in the vehicle

condition). The bar graph summarizes the displacement of the mountain along the two axes, and the error bars represent 95% confidence intervals surrounding the change in the parameter estimates. The 95% confidence interval surrounding the change in F_{hm} (red) includes zero, and thus the tiny displacement along the pulse-frequency axis fails to meet the criterion for statistical reliability. In contrast, zero falls well outside the 95% confidence interval surrounding the change in P_e, and thus, the much larger displacement of the mountain along the price axis easily meets the criterion for statistical reliability.

The fact that the radial sweeps in the vehicle and drug conditions pass slightly to either side of the intersection of the location parameters (panels *a*, *a'* and *b* of Figure 9) makes the 2D depictions of these sweeps (panels *e* and *f* in Figure 7) ambiguous with respect to the direction in which the mountain has shifted. This ambiguity is resolved by the contour-graph representation (Figure 9), which shows clearly that mountain was shifted rightward along the price axis by GBR-12909.

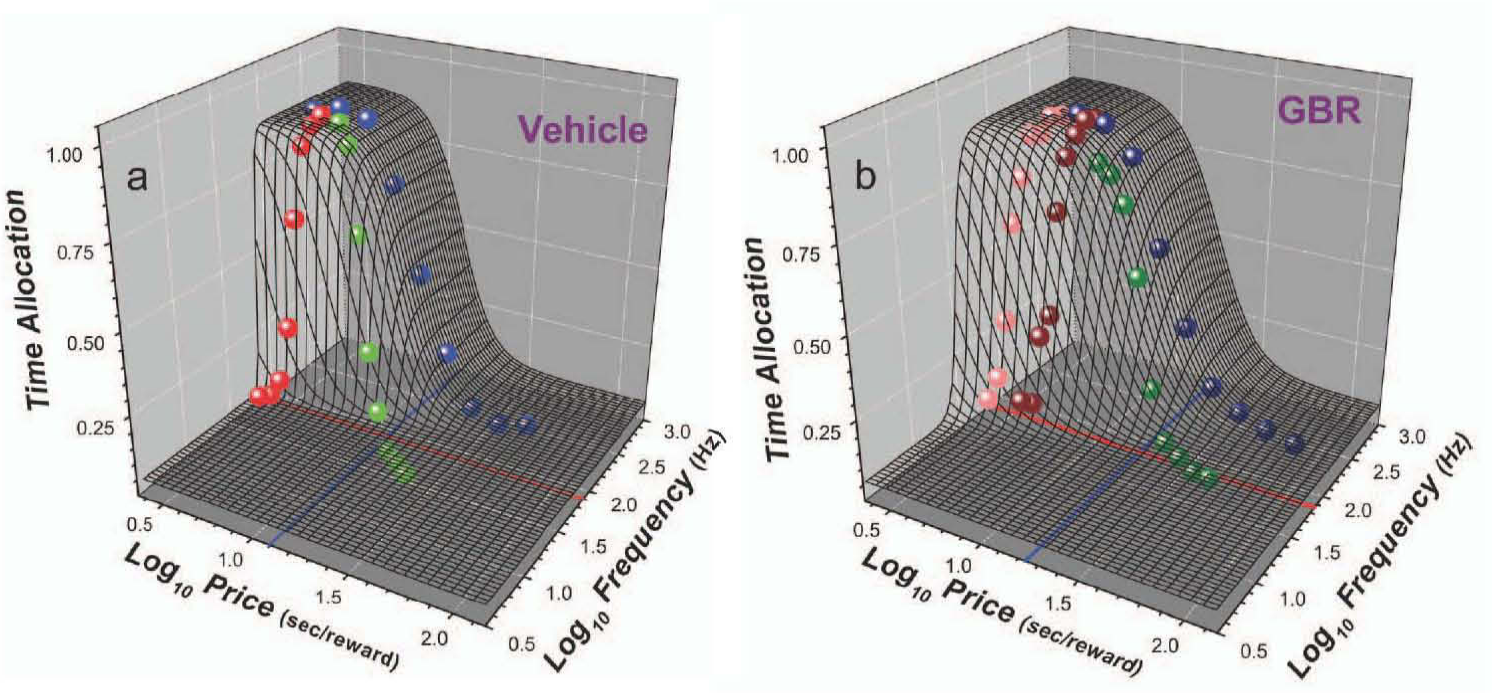

Figure 8: Fitted surfaces for rat 12. Panel *a* and *b* show the behavioral data from the vehicle and GBR-12909 conditions, respectively, along with the corresponding fitted wire-mesh surfaces. In panel *a*, the red, green and blue dots represent mean time-allocation values from the vehicle condition at each point along the frequency, radial and price sweeps, respectively. Along with the fitted wire-mesh surface, panel *b* shows mean time-allocation values for the low-price frequency sweep (light red), the high-price frequency sweep (dark red), the price sweep (blue), and the radial sweep (green). The red and blue lines on the floor of the figures represent the location parameters F_{hm} and P_e, respectively.

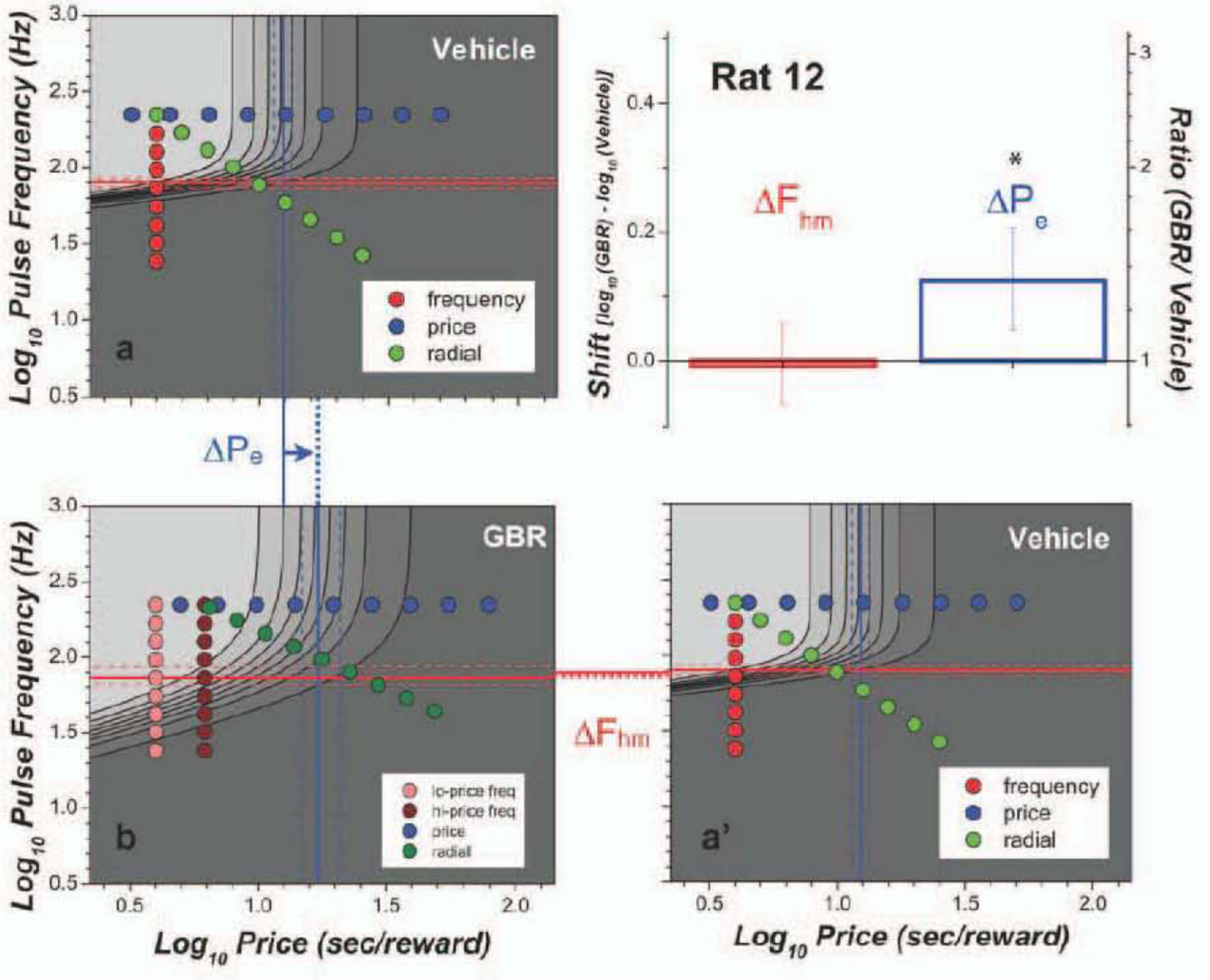

Figure 9: Contour graphs and bar graphs showing the drug-induced displacement of the mountain for rat 12. The contour graphs were constructed by projecting onto a plane the cross-sections obtained after horizontally slicing the fitted surfaces (Figure 8) at fixed intervals representing 10% changes in time allocation. Note that the contour graph for the vehicle condition is plotted twice (panel a and a'), so that the shifts along the two axes are readily visualized. The color-coded circles represent the parameter values tested along the frequency, price, and radial sweeps. The superimposed solid red and blue lines represent the position parameters, F_{hm} and P_e, respectively. These values determine the position of the mountain within the parameter space. The dashed lines denote the 95% confidence interval around each of the location-parameter estimates. As represented by the blue arrow, the structure was moved significantly rightward along the price axis by GBR-12909 (by 0.125 $\log_{10}$ units) but was hardly moved

at all along the pulse-frequency axis (by -0.009 $\log_{10}$ units). The bar graph summarizes the displacement of the mountain. Each bar represents the difference between the location-parameter values obtained in the drug and vehicle conditions. The confidence interval about the P_e estimate does not overlap zero and is thus considered to be statistically reliable. In contrast, zero falls near the middle of the confidence interval about the F_{hm} estimate, reflecting the failure of the drug treatment to displace the mountain along the pulse-frequency axis.

Figure 10 and Table 2 summarize the movement of the mountain along the pulse-frequency and price axes for all the subjects tested. In 7 of the 10 experimental subjects the displacement of the mountain along the price axis is statistically reliable, and in an eighth case, the shift falls just short of the criterion. The displacements vary across subjects between -0.013 and 0.367 $\log_{10}$ units, and the average displacement is 0.139 $\log_{10}$ units (SEM= 0.034). This means that on average the price at which the rats allocate half of their time in pursuit of a maximally intense reward strength was 1.38 times higher following administration of GBR-12909 (10mg/kg i.p.) than following administration of the vehicle.

The displacement of the mountain along the pulse-frequency axis varies across subjects from -0.041 and 0.23 $\log_{10}$ units; the average displacement is 0.021 $\log_{10}$ units (SEM=0.025). This means that on average the frequency that produced a half-maximal reward intensity was merely 1.05 times higher under the influence of GBR than in the vehicle condition. As shown in Figure 10, none of the displacements along the pulse-frequency axis meet the criterion for statistical reliability.

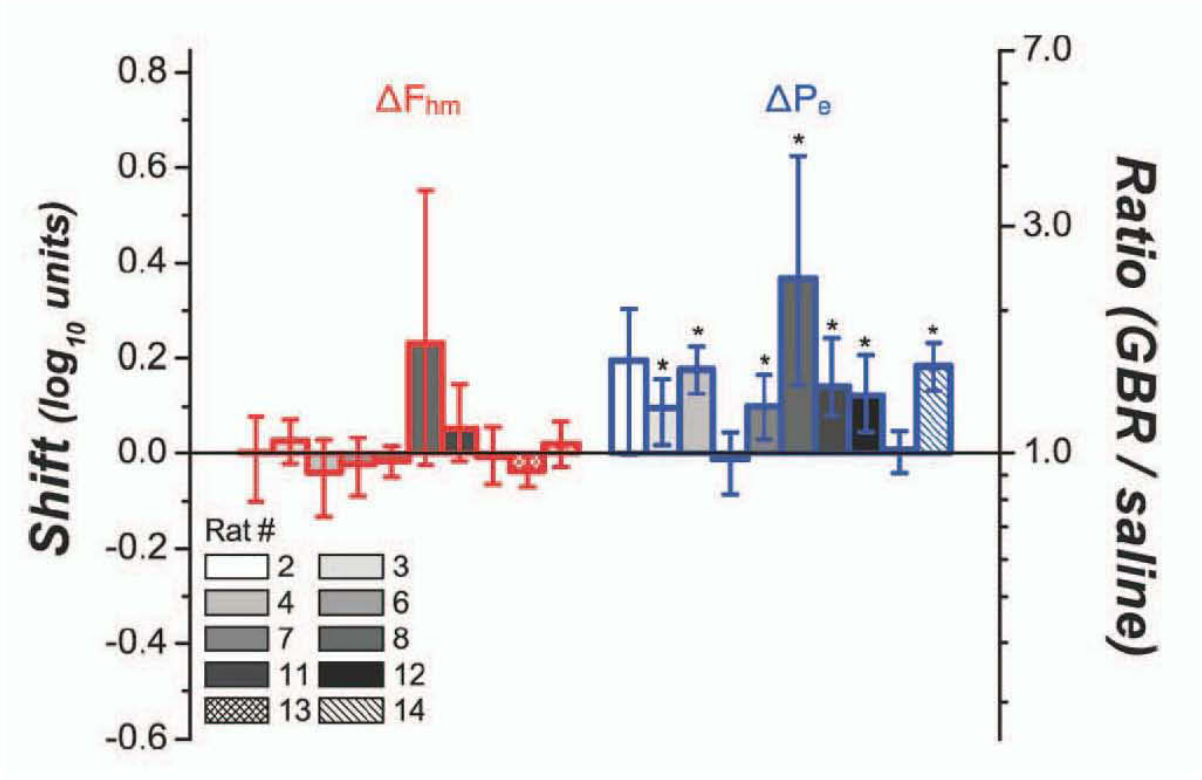

Figure 10: Drug-induced change in location-parameter estimates for all subjects. In 7 out of the 10 subjects, GBR-12909 shifted the mountain reliably along the price axis. The average drug-induced displacement of the reward mountain along the price axis was 0.139 $\log_{10}$ units (SEM= 0.03). This means that on average, the price at which the rats allocate half of their time to pursuit of a maximally intense reward was 1.4 times higher when they were injected with 10mg/kg i.p. of GBR-12909 than when they were injected with vehicle. In contrast, GBR-12909 shifted the reward mountain by only 0.021 $\log_{10}$ units (SEM=0.025) along the pulse-frequency axis. This means that on average, the pulse frequency that produced half-maximal reward intensity was merely 1.05 times higher when the subjects were tested under the influence of GBR than when they were injected with vehicle. None of the displacements along the pulse-frequency axis were statistically reliable.

Table 2. Changes in the location-parameter estimates produced by administration of GBR

Rat	F_{hm} CI $^-$	F_{hm} shift	F_{hm} CI $^+$	P_e CI $^-$	P_e shift	P_e CI $^+$
GBR2	−0.100	0.002	0.079	−0.003	0.195	0.303
GBR3	−0.023	0.027	0.073	0.018	0.098*	0.159
GBR4	−0.134	−0.041	0.029	0.128	0.179*	0.224
GBR6	−0.089	−0.023	0.034	−0.086	−0.013	0.047
GBR7	−0.050	−0.017	0.016	0.030	0.101*	0.168
GBR8	−0.025	0.230	0.553	0.146	0.367*	0.624
GBR11	−0.017	0.055	0.148	0.081	0.144*	0.241
GBR12	−0.065	−0.009	0.058	0.048	0.125*	0.207
GBR13	−0.075	−0.037	0.005	−0.042	0.009	0.050
GBR14	−0.030	0.021	0.070	0.134	0.184*	0.231
Minimum	−0.134	−0.041	0.005	−0.086	−0.013	0.047
Mean	−0.061	0.021	0.106	0.045	0.139	0.225
Maximum	−0.017	0.230	0.553	0.146	0.367	0.624
SEM		0.025			0.034	

CI, Confidence interval.

Table 2: Changes in the location-parameter estimates produced by administration of GBR-12909. The values in this table are shown graphically in Figure 1.9. Asterisks denote shifts that meet the statistical criterion. In these cases, zero falls outside the 95% confidence interval surrounding the difference between the location-parameter estimates obtained in the drug and vehicle conditions.

Discussion

ICSS can be altered by drug action at different stages of the underlying neural circuitry (Arvanitogiannis & Shizgal, 2008; Gallistel, 1978; Gallistel, Shizgal, & Yeomans, 1981; Hernandez et al., 2010). The first event is a volley of action potentials in the directly-stimulated neurons, the effects of which are integrated spatially and temporally (Gallistel, 1978; Gallistel et al., 1981; Simmons & Gallistel, 1994; Sonnenschein et al., 2003) to yield a neural signal representing reward intensity. The drug-induced

enhancement of ICSS by psychomotor stimulants was attributed initially to action on these early stages of the circuitry. For example, Wise (1980) proposed that drugs of abuse lower the threshold of the circuitry to exogenous excitation (presumably at the integration stage) or reduce the input required from the electrode due to pharmacological activation of the substrate. We refer to such effects as changes in the *sensitivity* of reward substrate, the variable that determines the strength of the electrical input required to drive the rewarding effect to a given proportion of its maximal value (Hernandez et al., 2010). The function that maps the strength (e.g., pulse frequency) of the stimulation into the intensity of the rewarding effect is called the *reward-growth function* (Leon & Gallistel, 1992). Changes in sensitivity displace this function along the strength axis just as changes in the affinity of a drug for a receptor displace the concentration-effect curve along the concentration axis.

Arvanitogiannis and Shizgal (2008) and Hernandez et al. (2010) demonstrated that two-dimensional measurement methods, such as the curve-shift or progressive-ratio methods, cannot distinguish changes in sensitivity from changes in a set of variables that includes reward probability, subjective effort cost, the value of alternate activities such as grooming, resting, and exploring, and reward-system *gain*, the variable that sets the vertical scale of the reward-growth function.

The reward-mountain method entails measurement of ICSS performance as a function of both stimulation strength (pulse frequency) and opportunity cost ("price"). Changes in sensitivity shift the mountain along the strength axis whereas changes in gain, reward probability, subject effort costs, or the value of alternate activities shift the mountain along the price axis. Changes in sensitivity are due to actions prior to the output of the reward-growth function whereas changes in gain, probability, subjective effort costs, and the value of alternate activities are due to actions downstream from this point in the reward circuitry. Manipulations that act prior to the output of the reward-growth function include changes in current, which alter the number of directly activated neurons, and changes in the train duration, which can alter the pulse frequency required to drive the output of the integrator to a particular level. Both manipulations shift the mountain along the pulse-frequency (strength) axis (Arvanitogiannis & Shizgal, 2008). Probability

discounting acts downstream from the output of the reward-growth function and shifts the mountain along the price axis (Breton et al., 2009).

In contrast with the explanation advanced in early studies of the effects of cocaine on ICSS (Crow, 1970; Esposito et al., 1978), Hernandez et al. (2010) showed that the principal effect of this drug is to shift the mountain along the price axis. This finding narrows down the stages of processing at which cocaine could be producing its performance-enhancing action but leaves open multiple explanations at the pharmacological level because cocaine blocks the norepinephrine transporter (NET) and serotonin transporter (SERT) as well as the DAT (Iversen, 2000).

In contrast to cocaine, GBR-12909 produces a highly-specific blockade of the DAT (Andersen, 1989). We show here that like cocaine, GBR-12909 shifts the reward mountain rightward along the price axis. Thus, the present findings implicate dopamine in the potentiation of performance for BSR by means of one or more actions at or beyond the output of the reward-growth function. These actions could include boosting reward-system gain, reducing subjective effort costs, and reducing the value of alternate activities.

Figure 11 shows that although 10 mg/kg of GBR-12909 (i.p.) displaced the reward mountain in the same direction as in the study by Hernandez et al. (2010), the magnitude of the shifts (mean = 0.14 $\log_{10}$ units) was substantially smaller than in response to continuous sub-cutaneous infusion of cocaine (mean = 0.38 $\log_{10}$ units). Whereas the shifts produced by cocaine were statistically reliable in all 7 rats tested in the study by Hernandez et al., the shifts produced by GBR-12909 met the statistical criterion in only 7/10 rats. The microdialysis data suggest that the similarities and differences in the behavioral effects of the two drugs reflect similarities and differences between their effects on monoaminergic neurons.

As shown in Figure 6a, 10 mg/kg of GBR-12909 (i.p.) produced an increase in dopamine levels in the NAc shell similar to that observed in response to continuous sub-cutaneous infusion of cocaine (1.75 mg/kg/h). In contrast, delivery of rewarding MFB

stimulation interacted differently with the two drugs. In the cocaine-treated rats, MFB stimulation produced a further boost in dopamine concentration; in the GBR-treated rats, dopamine concentration failed to rise further upon delivery of the stimulation (Figure 6b). This difference could well account for the larger displacements of the mountain along the price axis produced by cocaine.

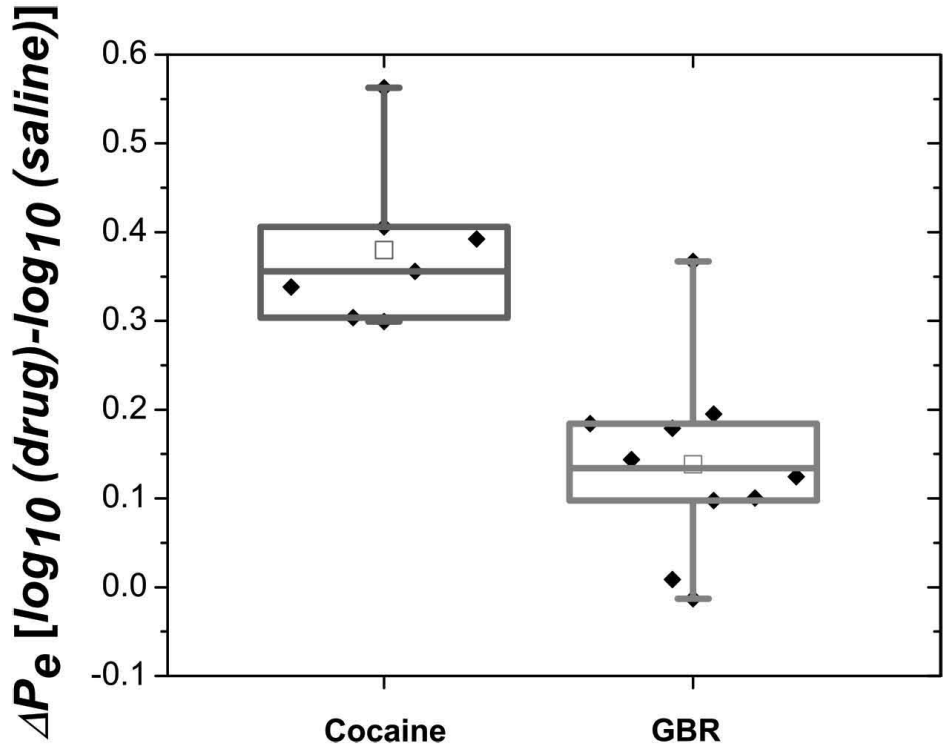

Figure 11: Box plot comparing displacements along the price axis produced by cocaine (Hernandez et al., 2010) and GBR-12909 (present study) under drug-administration regimens that produce similar elevations in nucleus accumbens dopamine levels in unstimulated rats (Figure 6a). The effect of cocaine is substantially greater than the effect of the matched dose of GBR-12909. Each grey diamond represents the drug-induced change in P_e for a given subject. Whiskers represent maxima and minima whereas the upper and lower borders of the boxes denote the 25th and 75th percentiles. The means are represented by the small squares and the medians by the bold horizontal lines bisecting the boxes.

Cocaine-induced blockade of the NET could have contributed to the higher dopamine levels and larger price shifts observed in response to cocaine than to GBR-12909 by potentiating the excitation of the VTA dopamine neurons by NE neurons in the locus coeruleus (Grenhoff, Nisell, Ferré, Aston-Jones, & Svensson, 1993). The NE neurons, in turn, could have been excited by input from hypothalamic orexin neurons (Bonnavion & de Lecea, 2010; Henny, Brischoux, Mainville, Stroh, & Jones, 2010; Sutcliffe & de Lecea, 2002) activated by the MFB stimulation.

Compounds acting at 5-HT_{1A} receptors have been shown to yield effects on ICSS opposite to those produced by compounds acting at 5-HT_{1B} and 5-HT_{2C} receptors (Hayes & Greenshaw, 2011). Such opposing effects are consistent with a report that the effectiveness of rewarding MFB stimulation was not changed by moderate doses of the specific SERT blocker, fluoxetine (Harrison & Markou, 2001). Thus, it is not clear what net effect, if any, would be contributed by blockade of the SERT during the regimen of cocaine administration employed here.

The effects on manipulating dopamine neurotransmission on operant performance for reward have been attributed to changes in reward intensity (Crow, 1970; Esposito et al., 1978; Wise, 1980). Rival accounts are couched in terms of changes in the proclivity to invest effort in pursuit of reward (Salamone, 2002; Salamone et al., 2005) or in subjective vigor costs (Niv et al., 2006). Hernandez et al. (2010) have argued that although the form in which Wise originally phrased the reward-intensity argument cannot explain the observed shifts along the price axis, his argument can be adapted to account for these effects by substituting changes in gain for changes in sensitivity. To distinguish this re-formulation of Wise's argument from the effort-based accounts, it will be necessary to adapt the mountain method so as to estimate the function mapping the work required to obtain a reward into its subjective effort costs (Hernandez et al., 2010).

Rats (Witten et al., 2011) and mice (Adamantidis et al., 2011; K. M. Kim et al., 2012) will perform operant responses for direct optical activation of VTA dopamine neurons. How

can these results be squared with the demonstrations that both cocaine and GBR-12909 shift the reward mountain along the price axis, an effect attributed to action beyond the output of the directly stimulated neurons?

The fine, unmyelinated axons of dopamine neurons have very high thresholds for activation by short-duration pulses of extracellular current (J. S. Yeomans et al., 1988) and are unlikely to constitute a major part of the directly activated substrate for MFB self-stimulation (Bielajew & Shizgal, 1986; Shizgal, 1997). Multiple glutamatergic (Geisler et al., 2007) and cholinergic pathways (Oakman, Faris, Kerr, Cozzari, & Hartman, 1995) are positioned to relay activation of non-dopaminergic MFB fibers to dopamine somata in the VTA, and there is considerable empirical evidence that these inputs are driven by rewarding MFB stimulation (Rada, Mark, Yeomans, & Hoebel, 2000; Sombers, Beyene, Carelli, & Wightman, 2009; You, Chen, & Wise, 2001). By analogy to an hypothesis advanced by Moisan & Rompré (Moisan & Rompré, 1998) Hernandez et al. (Hernandez et al., 2010) proposed that dopaminergic somata and/or their afferents may integrate input from directly activated, non-dopaminergic MFB fibers. On this view, reward intensity is represented by the firing of the dopamine neurons, whether induced directly by optogenetic means or indirectly by electrical activation of afferent pathways. DAT blockade would rescale upward the synaptic output of the dopamine neurons, increasing reward-system gain and shifting the mountain along the price axis. This hypothesis could be tested by specific optogenetic activation or silencing of dopaminergic neurons or their afferents. Optogenetic activation and silencing could also test the hypothesis (Lin, de Vaca, Carr, & Stone, 2007) that excitatory input to VTA dopamine neurons from locus coeruleus NE neurons makes a synergistic contribution to the rewarding effect of MFB stimulation. Thus, the combination of powerful new methods for altering signal flow in specific neural populations with the reward-mountain method should provide new insights about the neural circuitry underlying reward seeking.

Note: A movie that supplements this article can be found at http://spectrum.library.concordia.ca/974074/. This material has not been peer reviewed.

CHAPTER 2

A new view of the effect of dopamine receptor antagonism on operant performance for rewarding brain stimulation in the rat

Ivan Trujillo-Pisanty, Kent Conover & Peter Shizgal

Trujillo-Pisanty, I., Conover, K., & Shizgal, P. (2013). A new view of the effect of dopamine receptor antagonism on operant performance for rewarding brain stimulation in the rat. *Psychopharmacology*, *231*(7), 1351–1364. http://doi.org/10.1007/s00213-013-3328-x

Abstract

Rationale. Previous studies of neuroleptic challenges to intracranial self-stimulation (ICSS) employed two-dimensional (2D) measurements (curve shifts). Results so obtained are ambiguous with regard to the stage of neural processing at which the drug produces its performance-altering effect. We substituted a three-dimensional (3D) method that measures reward-seeking as a function of both the strength and cost of reward. This method reveals whether changes in reward seeking are due to drug action prior to the output of the circuitry that performs spatiotemporal integration of the stimulation-induced neural activity.

Objectives. The aim of this study was to obtain new information about the stage of neural processing at which Pimozide acts to alter pursuit of brain stimulation reward (BSR).

Methods. Following treatment with Pimozide (0.1 mg/kg) or its vehicle, the proportion of trial time allocated to working for BSR was measured as a function of pulse frequency and opportunity cost. A surface defined by Shizgal's reward-mountain model was fitted to the drug and vehicle data.

Results. Pimozide lowered the cost required to decrease performance for a maximal BSR to half its maximal level but did not alter the pulse-frequency required to produce a reward of half-maximal intensity.

Conclusions. Like indirect dopamine agonists, Pimozide does not alter the sensitivity of brain reward circuity but changes reward-system gain, subjective effort costs, and/or the value of activities that compete with ICSS. The 3D method is more sensitive and informative than the 2D methods employed previously.

Introduction

Animals will work vigorously at operant conditioning tasks to receive electrical stimulation of the medial forebrain bundle (MFB) (Olds & Milner, 1954). This behavior, known as intracranial self stimulation (ICSS), has been used extensively to study the pharmacological basis of reward. In this paper, we extend prior work on the role of dopamine (DA) in ICSS by applying a new measurement method (Arvanitogiannis & Shizgal, 2008; Breton et al., 2013; Hernandez et al., 2010). The results reported here complement recent findings that cast the role of DA neurons in a new light (Hernandez et al., 2010; 2012).

The most widely adopted method for measuring ICSS, the *curve-shift* method, (Edmonds & Gallistel, 1974; 1977; Miliaressis, Rompre, Laviolette, Philippe, & Coulombe, 1986b), employs electrical stimuli of different strength (e.g., pulse-frequency or current) as the independent variable and a measure of response vigor (e.g., response rate) as the dependent variable. The stimulation strength that produces a criterial level of performance is determined under control and experimental conditions. Commonly, half-maximal performance serves as the behavioral criterion. The pulse frequency required to meet this criterion is designated F_{m50}; this value specifies the position of the mid-point of the response rate-versus-pulse-frequency curve along the pulse-frequency axis. A decrease in F_{m50} corresponds to a leftward shift of the curve and is interpreted as facilitation of the rewarding effect, whereas an increase in F_{m50} corresponds to a rightward shift and is interpreted as attenuation of the rewarding effect. Dopaminergic agonists decrease F_{m50}, whereas dopaminergic antagonists increase F_{m50} (Wise, 1996). These findings constitute the principal foundation for a highly influential hypothesis: that the rewarding effects of electrical brain stimulation is encoded in the firing of dopamine (DA)-containing neurons.

Operant performance depends not only on reward strength but also on effort and opportunity costs (Breton et al., 2009; Hernandez et al., 2010; Niv et al., 2006), as well as on the value of activities, such as grooming, resting, and exploring, that compete with pursuit of the reward offered by the experimenter (Herrnstein, 1970; Heyman & Beer, 1987; Petry & Heyman, 1997). Taking these variables into account challenges the

assumption that changes in F_{m50} necessarily reflect facilitation or attenuation of the rewarding effect and offers alternate ways to interpret the effects of drugs that alter DA neurotransmission (Hernandez et al., 2010; 2012; Trujillo-Pisanty et al., 2011) .

Figure 12 integrates the processing of the stimulation-induced volley of action potentials that gives rise to brain stimulation reward (BSR) with task and environmental variables. The intensity of the rewarding effect is determined by spatial and temporal summation in a neural circuit or population that is activated trans-synaptically by the directly activated neurons. This circuit/population has been dubbed the *integrator*. The behavior of the integrator is well described by a *counter model* (Gallistel et al., 1981; Gallistel & Leon, 1991; Gallistel, Leon, Waraczynski, & Hanau, 1991; Simmons & Gallistel, 1994) that expresses the rewarding effect as a function of the aggregate rate of firing induced by the pulse train in the directly activated neurons. The rewarding effect grows non-linearly as a function of the induced rate of firing (Gallistel & Leon, 1991; Leon & Gallistel, 1992; Simmons & Gallistel, 1994) and the train duration (Sonnenschein et al., 2003). Later stages of neural processing compute a payoff by combining the peak reward intensity produced by the stimulation train with information about task variables, such as effort and opportunity costs (Arvanitogiannis & Shizgal, 2008; Hernandez et al., 2010; Shizgal, 2012). In concert with environmental variables, such as alternate sources of reward, the payoff from BSR determines the proclivity of the animal to invest time and effort to obtain electrical stimulation.

The depiction in Figure 12 reveals an ambiguity inherent in the curve-shift method: F_{m50} values can be altered similarly by very different manipulations acting at different points in the neural circuitry that processes information about the reward, the operant task, and the test environment (Arvanitogiannis & Shizgal, 2008; Breton et al., 2013; Hernandez et al., 2010). For example, the effect of changing the current, a manipulation that alters the number of neurons providing *input* to the integrator, can be indistinguishable from the effect of manipulations that act beyond the *output* of the integrator, such as altering the opportunity cost of the reward (the time required to earn a pulse train) or the value of competing activities (Video 1). This ambiguity limits the inferences about the reward

substrate that can be drawn from experiments in which ICSS is challenged by interventions such as drug administration, lesions, and alterations in physiological state.

By manipulating two independent variables rather than one, information lost in the curve-shift method can be retrieved, and the locus of action of an experimental manipulation can be resolved with respect to the output of the integrator. Instead of tracking shifts of a two-dimensional (2D) curve, shifts in the position of a three-dimensional (3D) surface are measured. Rats are trained to hold down a lever in order to receive rewarding stimulation. Both the pulse frequency and the cumulative time required to obtain a reward (the opportunity cost or *price* of the stimulation train) are varied across trials. The proportion of trial time invested in harvesting the reward (*time allocation*: TA) serves as the dependent variable. The resulting 3D representation, termed a *reward mountain*, expresses TA as a function of pulse frequency and price (Video 1, http://spectrum.library.concordia.ca/978205/5/ITP_etal_2013.mp4).

In the 2D curve-shift method, F_{m50} locates rate-frequency curves along the axis representing the single independent variable. In the 3D method, a pair of location parameters play an analogous role by locating the TA surface in the space defined by the two independent variables. The stimulation frequency that produces half-maximal reward (F_{hm}) determines the position of the surface along the pulse-frequency axis, whereas the price that produces half maximal TA for a maximal reward (P_e) determines the position of the surface along the price axis. These location parameters reflect different stages of neural processing. Manipulations acting prior to the output of the integrator (e.g., changes in stimulation current or train duration) shift the 3D structure along the pulse-frequency axis, thus altering F_{hm}. Changes at or downstream from the output of integrator displace the three-dimensional structure along the price axis, thus altering P_e (Figure 12, Video 1) (Arvanitogiannis & Shizgal, 2008; Breton et al., 2013; Hernandez et al., 2010).

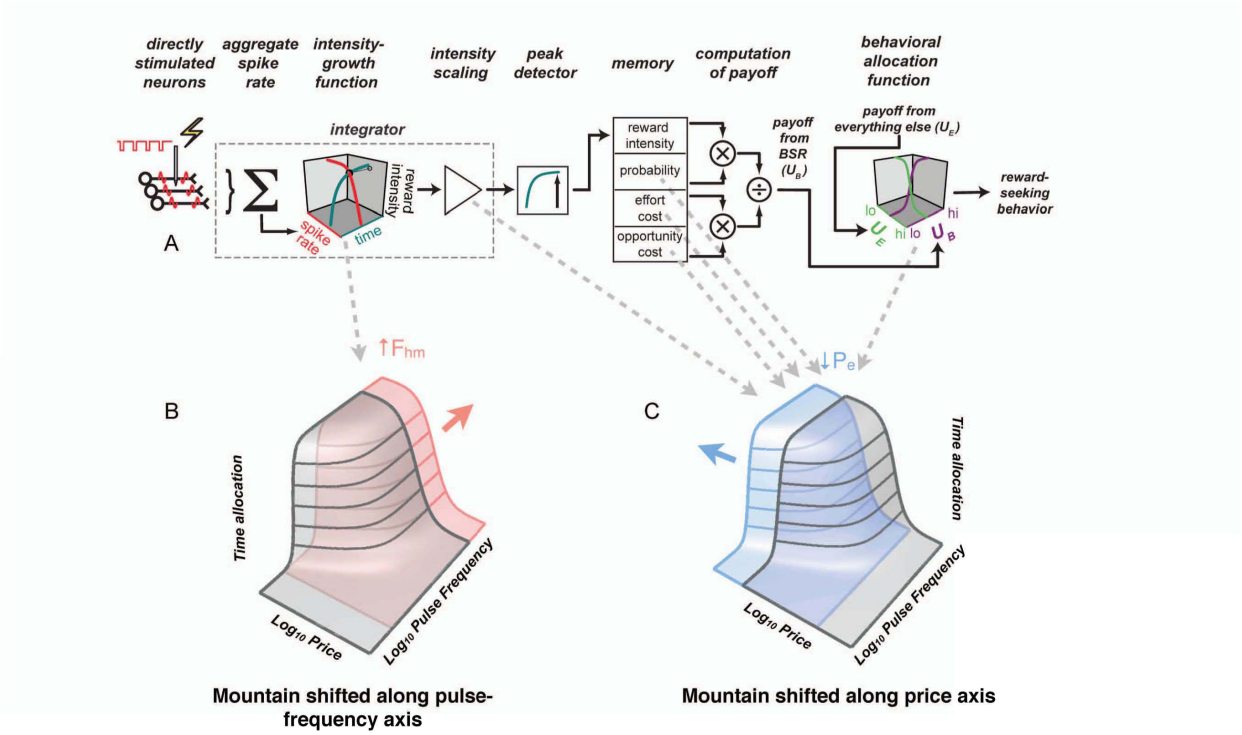

D

$$I = I_{\max} \times \frac{f^{g}}{f^{g} + f_{hm}{}^{g}}$$

$$U_B = \frac{I \times p}{(1+\xi) \times P};\ U_E = \frac{I_{\max} \times p}{(1+\xi) \times P_E}$$

$$TA = \frac{U_B{}^{a}}{U_B{}^{a} + U_E{}^{a}}$$

$$\therefore TA = \frac{\left(\frac{f^{g}}{f^{g} + f_{hm}{}^{g}}\right)^{a}}{\left(\frac{f^{g}}{f^{g} + f_{hm}{}^{g}}\right)^{a} + \left(\frac{P}{P_E}\right)^{a}}$$

a = price-sensitivity constant

f = stimulation frequency

f_{hm} = frequency producing a half-maximal reward

g = reward-growth constant

I = intensity of BSR; I_{max} = maximum intensity of BSR

ξ = perceived exertion;

p = reward probability; P = price of a stimulation train

P_E = price at which payoff from I_{max} = payoff from everything else (U_E)

TA = time allocation;

U_B = payoff from BSR; U_E = payoff from everything else

Figure 12. Graphical representation and summary of the mountain model. (A) In the initial stages of reward processing, the action potentials produced by direct electrical activation of MFB axons are integrated temporally and spatially by a neural circuit that transforms the effect of the stimulation-induce volley into a signal representing subjective reward intensity. The peak reward intensity by the stimulation is combined, in scalar fashion, with subjective estimates of the probability and cost of reward so as to compute the payoff from procurement of a stimulation train. The rat's allocation of time to pursuit of the rewarding stimulation depends on the computed payoff in relation to the value of competing activities (e.g., grooming, resting or exploring). (B) Time allocation is represented as a function of the strength (pulse frequency) and opportunity cost ("price") of the stimulation. Interventions acting prior to the output of the integrator shift the three dimensional (3D) structure along the

pulse-frequency axis. Such shifts are measured as changes in the parameter of the reward-mountain model, F_{hm}, that locates the 3D structure along the pulse-frequency axis. (C) Interventions acting at or beyond the output of the integrator shift the 3D structure along the price axis, as measured by a change in the parameter of the reward-mountain model, P_e, that locates the structure along this axis. (D) Formal statement of the reward-mountain model. Modified from Trujillo-Pisanty *et al.* (2011).

The procedure based on the 3D reward-mountain model has been used successfully to disambiguate the level of neural processing at which DA agents act to alter ICSS of the MFB. The work shows that enhancement of DA signaling consistently increases the value of P_e but rarely affects F_{hm} (Hernandez et al., 2010; 2012). Based on the 2D curve-shift analysis, the effects of DA agents have been likened to those produced by changing the current (Edmonds & Gallistel, 1977; Miliaressis, Rompre, Laviolette, Philippe, & Coulombe, 1986b), a manipulation that acts upstream from the integrator. In contrast, the 3D analysis positions the locus of the drug effect at or beyond the output of the integrator, a stage at which multiple variables, including subjective effort costs, act to alter reward seeking (Figure 12; Arvanitogiannis & Shizgal, 2008; Breton et al., 2013; Hernandez et al., 2010).

In the present study, we used the 3D method to assess the effects of Pimozide, a DA antagonist, on ICSS, thus complementing earlier work carried out with indirect DA agonists (Hernandez et al., 2010; 2012). On the basis of the prior work, we predicted that Pimozide would decrease P_e without affecting F_{hm}.

Materials and Methods

Subjects. Eight, 350-400 g, male, Long-Evans rats (Charles River breeding farms) were housed in pairs in Plexiglas cages in a vivarium with a reversed 12 h dark/light cycle (lights “on” at 8:00 A.M.). All behavioral tests were conducted during the dark cycle (between 8:00 A.M. and 2:30 P.M.). Rats were housed individually following electrode implantation.

Electrode implantation. Atropine sulfate (0.05mg/kg, s.c.) was administered to reduce bronchial secretions, a ketamine-xylazine mixture (10/100 mg/kg, i.p.) was used to induce anesthesia, and penicillin (0.3ml/kg, s.c.) was used to prevent infections. Xylocaine jelly was applied to the external auditory meatus to reduce discomfort from the stereotaxic ear bars. Once the rat was mounted on the stereotaxic frame, anesthesia was maintained by isoflurane vapor administered through a snout mask.

Six stainless-steel screws were threaded into pilot holes drilled in the skull. One end of a copper wire was wrapped around two of the screws, which served as the current return (anode); the other end was terminated in a gold-plated Amphenol connector. Monopolar stainless-steel electrodes were custom-made from 000 insect pins, which were insulated with Formvar enamel to within 0.5mm from the bare tip; the unsharpened end was soldered to a copper wire, which, in turn, was attached to a gold-plated Amphenol connector.

The electrodes were aimed bilaterally at the MFB, at the level of the lateral hypothalamus (LH, AP: -2.8 from bregma, ML: ±1.7, DV: 8.8-8.9 from skull surface), and secured to the skull with dental acrylic. The Amphenol connectors were inserted into a McIntyre miniature connector (Scientific Technology Centre, Carleton University, Ottawa, ON, Canada), which was attached to the skull and skull-screw anchors with dental acrylic. Rats were allowed at least five days of post-surgical recovery before behavioral screening commenced.

Apparatus. The experimental chambers (30 X 21 X 51 cm) have mesh floors and a transparent Plexiglas front panel. An amber flashing light is mounted 10 cm above the mesh floor, a retractable lever (ENV-112B, MED Associates) is mounted on the right side panel, and a 1 cm cue light is located 2 cm above the lever. An electrical swivel located at the top of the box allowed the animal to circle without tangling the stimulation leads.

A computer-controlled digital pulse generator and a constant-current amplifier were used to set the temporal parameters of the electrical stimulation and the pulse amplitude, respectively. A custom-written computer program ("PREF", Steve Cabilio,

Concordia University, Montreal, QC, Canada) controlled the experiments and logged the data.

Self-stimulation training. Each rat was screened to determine the electrode and the combination of electrical current and pulse frequency that best supported vigorous lever pressing with minimal motoric and/or aversive side effects. From this point onwards, the most effective electrode was used and the current was kept constant. Rats were trained to depress the lever for 4 s on a *cumulative-handling-time schedule* (Breton et al., 2009) to receive a 0.5 s train of 0.1 ms cathodal pulses. This schedule delivers a reward when the cumulative time that the lever has been depressed reaches an experimenter-defined criterion, called the *price* of the stimulation. Once performance on the cumulative handling-time schedule was stable, the rats were gradually trained on the different subtasks that provide the data required to fit the mountain model: *frequency sweeps, price sweeps,* and *radial sweeps.*

A frequency sweep consisted of eleven 80 s trials; given the 4 s price, the rat could harvest a maximum of 20 reinforcements per trial. Within each trial, the pulse-frequency and price were held constant. A black-out delay (BOD) followed delivery of the reward: during this delay, the lever was disarmed and retracted for 2 s, and the trial-duration timer was paused. The pulse frequency of the stimulation on the first three trials of each sweep was set to the maximal value the rat could tolerate without manifesting pronounced forced movements or signs of aversion; the pulse frequency was then decreased in equal proportional steps across the remaining trials. The step size was adjusted for each rat so as to yield a sigmoidal relationship between TA and the logarithm of the pulse frequency, with an upper asymptote above 0.8, a lower asymptote below 0.2, and a transitional region positioned roughly mid-way between the upper and lower TA asymptotes. The first two trials of each sweep served as warm-ups and were excluded from the analysis. A 10 s inter-trial interval (ITI) signaled the beginning of a new trial; the amber light flashed during this period, and a non-contingent (priming) stimulation train at the maximal pulse-frequency was delivered at the 8 s and 10 s timepoints. The computer time-stamped and logged each transition of the lever (from up to down or down to up).

Once consistent sigmoidal-shaped TA-frequency curves were obtained, the rat was trained to perform on price sweeps. These consisted of eleven trials during which the reward strength was maximal, but the price was increased systematically across trials. The price on the first three trials was set to either 3 or 4 s; the first two trials were considered warm-ups and were excluded form analysis. The trial duration was adjusted to allow the rat to harvest a maximum of twenty rewards per trial. The values of the ITI, BOD and priming parameters were the same as those used on frequency sweeps. During this phase of training, test sessions consisted of 3 price sweeps randomly intercalated with 4 frequency sweeps. The size of the proportional price changes was adjusted for each rat so as to produce well-formed sigmoidal TA-price curves, as described above in the case of the frequency sweeps.

Radial sweeps were incorporated in the training sessions once consistent sigmoidal TA-prices curves were obtained. On radial sweeps, we both decreased the pulse-frequency and increased the price systematically across trials. Eleven trials were run, with the first two defined as warm-ups and excluded from the analysis. The sizes of the proportional changes in pulse-frequency and price were adjusted so that the resulting TA-frequency and TA-price curves were sigmoidal and so that the trajectory of the radial sweep in the space defined by the pulse frequency and price (see the green points in Figure 5) passed close to the point defined by the two location parameters (Pe, F_{hm}). The empirical objective of the 3D analysis is to measure drug-induced shifts of this point. Thus it is important that behavioral measurements be obtained as close to the location parameters (Pe, F_{hm}) as possible. To achieve this, we used a simulator implemented by Yannick Breton in MATLAB (the MathWorks, Natick, MA) to aim the radial sweep at (Pe, F_{hm}) on the basis of the data from the frequency and price sweeps and estimates of slope parameters based on previous studies. As data obtained from radial sweeps accumulated, preliminary fits of the 3D reward-mountain model were performed as described below (Model fitting and comparisons), and the trajectory of the radial sweep was adjusted accordingly.

After the introduction of radial sweeps, test sessions consisted of 3 frequency sweeps, 2 price sweeps and 2 radial sweeps. The first sweep was always a warm-up frequency

sweep, which was excluded from the analysis. We refer to the dataset composed of a frequency sweep, a price sweep and a radial sweep as a *survey*, the minimal dataset that suffices to fit the mountain model. Within a survey, sweep types were ordered pseudorandomly. Each test session included two surveys, performed sequentially. Four of these sessions were run, and then the data were fit using a resampling strategy, as described below (Model fitting and comparisons). If any of the sweeps lacked well-defined lower and upper asymptotes, or if the radial sweep strayed too far from (P_e, F_{hm}), the pulse frequencies and/or prices were adjusted, and four extra sessions were run. This process was repeated until the data met the criteria, at which point the rats were considered ready for drug testing. Two rats failed to perform all of the stages of training described above and were excluded from the experiment.

Drug testing. Each drug and vehicle session started with a warm-up frequency sweep, followed by two surveys, which each required 2-3 h to complete. Each type of sweep within a survey was presented in pseudorandom order. Pimozide (0.1 mg/kg; Tocris Bioscience) was diluted in physiological saline and administered at a volume of 1.0 ml/kg, i.p., 180 min before each behavioral test. This dose was determined from previous experiments (Atalay & Wise, 1983; Gallistel & Freyd, 1987) and from our own pilot tests, in which responding ceased or was unacceptably weak at doses of 0.25 - 1.0 mg/kg (data not shown). Rats were tested following vehicle injections on Mondays and Thursdays, and after drug injections on Tuesdays and Fridays. Wednesdays and weekends served as drug elimination days. During vehicle sessions, the rats were presented with the same sets of sweeps determined during training. On drug sessions, all prices from the price sweep were decreased by 0.1-0.2 log10 units (1.25-1.58 s) because our pilot tests suggested leftward shifts of this magnitude along the price axis. Had we not done this, we would have risked losing the upper asymptote of the price sweep, which would have compromised the fit of the model.

Six sessions, each 5-6 h long, were run with each rat in the vehicle and drug conditions, and thus, all rats received the 0.1 mg/kg dose of Pimozide six times. Rats Pharm2 and Pharm3 also received four injections each at Pimozide doses ranging from 0.25 - 1.0 mg/kg during pilot tests carried out prior to the experiment proper.

A second frequency sweep, carried out at a lower price, had to be included in all drug sessions conducted with subject Pharm3. This was necessary because in this subject, TA decreased very steeply as a function of price (data not shown). Performance on the 4 s frequency sweep no longer attained a sufficiently high TA to provide a good estimate of the upper asymptote. The addition of the low-price frequency sweep provided the needed information. The objective of estimating the upper asymptote in the drug condition was addressed in rats Pharm10, Pharm11 and Pharm13 by decreasing the price during frequency-sweep trials to 3 s.

On average, it took three months following surgery to finish the experiment with each rat.

Following data acquisition, the rats were overdosed with ketamine-xylazine. The location of the electrode tip was determined by staining the tissue with the Prussian-Blue method and examination of brain sections by means of low-magnification microscopy (Hernandez et al., 2006).

Model fitting and comparisons. The mountain model and the fitting approach have been described in detail elsewhere (Hernandez et al., 2010; 2012; Trujillo-Pisanty et al., 2011). Briefly: the six and seven parameter versions of the mountain model (Hernandez et al., 2010; 2012; Trujillo-Pisanty et al., 2011) were fit to the drug and vehicle datasets separately for each rat. Both models include parameters that specify the location and slope of the fitted surface along both the price and pulse-frequency axes as well as the maximal and minimal TA. The 7-parameter version includes an additional term that estimates the contribution of conditioned reward (Hernandez et al., 2010), thus accommodating the possibility that the lever and/or the act of lever depression come to serve as secondary reinforcers. The fits were carried out using a MATLAB (the MathWorks, Natick, MA) procedure developed by Kent Conover, based on the non-linear least-squares routine in the optimization toolbox and resampling methods (Efron & Tibshirani, 1994). The data from each rat under the drug and vehicle conditions were resampled with replacement 1000 times by survey. The model was fit to each of the resulting datasets. Mean values for each parameter within condition were obtained by averaging the 1000 estimates. Confidence intervals were obtained by excluding the

lowest and the highest 25 values of the 1000 estimates. This strategy allowed us to obtain unbiased estimates of the location parameters (P_e and F_{hm}) and their dispersions for each subject under each condition. Two different fitting strategies were used per model: in the location-specific approach, location parameters were estimated for each survey; the all-parameters-common approach estimated single location parameter values for an entire dataset (Hernandez et al., 2010; 2012; Trujillo-Pisanty et al., 2011). The Akaike information criterion (AIC) (Akaike, 1974) was used to select the model and strategy that provided the best fit of the data. Difference vectors were then constructed by subtracting each of the 1000 parameter location-parameter estimates for the vehicle condition from the corresponding estimates for the drug condition. Confidence intervals were derived from the 2.5th and 97.5th percentiles of the difference vector. Differences were regarded as significant with an alpha level of 0.05 when zero fell outside the 95% confidence interval. This strategy allowed us to assess the effects of the drug within subject.

Results

Two rats were unable to meet the performance criteria and were excluded from the experiment. The six remaining rats learned to perform appropriately on frequency, price, and radial sweeps. Figure 13 shows the mean TA from a representative rat (subject Pharm10), for every trial in each type of sweep. Note that as expected, TA increased as a function of pulse frequency and decreased as a function of price. In other words, the stronger and cheaper the electrical reward, the more it was sought out by the rat and the less the rat engaged in alternate activities. In all sweeps, the upper asymptote is above 0.8 and the lower asymptote below 0.2.

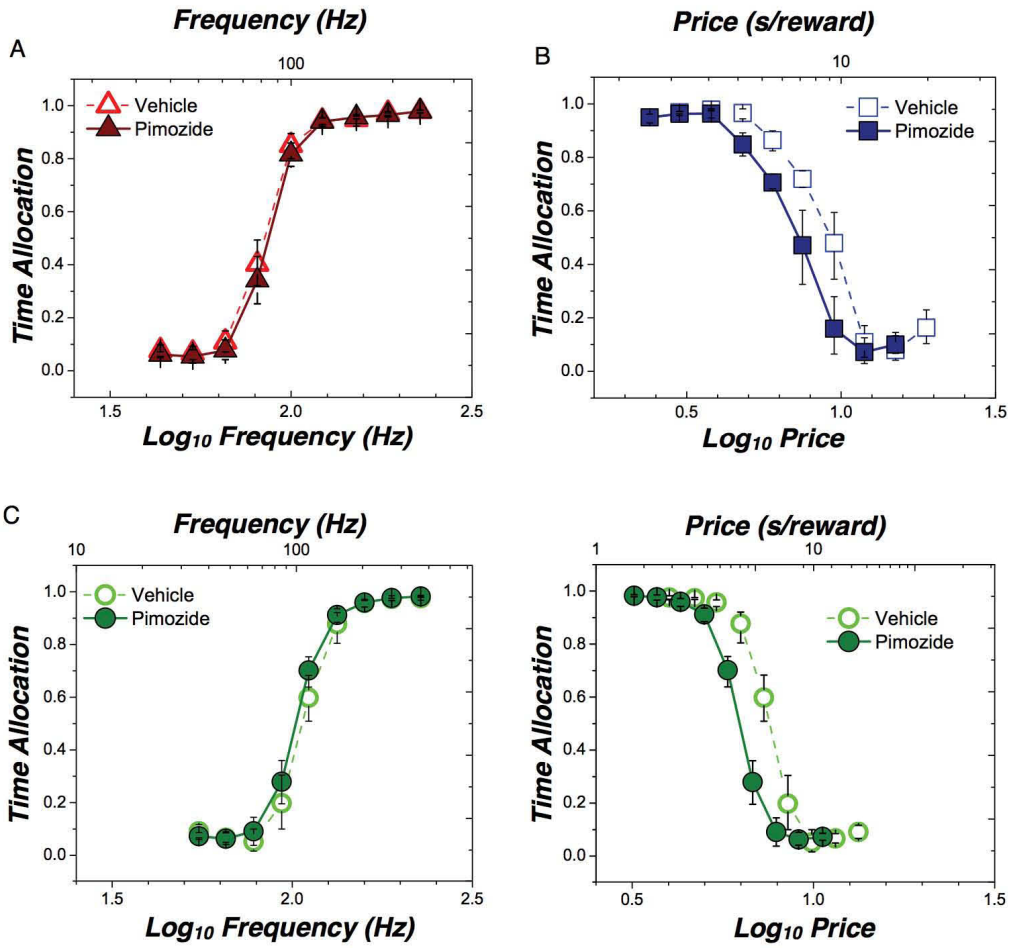

Figure 13. Time allocation data from subject Pharm10, under vehicle and Pimozide conditions. Data shown are means and 95% confidence intervals. (A) During *frequency sweeps*, the pulse frequency varied across trials and the price was held constant. (B) During *price sweeps*, the price varied across trials, and the frequency was kept at a value that yielded maximal reward. (C) during r*adial sweeps*, frequency and priced varied conjointly across trials. The same data are shown twice, once from the viewpoint of the pulse-frequency axis and once from the viewpoint of the price axis. In all cases the upper asymptote is above 0.8, and the lower asymptote is below 0.2.

Histological analysis confirmed that the electrode tips were located within the MFB, at the level of the LH, in all the rats included in the experiment (Figure 14).

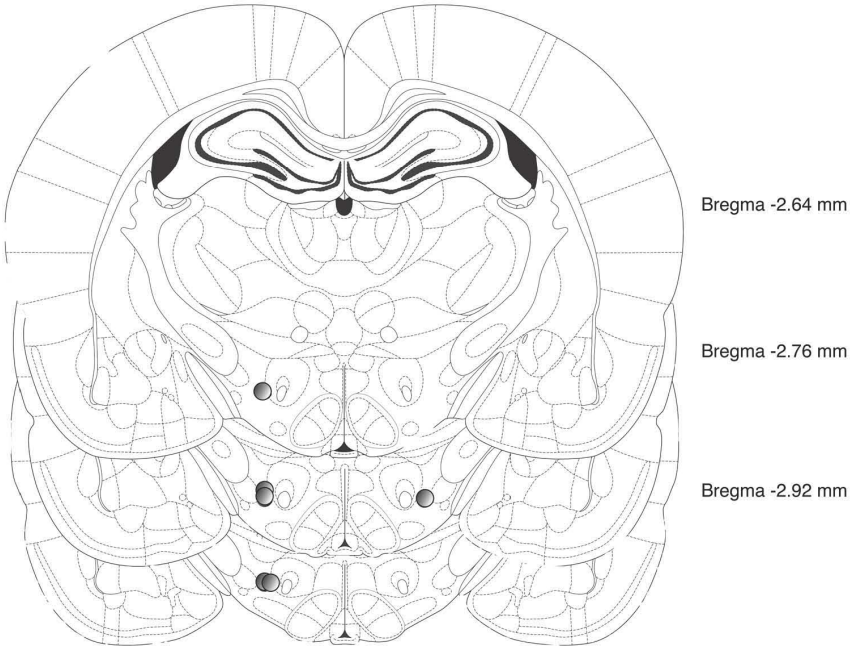

Figure 14. Electrode placement. The location of each electrode tip is shown. All placements fell within the boundaries of the MFB, at the level of the LH, as determined using low magnification microscopy and the Paxinos and Watson atlas (2007).

The fitting strategy allowed us to perform within-subject analysis and comparisons. An example is shown in Figure 15, which depicts the vehicle and drug data from subject 10, along with the corresponding surface fits and contour plots. The horizontal line with right-pointing triangular endpoints and the vertical line with diamond endpoints represent the estimated F_{hm} and P_e values, respectively; the surrounding shaded bands denote 95% confidence intervals. Note that the trajectory of the radial sweep passes close to (P_e, F_{hm}), as intended. In all rats, the model fit the data well: adjusted R^2 values ranged from 0.965-0.989 in the vehicle condition and 0.961-0.988 in the drug condition.

Figure 16 replots the data in Figure 15 so as to highlight any drug-induced shifts of the fitted 3D surface, The contour graph for the vehicle condition is shown twice, in the upper left as well as in the lower right quadrant. Note that Pimozide did not move the mountain along the frequency axis (as indicated by the horizontal lines with right-

pointing triangular endpoints positioned at F_{hm}), whereas a clear (-0.0857 $\log_{10}$ units) leftward shift along the price axis is evident (as indicated by the arrowhead between the projections of the vertical lines with diamond endpoints representing P_e). The bar graph summarizes the effect of the drug on the position of the mountain along the two axes.

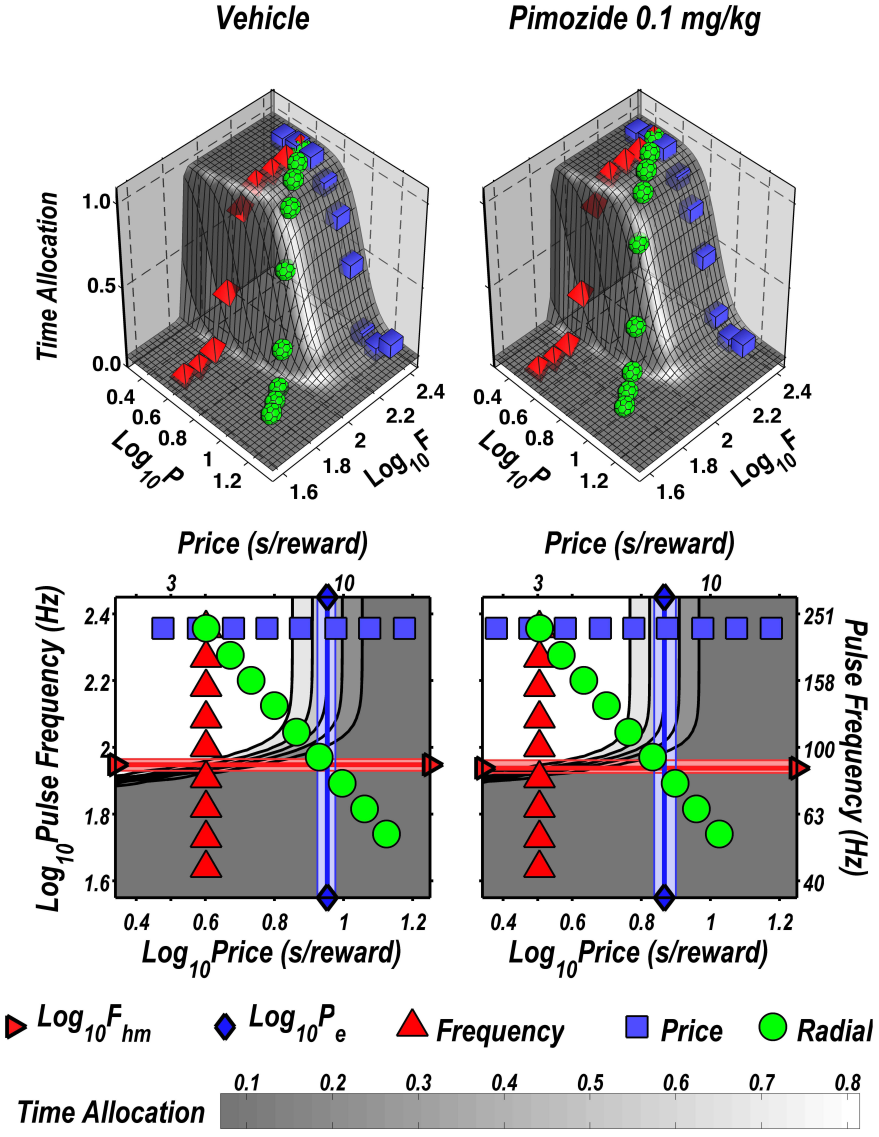

Figure 15. Mean time allocation, fitted surfaces, and contour maps. The data are from rat Pharm10. In the 3D graphs in the upper row, the fitted surfaces are shown in grey, frequency-sweep data are designated by pyramids, price-sweep data are designated by cubes, and radial-sweep data are designated by polyhedrons. Contour graphs of the fitted surfaces are shown in the lower row. In these graphs, values of the independent variables along frequency sweeps are designated by

Figure 16. Contour-graph representation of the effect of Pimozide in rat Pharm10. The contour map for the vehicle condition is shown twice (upper left and lower right) to facilitate across-condition comparison of location-parameter values ($Log_{10}F_{hm}$, $Log_{10}P_e$) along the frequency and price axes. The bar graph shows the size of the drug-induced change in the values of the location parameters. Pimozide failed to shift the reward mountain along the frequency axis but displaced the mountain leftward along the price axis.

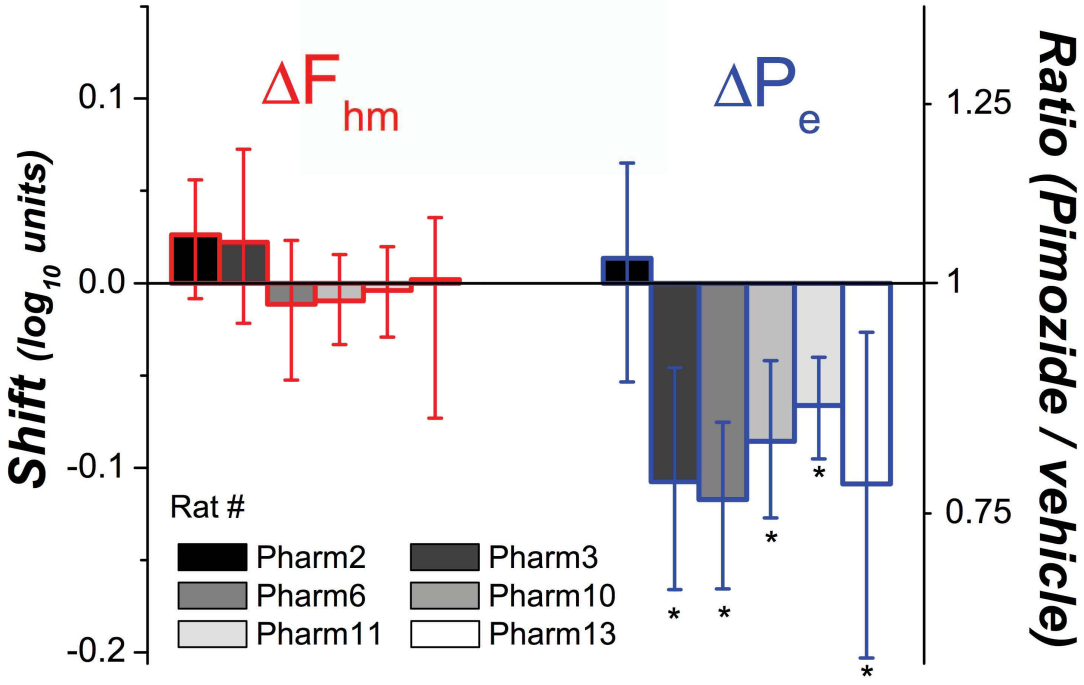

Figure 17. Pimozide-induced shifts for all subjects. Error bars denote 95% confidence intervals. In no case did the drug reliably alter F_{hm}, whereas it decreased P_e reliably in 5/6 subjects.

If the effect of Pimozide had varied systematically across test sessions as a result of tolerance or sensitization, this would have inflated the variance of the location-parameter estimates. Similar inflation of error variance would have been produced by systematic changes in baseline values as a result of the repeated drug administration. Figure 18 shows that the location-parameter estimates obtained in the vehicle and drug

sessions did not vary systematically across test sessions. The values shown are expressed as within-session deviations from vehicle means and are averaged across subject.

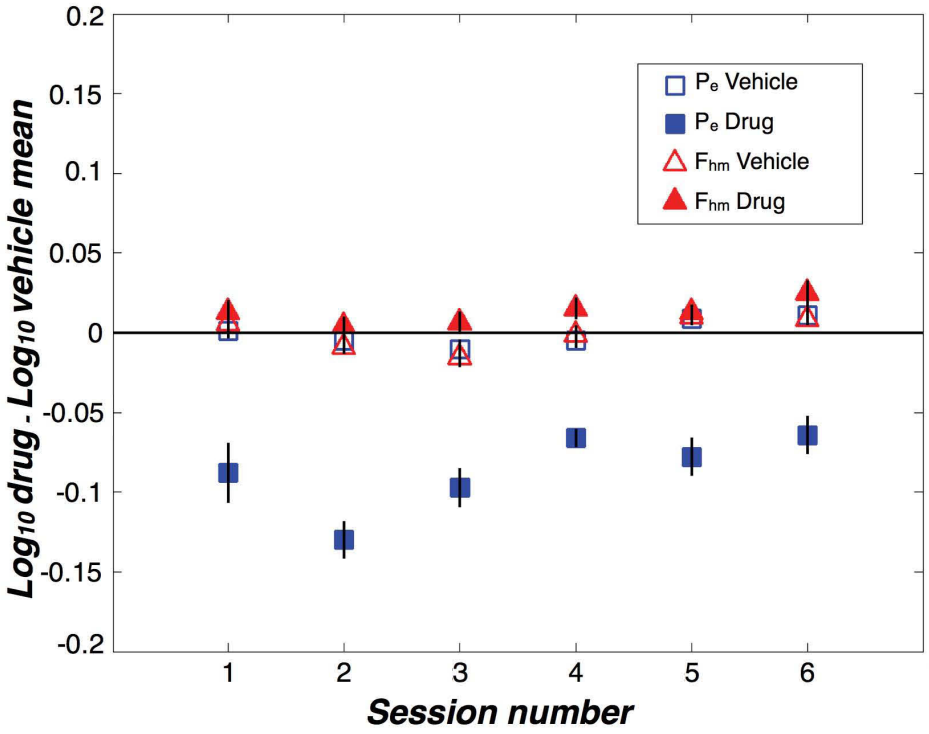

Figure 18. Normalized shifts in location-parameter values across sessions. Two surveys of the reward mountain were carried out in each session. For each rat, the two estimates of each location parameter for each session were averaged so as to produce a single estimate for that session. A set of difference scores for each rat was then obtained by subtracting the average location-parameter estimate obtained for that rat across the 6 vehicle sessions from the estimate for each individual session. This causes the values for the vehicle sessions to fluctuate around zero and expresses the values for the drug sessions as deviations from the vehicle baseline. The difference scores were then averaged across the 6 rats to obtain the plotted values (open symbols: vehicle; filled symbols: drug). The error bars represent

the standard error of the mean. As expected from the within subject analysis (Figure 17), the F_{hm} values for the drug and vehicle conditions overlap, whereas the P_e values fall consistently below the vehicle baseline. These plots provide no indication of the systematic shifts over sessions that would be expected from tolerance or sensitization effects.

Discussion

The importance of the 3D perspective. A researcher studying ICSS by means of the conventional curve-shift method is, in effect, viewing the silhouette of the reward mountain in 2D while facing the pulse-frequency axis (Hernandez et al., 2010). When the silhouette shifts to the right, such an observer cannot be sure what movement of the mountain is responsible (Video 1, Figure 2). Although it is possible that the 3D structure indeed has moved rightward, it is also possible that the mountain has retreated along the price axis. Due to the diagonal orientation of the mountain surface, a displacement towards lower values along the price axis (hidden in the 2D view) drags the silhouette rightwards along the pulse-frequency axis. When we examine the results of the previous studies of Pimozide-induced changes in ICSS by means of the curve-shift method, we are confined to the 2D perspective of the observer described above. As a result, we cannot be sure whether the reported rightward displacement of rate-frequency curves reflects movement of the mountain along the pulse-frequency or price axes (Figure 2). In the present study, we eliminated this ambiguity by using a 3D measurement method that provides a view of the mountain from above, thus making the components of its displacement along the two axes readily apparent (Figure 16, Video 1). Whereas Pimozide produced no reliable movement along the pulse-frequency axis, the direction of the shifts reported in 2D studies (Gallistel & Freyd, 1987; Miliaressis, Rompre, Laviolette, Philippe, & Coulombe, 1986b; Rompré & Wise, 1989), the drug consistently displaced the reward mountain along the dimension that was hidden in the prior work: the axis representing reward cost.

Comparison to previous 2D results. The reliable shifts revealed by our 3D method in 5 of 6 rats following administration of Pimozide at a dose of 0.1 mg/kg contrast with the results reported for doses in the 0.1-0.175 mg/kg range in 2D curve-shift studies. A 0.1

mg/kg dose failed to produce statistically reliable shifts in a study by Franklin (Franklin, 1978), who used a runway to measure ICSS performance and the number of pulses in a fixed-frequency train as the strength variable. In a later runway study carried out by Stellar et al. (Stellar, Kelley, & Corbett, 1983), 0.125 mg/kg produced a reliable shift along the pulse-frequency axis in only 1 of 6 rats. In studies carried out in operant conditioning chambers, the small leftward shifts in rate-frequency curves reported by Gallistel and Freyd (Gallistel & Freyd, 1987) failed to meet their criterion for statistical significance at a 0.1 mg/kg dose, as did the shifts reported by Rompré and Wise (Rompré & Wise, 1989) at a 0.175 mg/kg dose. Doses in the 0.2 - 0.35 mg/kg range produced statistically significant leftward curve shifts in all the aforementioned studies.

Why were reliable shifts seen in the present 3D study but not in previous 2D work carried out with similar doses? We have demonstrated previously (Hernandez et al., 2010; 2012) that shifts along the price axis displace the silhouette of the mountain along the pulse-frequency axis, creating the illusion of movement along an axis orthogonal to the one along which the 3D structure is actually displaced. If so, why weren't shifts in the 2D silhouette seen in the prior work? Inspection of the contours in Figures 15 and 16 reveals that such shifts would have been very hard to detect in 2D studies. Note that the slope of the diagonal portion of the contour lines is shallow: the effect of a large change in price is offset by a modest change in pulse frequency. This follows from the fact that the intensity of BSR produced by MFB stimulation rises steeply as a function of pulse frequency (Hernandez et al., 2010; 2012; Leon & Gallistel, 1992; Simmons & Gallistel, 1994; Trujillo-Pisanty et al., 2011). Given that the shifts along the price axis reported here are only on the order of 0.1 common logarithmic units, the correspondingly smaller displacement of the silhouette of the mountain along the pulse-frequency axis would likely have fallen below the detection threshold in 2D studies. The 3D method offers greater sensitivity than the 2D method because shifts along either or both axes can be detected.

The benefits obtained from the 3D method do have a cost: three months were required to obtain a dataset from a single rat in the present study. Given the long period required for training and testing, obtaining dose-response information is very expensive.

Regardless of the testing paradigm, Pimozide and other neuroleptics pose particular problems in this respect. Gallistel and Freyd (1987) did not discern a dependence of 2D curves shifts on the dose of Pimozide in the range of 0.2 - 0.6 mg/kg. As the dose was raised (to 0.4 mg/kg and above), an increasing proportion of subjects ceased to perform. Rompré and Wise (1989) have argued that the attenuation and ultimate cessation of performance as the dose of neuroleptic is increased likely reflects depolarization inactivation of DA neurons due to summation between the excitatory influence of the electrical stimulation and the disinhibition of DA somata by blockade of autoreceptors. The attenuation of ICSS performance is exacerbated in our paradigm because of the requirement to pay much higher opportunity costs than those demanded in 2D curve-shift studies carried out in operant chambers. Typically the rat must only make a single lever press of infinitesimal duration to earn a reward in such 2D curve-shift studies. In contrast, the rats had to keep the lever depressed for substantial periods of time to earn a reward in the present study; the highest prices tested ranged from 18.9 - 38.1 s. Given the high reward costs and the likely onset of depolarization inactivation, it is not surprising that we could not obtain reliable performance with doses of 0.25 or above. The dose window for 3D tests is very narrow indeed in the case of this drug. In future work, 2D studies may play a role complementary to 3D studies by providing information about wider dose ranges, albeit with lower sensitivity and interpretative power.

Comparison to previous 3D results. The results of the present study are highly consistent with those obtained by means of the 3D method with drugs that block the dopamine transporter. Cocaine and GBR-12909, displaced the mountain rightward along the price axis (Hernandez et al., 2010; 2012), whereas we show here that Pimozide displaces the mountain leftward along the same axis. Thus, the mountain moves in opposite directions in response to indirect agonists and to a receptor antagonist. Both Pimozide in the present work, and GBR-12909, the more specific of the DAT blockers employed in the previous work, failed to produce any statistically reliable shifts of the mountain along the pulse-frequency axis. In contrast, the tested

doses of Pimozide and GBR-12909 produced reliable shifts along the price axis in 5/6 and 7/10 rats, respectively.

Interpretation of the shift along the price axis. The confinement of the shifts to the price axis has important implications in terms of the stage of processing at which DA neurotransmission contributes to BSR. In early work on the role of DA in ICSS, it was often proposed or implied that the rewarding effect arose from direct excitation of midbrain DA neurons that give rise to MFB projections (Anlezark, Arbuthnott, Christie, Crow, & Spear, 1974; Arbuthnott, Crow, Fuxe, Olson, & Ungerstedt, 1970; Corbett & Wise, 1980; Crow, 1972; Fibiger, LePiane, Jakubovic, & Phillips, 1987). However, the axons of these neurons have high thresholds to activation by extracellular stimulation, and their excitability and conduction properties are poorly matched to the inferred properties of the directly stimulated substrate for self-stimulation of the MFB (Anderson et al., 1996; Bielajew & Shizgal, 1982; Gallistel et al., 1981; Shizgal, 1997; Shizgal et al., 1980; J. S. Yeomans et al., 1988). Moreover, the behaviorally relevant direction of conduction in at least a portion of the directly stimulated neurons subserving the rewarding effect is rostro-caudal, opposite to the direction in which the midbrain DA neurons project to forebrain targets (Bielajew & Shizgal, 1986). To accommodate both the psychophysically derived portrait of the directly stimulated substrate and the ample evidence that DA neurons play an essential role in ICSS, the “descending-path” hypothesis was proposed (Bielajew & Shizgal, 1986; Shizgal, 1997). This hypothesis states that the rewarding effect of MFB stimulation arises from the direct excitation of descending, myelinated projections of forebrain neurons that provide trans-synaptic input to midbrain DA neurons. Supporting evidence is provided by recent demonstrations that direct optical excitation of descending MFB inputs to the ventral tegmental area (VTA) supports operant responding. These inputs excite VTA DA neurons either directly (Kempadoo et al., 2013) or via disinhibition mediated by local GABAergic interneurons (Jennings et al., 2013b).

Rate-frequency curves obtained via 2D measurements of ICSS have often been likened to dose-effect curves in pharmacology (Bauco, Wang, & Wise, 1993; Wise, 1996). This analogy would work well if direct activation of DA neurons were responsible for the

rewarding effect of MFB stimulation. Just as the dose of a drug required to produce an effect of a given magnitude would be increased due to partial blockade of the receptors at which the drug acts, the "dose" (e.g., pulse frequency) of stimulation required to produce a given ICSS response rate would be increased by a DA receptor antagonist. However, this analogy may no longer hold if, as modern evidence suggests, the activation of the DA neurons is largely of trans-synaptic origin. Whether or not the analogy remains valid in the case of trans-synaptic activation depends on where the DA neurons are positioned in the depiction provided by Figure 1.

The key pivot point in Figure 1 is at the output of the integrator, the circuit or neural population responsible for spatio-temporal integration of the post-synaptic signals arising from the volley of stimulation-induced action potentials in the directly stimulated neurons. The analogy between rate-frequency and dose-effect curves would remain valid if the DA neurons functioned merely to relay signals from the directly stimulated neurons to the *input* of the integrator. In that case, a DA antagonist, such as Pimozide, would increase the pulse frequency required to drive integrator output to a given level. We have termed such an effect a change in the *sensitivity* of the BSR substrate, an effect strictly analogous to a change in the K_D of a receptor or the K_m of an enzyme. In early studies, the effect of DA agents on ICSS was attributed to such changes in sensitivity (Crow, 1970; Esposito et al., 1978), which are expressed in the mountain model as a change in F_{hm} (Hernandez et al., 2010). The results of both our prior studies of the effects of indirect DA agonists (Hernandez et al., 2010; 2012) and the present work with a DA antagonist are inconsistent with such a view: these agents shift the mountain reliably along the price axis (i.e., they change P_e) while producing little or no change along the pulse-frequency axis (as indexed by F_{hm}). These consistent findings show that the DA agents act at or beyond the output of the integrator.

One way in which the action of a drug at or beyond the output of the integrator could alter ICSS is by rescaling that output (as represented by the right-facing triangle in Figure 1). We describe such an effect as a change in *gain* (Hernandez et al., 2010), an adjustment that alters the maximum payoff attainable without changing the pulse frequency required to reach this plateau. A change in gain is analogous to a change in

the V_{max} of an enzymatically catalyzed reaction or a change in the receptor density. Changes in sensitivity and gain are independent (as are changes in K_m and V_{max}).

A model proposed by Moisan and Rompré (Moisan & Rompré, 1998) predicts that manipulations of DA neurotransmission will alter reward-system gain. According to their model, rewarding stimulation of the posterior mesencephalon activates midbrain DA neurons trans-synaptically. Spatiotemporal integration of the effects of the stimulation-induced volley underlying the rewarding effect occurs either in the dendritic arbor of the DA neurons and/or in a neural network that feeds input to the DA neurons from the directly stimulated population. If so, indirect DA agonists and Pimozide would not change the pulse frequency required to produce a given level of firing in the DA neurons, which will have already been determined before the stimulation-induced signal reached the spike-generating region. In contrast, the post-synaptic impact of the induced level of firing would be altered by indirect DA agonists and Pimozide as they boost release or block post-synaptic receptors, respectively. The results obtained in the present study using Pimozide and in previous 3D studies using indirect DA agonists are consistent with such drug-induced changes in gain and thus with transposition of the Moisan and Rompré model to the MFB.

An alternative interpretation of the results follows from the treatment of payoff that the reward-mountain model has inherited from the generalized matching law (Baum & Rachlin, 1969; Killeen, 1972; Rachlin, 1971). In those accounts and in the reward-mountain model, payoff is computed by scalar combination of variables such as reward quality, reward probability, and reward costs. A property of scalar combination is that a change in the value of an input variable simply rescales the result of the calculation, increasing or decreasing it by a given proportion. Thus, a change in reward cost can have the same effect as a change in gain.

An influential view of the role of DA neurons in operant performance couches their contribution in terms of the proclivity to invest effort in pursuit of rewards (Niv, Daw, Joel, & Dayan, 2006; Salamone, Correa, Farrar, Nunes, & Pardo, 2009; Salamone, Correa, Farrar, & Mingote, 2007; Salamone, Correa, Mingote, & Weber, 2003). This view is consistent with the notion that the effect of Pimozide reported here is related to

subjective reward costs rather than to reward-system gain. For example, the drug may have altered the rats' perception and/or evaluation of the effort required to hold down the lever. Such an effect differs from the deficit in response initiation typically associated with neuroleptic action: it operates in a different plane. Delayed initiation would have depressed maximal time allocation, compressing the mountain vertically. However, the low dose of Pimozide employed here failed to do so: As shown in Table 3, TA_{max} values for the vehicle and drug conditions were reliably different in only 1 of 6 rats (Rat Pharm3). Rather than lowering the "altitude" of the mountain, the drug shifted its position horizontally along the price axis. By substituting manipulation of effort costs for the manipulation of opportunity costs used in the present study, it may prove possible, in future studies, to distinguish between the contribution to such changes in position due to alteration of reward-circuit gain and alteration of subjective perception and/or evaluation of the effort required to procure a reward.

Herrnstein's conceptualization of single-operant performance in terms of choice between pursuit of an experimenter-controlled reward and engagement in alternate activities (Herrnstein, 1970; 1974) provides a third interpretation of the results. Given this view, the effect of Pimozide observed in the present study could be attributed to a drug-induced increase in the value of alternate activities. That said, we have argued elsewhere that a change in the value of alternate activities is unlikely to account for the large rightward shifts of the reward mountain along the price axis that are produced by continuous infusion of cocaine (Hernandez, Breton, Conover, & Shizgal, 2010).

Rat	TA_{max} vehicle	TA_{max} drug	Significant
Pharm2	0.949	0.948	False
Pharm3	0.976	0.918	True
Pharm6	0.999	1.000	False
Pharm10	0.963	0.951	False
Pharm11	0.832	0.823	False
Pharm13	0.986	0.967	False

Table 3. Estimates of maximal time allocation (TA_{max}) in the vehicle and drug conditions. The criterion for statistical reliability is whether or not zero falls within the 95% confidence interval surrounding the difference between the estimates for the vehicle and drug conditions. In five of six cases, administration of Pimozide (0.1 mg/kg) had no reliable effect on TA_{max}.

Conclusions. By applying a 3D measurement method, we demonstrate consistent effects of Pimozide on ICSS at a dose below the detection threshold in earlier 2D studies and we resolve an ambiguity inherent in the 2D methods. Whereas the 2D methods cannot determine the stage of neural processing at which drugs alter ICSS, the 3D method reveals that Pimozide acts at or beyond the output of the circuitry that performs spatiotemporal integration of the neural signals arising from MFB stimulation. Previous studies employing indirect DA agonists (Hernandez et al., 2010; Hernandez, Trujillo Pisanty, Cossette, Conover, & Shizgal, 2012) show that the effects of those drugs on MFB ICSS also arise from action at or beyond the output of the integrator. As expected, the direction of the effects produced by Pimozide and the indirect agonists are opposite. Positioning midbrain DA neurons at or beyond the output of the integrator is consistent with both psychophysical (Bielajew & Shizgal, 1982; 1986; Gallistel, Shizgal, & Yeomans, 1981; Shizgal, 1997; Shizgal, Bielajew, Corbett, Skelton, &

Yeomans, 1980) and optogenetic (Jennings et al., 2013; Kempadoo et al., 2013) findings.

The introduction of optogenetic methods (Yizhar, Fenno, Davidson, Mogri, & Deisseroth, 2011) is rapidly providing new information about the structure of brain reward circuitry and the neurochemical identity of its components (Jennings et al., 2013; Kempadoo et al., 2013; Tsai et al., 2009; Witten et al., 2011). For these and other new tools to realize their full potential, behavioral methods with the appropriate sensitivity and specificity are required. The reward-mountain model and the associated 3D measurement method are very promising in this respect. Combining these with optogenetic interventions should help link effects of drugs on reward seeking to well-defined actions at particular points in an increasingly detailed and accurate map of the underlying neural circuitry.

CHAPTER 3

Robust optical fiber patch-cords for *in vivo* optogenetic experiments in rats

Ivan Trujillo-Pisanty, Christian Sanio, Nadia Chaudhri, and Peter Shizgal

Trujillo Pisanty, I., Sanio, C., Chaudhri, N., & Shizgal, P. (2015). Robust optical fiber patch-cords for in vivo optogenetic experiments in rats. *MethodsX*, *2*, 263–271. http://doi.org/10.1016/j.mex.2015.05.003

ABSTRACT.

In vivo optogenetic experiments commonly employ long lengths of optical fiber to connect the light source (commonly a laser) to the optical fiber implants in the brain. Commercially available patch cords are expensive and break easily. Researchers have developed methods to build these cables in house for in-vivo experiments with rodents (Aravanis et al., 2007; Klorig & Godwin, 2014; Sparta et al., 2011; Ung & Arenkiel, 2012). However, the half-life of those patch cords is greatly reduced when they are used with behaving rats, which are strong enough to break the delicate cable tip and to bite through the optical fiber and furcation tubing. Based on Sparta et al. (2011) we have strengthened the patch-cord tip that connects to the optical implant, and we have incorporated multiple layers of shielding to produce more robust and resistant cladding. Here, we illustrate how to build these patch cords with FC or M3 connectors. However, the design can be adapted for use with other common optical-fiber connectors. We have saved time and money by using this design in our optical self-stimulation experiments with rats, which are commonly several months long and last four to eleven hours per session. The main advantages are:

- Long half-life
- Resistant to moderate rodent bites
- Suitable for long *in-vivo* optogenetic experiments with large rodents.

KEYWORDS: Optogenetics, optical fiber, behavior.

GRAPHICAL ABSTRACT

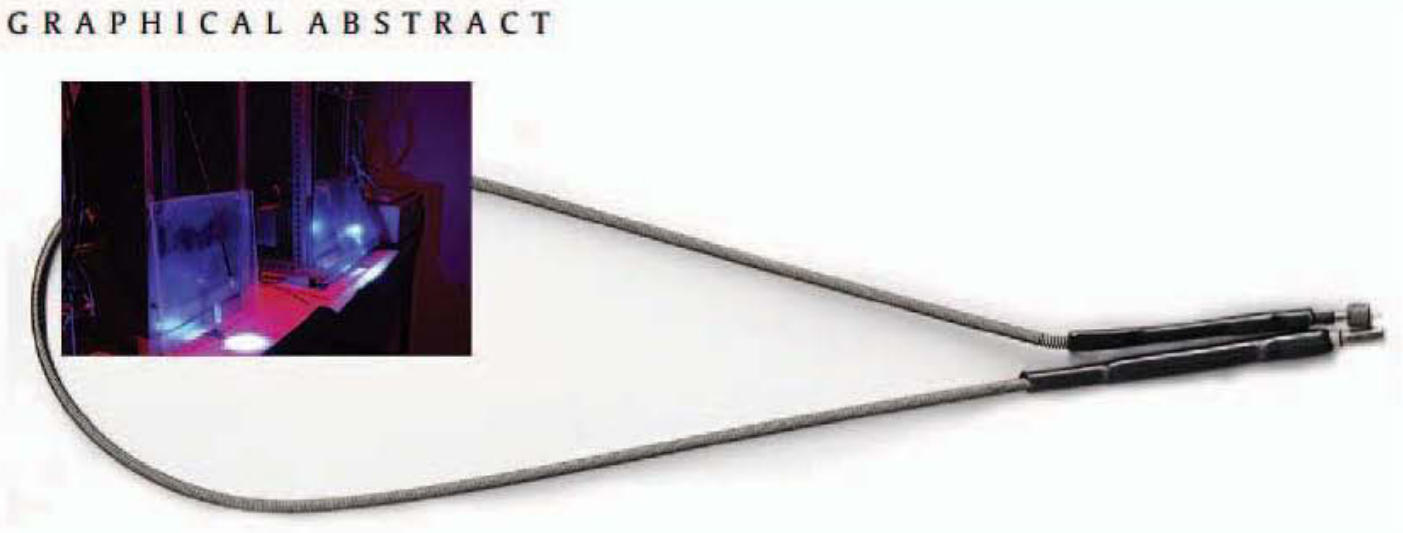

METHODS.

The following steps illustrate how to build a robust optical patch-cord suitable for in vivo experiments with rats. Overall, we start with a 200 µm core multi-mode optical fiber of the desired length. We then attach the appropriate connector to be used with the behavioral testing setup (FC or M3 in this protocol). The length of the optical fiber is strengthened and protected by incorporating a layer of black shrink tubing and a stainless steel compression spring. We strengthen the opposite tip of the patch cord, which is attached to the optical implant on the animal's head, by merging two stainless alloy ferrules and adding several layers of shrink tubing. This results in a strong and semi-rigid tip that serves as a holder and it is resistant to being dislodged when the animal moves around the setup.

Step 1: Before you begin, read this section completely and refer to Table 4 for a list of required materials. The assembling process takes sixty to ninety minutes. We prefer to use optical fibers with a smaller diameter core and/or smaller numerical aperture than that of the optical implant to which the patch-cord will be attached to. This is a preventive measure to avoid light loss. In principle, increasing the core diameter and/or the numerical aperture should retain light transmission in the face of small alignment errors. When two ferrules are joined by means of a ceramic sleeve, alignment may well vary somewhat as a function of the animal's movements. Avoiding variation in light transmission is of particular importance in psychophysical experiments, which require tight, graded control of optical power. The following steps and inventory are appropriate to make a 200 µm core multi-mode 0.39 NA fiber patch-cord compatible with a 300 µm multimode implant, but they can be adapted for other core diameters, specially if experimenters are concerned about the larger tissue damage produced by using thicker fibers.

Inventory.

Material	Company	Catalog no.	Quantity
200 μm, 0.39 NA multimode optical fiber	Thorlabs Inc., Newton, New Jersey, USA	FT200EMT	Cut to desired length
200 μm optical fiber stripper	Thorlabs Inc., Newton, New Jersey, USA	T12S21	1
Heat curable epoxy resin part A	Precision Fiber Products Inc., Silicon Valley, California, USA	PFP-353ND-16OZ-A	1 ml
Heat curable epoxy resin part B	Precision Fiber Products Inc., Silicon Valley, California, USA	PFP-353NC-16OZ-B	0.1 ml
M3-230 μm connector[a]	Doric Lenses Inc., QC, Canada	F210-0409	1
FC alloy connector drilled to 240 μm[b]	Fiber Instruments Sales Inc., New York, USA	30126G2-240	1
FC crimp tool[b]	Thorlabs Inc., Newton, New Jersey, USA	CT042	1
Diamond wedge scribe	Fiber Instruments Sales Inc., New York, USA	FO9OW	1
3/64″ shrink tubing	Newark Element14. Palatine, IL, USA	84N583	~10% shorter than fiber
1/4″ shrink tubing	Newark Element14., Palatine, IL, USA	84N588	~2″
0.125′′ ID adhesive shrink tubing	Newark Element14., Palatine, IL, USA	48W4786	~2″
Stainless steel compression spring, 0.1″ ED, 0.07′′ ID	Heilplex east end., Montreal, QC, Canada	Custom order	Cut to desired length
Stainless alloy ferrule drilled to 240 μm	Fiber Instruments Sales Inc., New York, USA	F10061F240	2
Ceramic split sleeve	Fiber Instruments Sales Inc., New York, USA	F18300SSC25	2
5 μm silicon carbide polishing paper	Thorlabs Inc., Newton, New Jersey, USA	LFG5P	1
3 μm aluminum oxide polishing paper	Thorlabs Inc., Newton, New Jersey, USA	LFG3P	1
1 μm aluminum oxide polishing paper	Thorlabs Inc., Newton, New Jersey, USA	LFG1P	1
0.3 μm aluminum oxide polishing paper	Thorlabs Inc., Newton, New Jersey, USA	LFG03P	1
Polishing puck	Thorlabs Inc., Newton, New Jersey, USA	D50-PC	1
Polishing pad and polishing plate	Thorlabs Inc., Newton, New Jersey, USA	NRS913A CTG913	1
200× fiber scope	Thorlabs Inc., Newton, New Jersey, USA	FS200	1
Digital power meter	Thorlabs Inc., Newton, New Jersey, USA	PM100D	1
Photodiode power sensor	Thorlabs Inc., Newton, New Jersey, USA	S121C	1
Threaded fiber adapter for sensor	Thorlabs Inc., Newton, New Jersey, USA	S120-FC	1

List of required materials and tools.
[a] The M3 connector is not necessary if working with the FC connector.
[b] These materials are not necessary if working with the M3 connector.

Table 4. List of required materials and tools. #The M3 connector is not necessary if working with the FC connector. *These materials are not necessary if working with the M3 connector.

Step 2: Use the optical fiber stripper to remove the optical fiber buffer and expose 35 mm of the optical-fiber clading (Figure 19A). Measure the optical fiber from the unstripped edge (Figure 19B) and cut it to the desired length using scissors or wire cutters.

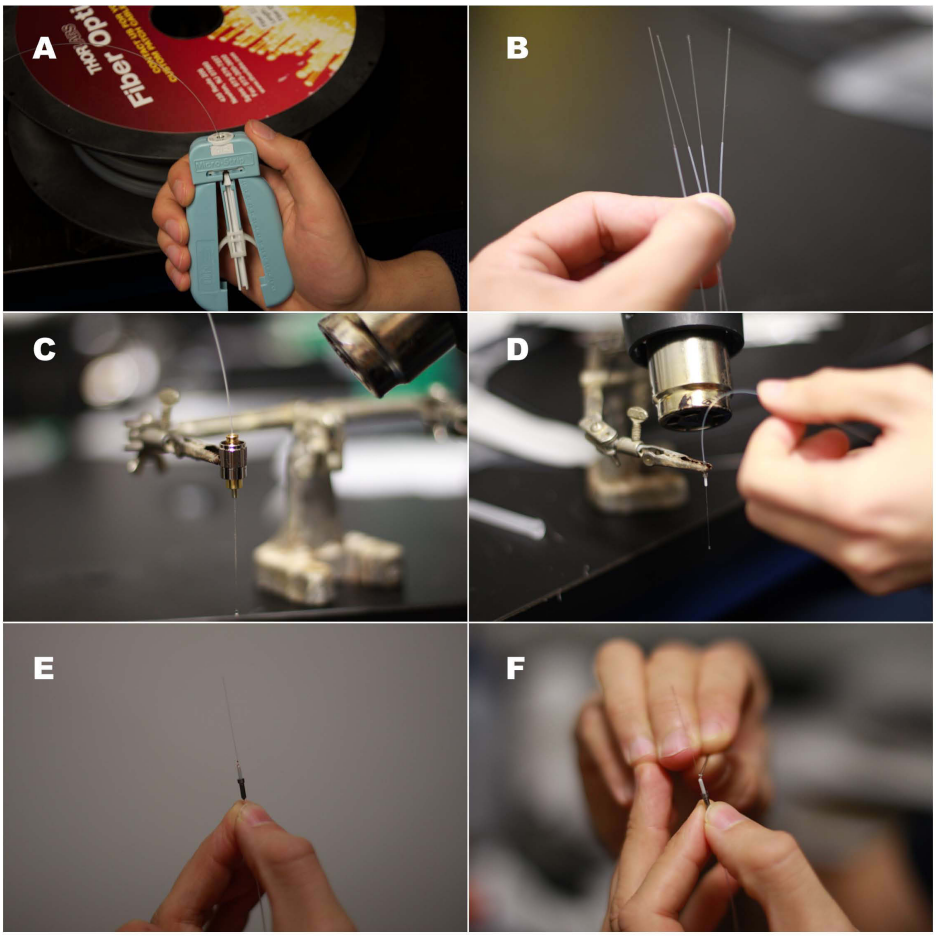

Figure 19. **A** Stripping 200 µm multimode optical fiber. **B** 35 mm of exposed optical fiber core in four optical fiber threads. **C** FC connector on third hand. Notice that the clamping occurs away from the tip of the connector. **D** Curing the resin inside the M3 connector. The process is similar for FC connectors. Warning: following this step the connectors will be very hot. **E** Cured resin at the tip of the M3 connector. The fiber should be glued to it rigidly and should cover the lumen. **F** Troubleshooting when there is no excess of resin at the tip of the connector. A very small amount of resin is applied to the lumen of the connector.

Step 3: Mix the heat curable epoxy resin according to the manufacturer's instructions, and load a 3 ml syringe with the mixed resin. Attach a 21 gauge blunt tip needle (Braintree Scientific, Inc. Braintree, MA) to the syringe.

Place the FC (Fiber instruments sales Inc. New York, USA) or M3 (Doric lenses, Québec, Québec, Canada) connector (Figures 19C and 19D) on the third hand with the small lumen facing downwards. Fill the internal volume of the connector with resin. Insert the fiber core all the way through the connector, leave in place, and cure the resin with the heat gun until it darkens. Be careful not to overheat the epoxy: some optical fibers may be damaged by excessive heat, resulting in lower light transmission. Any resin spills on the connector should be wiped off before heat-curing the resin.

When the resin has cured, the tip of the M3 or FC connector should have a small excess drop of resin on the 240 µm lumen (Figure 19E), which will hold the optical fiber core in place when the end of the fiber is polished. If the excess resin is not present, a 26 gauge needle or a piece of optical-fiber buffer can be used to apply a small drop of resin to the area (Figure 19F).

Step 4: Use the diamond scribe to make a small straight groove in the side of the optical fiber core, right at the edge of the hardened resin on the tip of the connector (Figure 20A). Flick-off the protruding length of optical fiber core to leave a level surface. Avoid breaking the core with the diamond scribe.

If working with the M3 connector, insert the internally threaded nut (provided by the manufacturer) until it reaches the connector (Figure 20B).

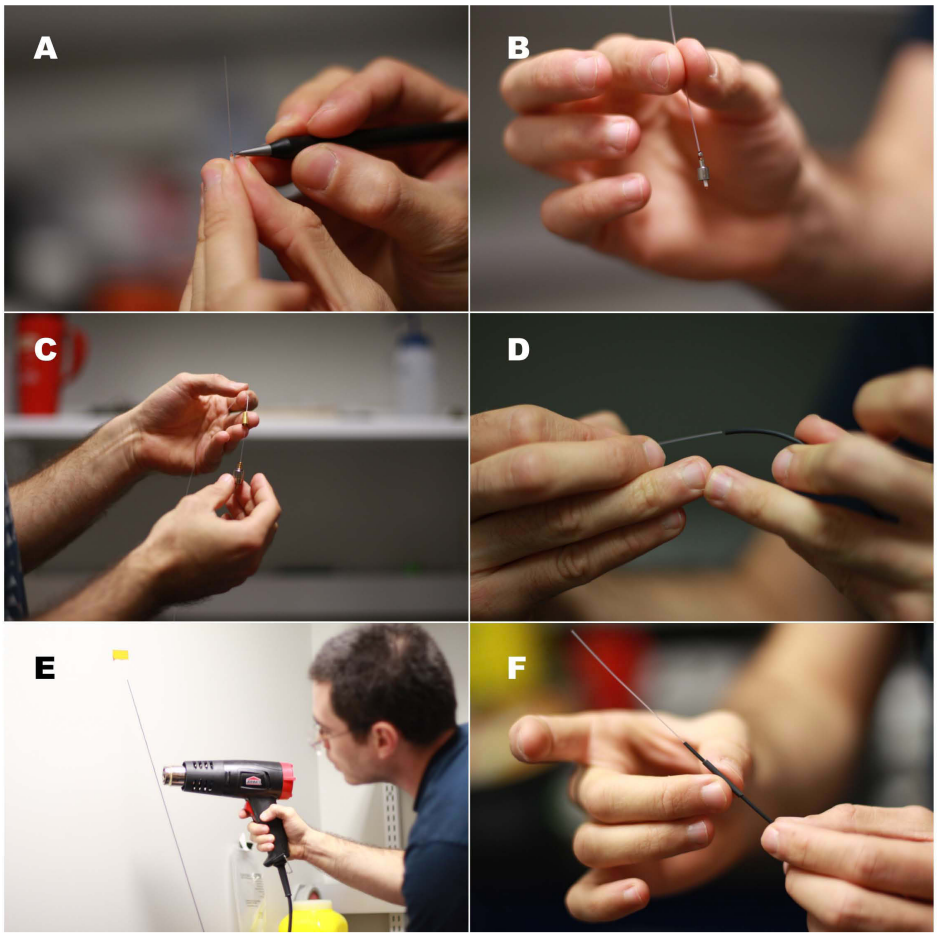

Figure 20. **A** Making a groove at the edge of the fiber. Notice that the diamond wedge scribe is kept horizontal. Do not break the optical fiber core doing this. **B** An M3 connector with the leveled cut and the bolt. **C** The boot of the FC connector is inserted. The boot should be crimped-on tightly using the specialized crimping tool. **D** Inserting the optical fiber through the 3/64" shrink tubing. **E** Shrinking the 3/64" shrink tubing tightly onto the fiber. Make sure it is even, "bumps" would not allow the stainless steel compression spring to fit through. **F** Insert the small shrink tubing provided with the M3 connector over the new cladding. Push it all the way through but do not shrink it yet.

If working with an FC connector, pass the optical fiber through the metal boot (Figure 20C) and crimp it in place using the special-purpose tool (not shown).

Step 5: Cut a piece of 3/64" shrink tubing (approximately 10% shorter than the length of the optical fiber), and pass the optical fiber through it in until it is in contact with the

connector (Figure 20D). Secure the fiber to a vertical surface, and with the connector facing downwards, apply heat to evenly and tightly shrink the tubing around the fiber (Figure 20E). Make sure that the shrink tubing cladding is even; avoid having bumps on the tubing.

If working with M3 connectors, pass the small-bore shrink tubing (provided by the manufacturer, Figure 20F) over the fiber until it protrudes slightly beyond the metallic end of the M3 connector. Do not shrink this tubing until the fiber tip has been properly polished (see Step 11).

If working with the FC connector, slide the rubber protector provided by the manufacturer over the metallic boot (not shown).

Step 6: Pass the optical fiber through the stainless-steel compression steel spring (Figure 21A), and strip 45-50 mm of the optical fiber beyond the connector (Figure 21B). When stripping, avoid leaving a large gap of unstripped fiber between the shrink tubing and the exposed optical fiber cladding (a small gap, between 5 and 8 mm long, is acceptable, Figure 21C).

Step 7: Place a stainless-steel ferrule in the third hand. (The 240 µm drilled part should face downwards). Fill up the internal volume of the ferrule with heat-curable epoxy, and pass the long section of exposed fiber core all the way through until it cannot be pushed any further. It is very important to remove all traces of resin from the inserted optical-fiber core. This can be done using a delicate-task wipe and alcohol. Do not cure the resin inside the ferrule until certain that the fiber core is resin free. Apply heat to cure the resin and fix the ferrule in place, making sure to leave approximately 40 mm of optical fiber core protruding from the ferrule (Figure 21D).

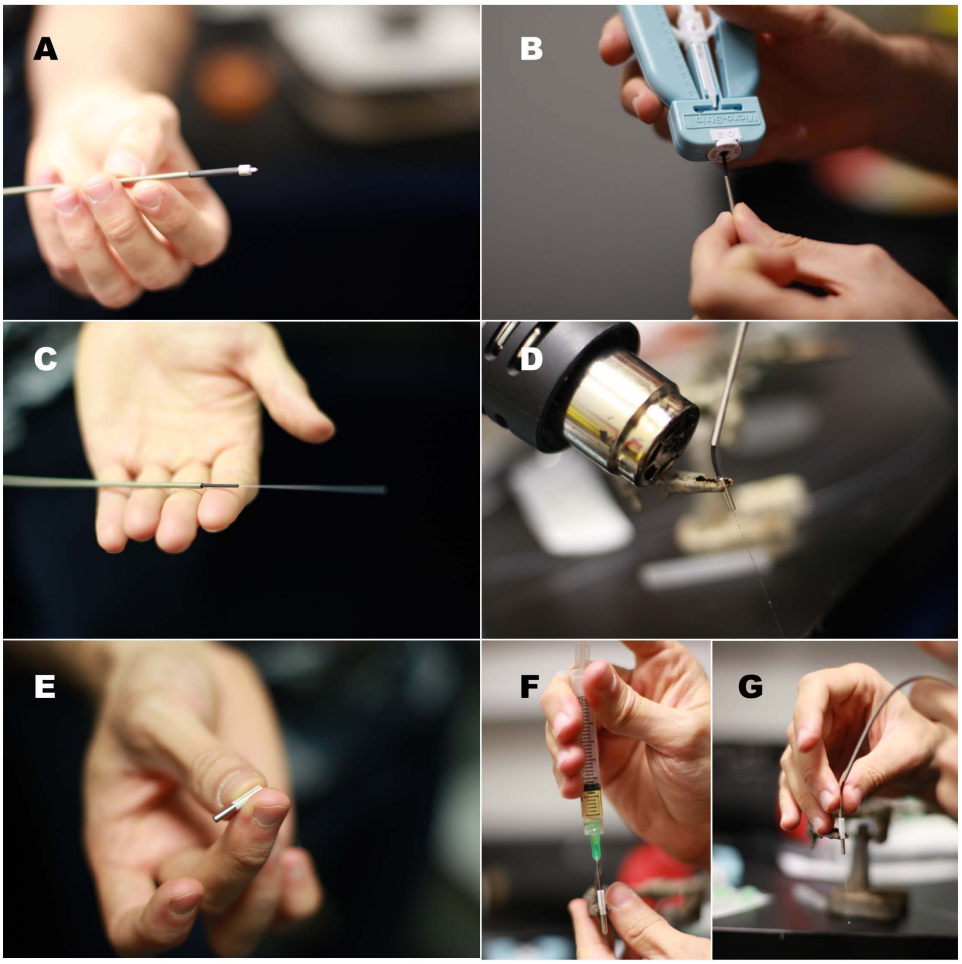

Figure 21. **A** An unfinished patch cord with the stainless steel compression spring and the small shrink tubing from the M3 connector inserted through it. **B** Striping the other end of the optical fiber. **C** The spring, shrink tubing, and exposed optical fiber cladding are shown. **D** The exposed optical-fiber core is passed through a ferrule loaded with resin. The drops of resin that accumulate on the core should be wiped off before heat-curing the resin. **E** A ceramic split sleeve is attached to the edge of a ferrule (on the side with the large opening). **F** The component shown in Figure 3E is loaded with resin. A thin layer of resin should also cover the internal walls of the ceramic sleeve. **G** The optical fiber core shown in Figure 3D is passed through the second ferrule until both ferrules are in direct contact.

Step 8: Fasten a ceramic split sleeve to another ferrule, making sure the 240 µm lumen is facing away from the sleeve and that most of the ferrule remains exposed (i.e. about 1/4 of the length of the ferrule should enter the ceramic sleeve, Figure 21E). Step 8:

“Attaching this second ferrule to the patch cord provides a rigid area to grip when attaching and detaching the cable. This also prevents the cable from bending sharply as the animal makes sudden movements and reduces the likelihood that contact with the levers or the chamber walls will detach, break, or dislodge the patch cord. In our hands, cables with single ferrules at the tip have a shorter half-life than those built using two ferrules in tandem.

Place the attached ferrule on the third hand and load it with heat curable epoxy (Figure 21F). Allow for some resin to reach the inside of the ceramic sleeve. Insert the optical fiber core through the ferrule, until both ferrules are in contact with each other within the ceramic sleeve (Figure 21G). Remove excess resin and heat cure the remainder in place.

When the resin has cured, a small excess should remain at the tip of the ferrule. If not present, gently apply a very small amount of resin to the area (as in Figure 19F). Again, use the diamond scribe to make a groove on the side of the optical fiber core, at the edge of the cured resin. Make sure not to break the fiber when making the groove. Flick to cut the fiber at the level of the groove.

Step 9: Push the spring over the fiber until it is in contact with the ferrule. Insert the end with the attached ferrules through a 2” piece of the adhesive shrink tubing (Figure 22A). Push the ferrules through the adhesive shrink tubing until the ferrule glued to the tip of the cord protrudes completely and some shrink tubing covers a section of the spring; the attached ceramic sleeve should be almost completely covered by the tubing. Heat-shrink the tubing in place, making sure the spring is in close contact with the ferrule. Apply light pressure around the tubing while it is still hot to produce tight contact with the spring and the ceramic sleeve below it. (Be careful: the tubing can be very hot!). Some adhesive from the inside of the tubing may spill out. Avoid getting it on the exposed ferrule. This step stiffens the tip of the patch cord and secures the spring in place (Figure 22B).

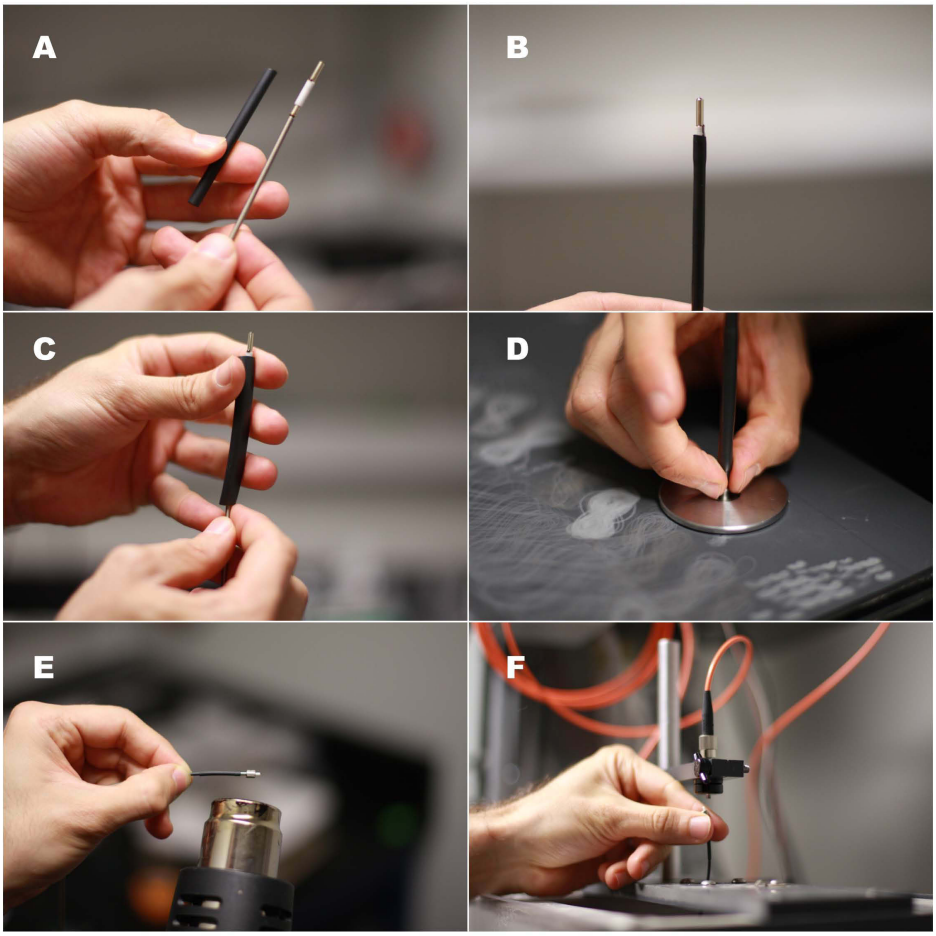

Figure 22. **A** A piece of adhesive shrink tubing is inserted through the tip of the patch cord, keeping the spring in contact with the ferrule. Note that the excess optical-fiber core has already been flicked off at this point, similarly to Figure 2A. **B** The aspect of the semi-rigid tip when the adhesive shrink tubing has been fixed in place. **C** Adding an extra layer of protection and rigidity by inserting a piece of 1/4" shrink tubing. **D** Use the 5 µm silicon carbide polishing paper and disk to polish the cured resin off the tip. Notice the "eight shape" marks left on the paper. The polishing disk can also be used with FC connectors. **E** Shrink the short piece of shrink tubing provided with the M3 connector in place. Make sure to wrap it onto the metallic part of the connector and the covered optical fiber. Do not do this until the fiber has been properly polished: it may make visualizing through the 200X fiber scope more difficult. **F** Attaching the M3 connector to the corresponding 1x1 optical swivel (Doric lenses, Québec, Québec, Canada) for testing.

Step 10: Strengthen the tip by inserting it into a piece of 1/4" shrink tubing (approximately 2" long) and heat-shrinking this tubing over the already stiffened patch-

cord tip (Figure 22C), taking care to leave the ferrule exposed. This step can be repeated until the desired rigidity or external diameter is achieved. We recommend using at least one layer of 1/4 inch shrink tubing.

Step 11: Fibers need to be adequately polished to achieve optimal performance; instructions can be downloaded for free from the manufacturer's web site: https://www.thorlabs.com/thorproduct.cfm?partnumber=FN96A. Polish the tip of the patch cord on the 5 µm silicon carbide polishing paper by repeatedly tracing a figure eight pattern with the exposed ferrule tip. Use the polishing puck to keep the ferrule vertical while polishing (Figure 22D). Applying too much pressure when polishing can damage the optical-fiber core. Once the cured resin at the tip of the ferrule has been polished away, clean the tip of the fiber using isopropyl alcohol and a delicate-task wipe. Replace the silicon carbide paper with the 3 µm polishing paper and repeat the polishing process. It is helpful to keep this fine polishing paper clean between polishes by using isopropyl alcohol and delicate-task wipes. Lubricatin the patch-cord tip with a drop of distilled water makes the polishing process easier. Repeat the process with progressively finer polishing paper (i.e. 1 µm and 0.3 µm) until the polished optical fiber core appears circular, smooth, light gray, and without scratches when viewed through the 200X fiber scope. Repeat these steps to polish the FC connector.

If using an M3 connector, clamp a straight hemostat to the connector tip and keep it flat against the polishing paper (Sparta et al, 2011). Make sure the long axis of the tip of the connector is perpendicular to, and in touch with, the paper. Polish by drawing a series of figure eight on the silicon-carbide paper with the tip of the connector. The hemostat should help avoid uneven polishing. Continue the process on progressively finer paper, as you did to the other end of the patch cord. The optical fiber core should be circular, light gray, and glossy when viewed through the fiber scope. The small shrink tubing from the M3 connector should extend slightly over the metallic part of the connector so as to wrap around it and the optical fiber, while still allowing the threaded nut to rotate and move along the base of the connector (Figure 22E).

Step 12: Test the patch cord in the behavioral apparatus. Attach the patch-cord connector to the optical rotary joint (Figure 22F) or the corresponding light output of

your setup. Carefully point the patch cord tip towards a vertical non-reflective surface and turn on the light source. (Caution: do not use full laser power in this test, and wear appropriate protective goggles, except when you are certain that the beam is pointing away from you, and you wish to view the pattern it forms on the non-reflective surface). A properly polished patch cord will produce a pattern of closely spaced concentric rings (Figure 23A). Confirm that the desired optical power is emitted by the patch cord by using the photodiode sensor and the optical-power meter. Adjust the laser power to determine the maximal light output from the cord. If the patch cord is properly built and polished, the light loss should not exceed 15% per connection (top and bottom). It is best to provide "headroom" by using patch cords that exceed the required output. Avoid using patch cords that cannot transmit at least 10% more power than required in the experiment. Insert the metal ferrule at the patch-cord tip halfway into a ceramic sleeve (Figure 23B). The metallic ferrule attached to the optical implant should fill the empty half of the ceramic sleeve so that both ferrules are in close contact inside the sleeve (Figure 23B inset).

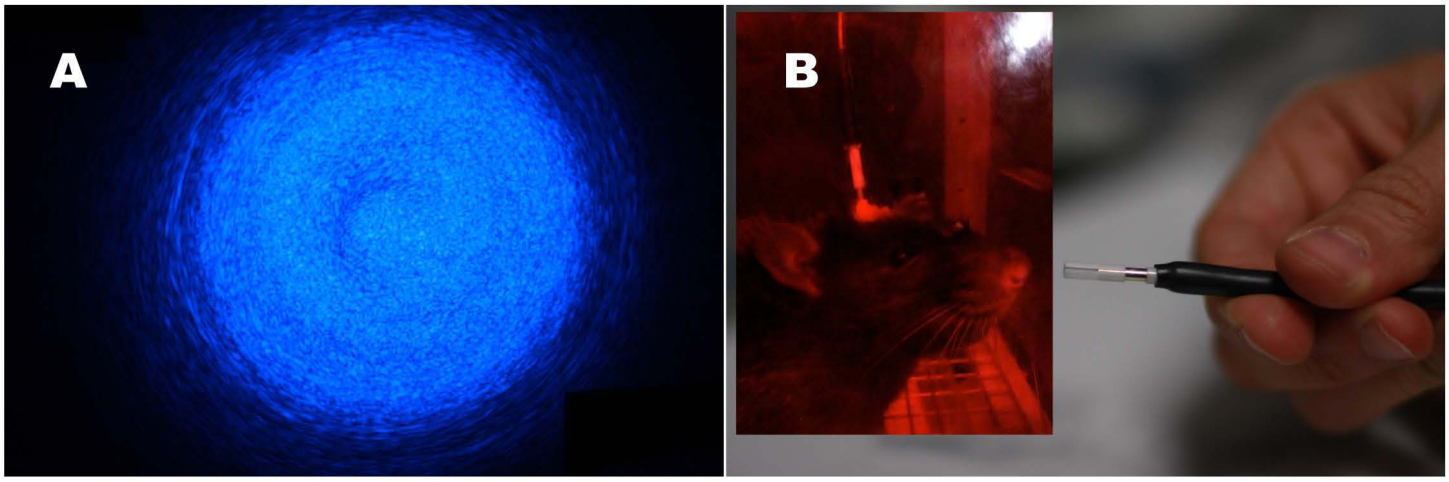

Figure 23. **A** Visual inspection. The light coming out from the patch cord tip should be concentric. **B** A ceramic sleeve is attached halfway through the tip of the patch cord. *Inset:* The ferrule from the implanted fiber on the rat's head should occupy the other half, keeping both ferrules in direct contact with each other.

These patch cords have held up well for several months under heavy use in daily experimental sessions lasting from four to eleven hours. We have used them successfully with or without a counterbalancing arm (MED associates inc. St. Albans, VT. Product number: PHM-110-SAI). When cut to a length of 2.32 ft (71 cm) the patch cords weigh approximately 0.49 oz (14 g).

ADDITIONAL INFORMATION: "DAMAGE PREVENTION AND MAINTENANCE"

Always handle the patch cord by the reinforced ferrule tip. This is particularly important when detaching it from the optical implant: pulling directly on the cord may damage it.

On rare occasions, the patch cord may detach from the rat's head during an experimental session, and the rat may seize it and bite it. This can be prevented by routinely replacing the ceramic sleeve that connects the cord to the optical implant; these sleeves tend to loosen with continued use.

The metallic shielding and tubing layers tend to survive some nibbling by a rat. When this occurs, new layers of 1/4" shrink tubing can be used to re-strengthen the damaged part. In rare cases, a rat may become adept at detaching the patch cord, and may destroy it if given enough time. Thus, it is useful to apply a few drops of a quinine solution to the patch cord tip to dissuade the animal from biting.

After several months of usage, some loss of power may occur. This can be remedied by gently wiping the ferrule end with alcohol, or by re-polishing it if the problem persists.

CHAPTER 4

Two-stage integration of reward intensity in midbrain dopamine neurons and in their afferents

Ivan Trujillo-Pisanty[1], Pavel Solis[1], Daniel Palacios[1], Dayane Karkouti[1], Kent Conover[1], Marie-Pierre Cossette[1], Ilana Witten[2] , Karl Deisseroth[3], and Peter Shizgal[1+]

[1]Department of Psychology, CSBN, Concordia University, Montreal, QC, Canada, H4B 1R6.

[2]Department of Psychology, Princeton University, Princeton, NJ, 08540.

[3]Department of Bioengineering, Stanford University, Stanford CA, 94305.

Unpublished manuscript, in preparation.

ABSTRACT

We have demonstrated previously that DA signaling affects electrical IntraCranial Self-Stimulation of the MFB (eICSS) downstream from the spatio-temporal integrator that computes reward growth: the DA reuptake blocker, GBR12909, increases the opportunity-cost that maintains half-maximal allocation of time to pursuit of a maximal reward (the P_e location parameter) but does not alter the electrical pulse frequency required to attain a half-maximal reward intensity (the F_{hm} location parameter) (Hernandez et al., 2012). Here, we show partially contrasting results in TH::Cre rats working for optical IntraCranial Self Stimulation (oICSS) of midbrain-DA neurons. As in the eICSS paradigm, GBR12909 increased P_e, but unlike its action in the eCISS paradigm, the drug decreased F_{hm}. This dissociation proves that the directly stimulated neural substrates supporting eICSS and oICSS are neurochemically different. In a companion experiment, the rewarding signal recruited in oICSS of midbrain DA neurons was shown to vary as a function of pulse-frequency and power. This implies that the rewarding signal from DA stimulation is integrated spatio-temporally, as is the rewarding signal arising from the activation of the non-DA neurons subserving eICSS. Overall the results support the view that eICSS and oICSS arise from direct activation of different stages of the reward processing system, which computes reward intensity by means of an integration process comprising more than one stage. DA signaling may be involved in multiple computational processes that determine reward seeking.

KEYWORDS: Dopamine, reward, GBR12909, TH::Cre rats, neuroeconomics.

INTRODUCTION

Electrical stimulation of the Medial Forebrain Bundle (MFB) at the level of the lateral hypothalamus is rewarding (Gallistel et al., 1981; Olds & Milner, 1954): laboratory animals will work vigorously to deliver trains of electrical pulses to this pathway (electrical IntraCranial Self-Stimulation, eICSS). Similarly, selective optogenetic activation of midbrain dopamine (DA) neurons is sufficient to support operant behavior

(optical Intracranial Self-Stimulation, oICSS) (Ilango et al., 2014; Witten et al., 2011). Even though eICSS and oICSS yield behavioral outputs that are similar *prima facie* (Steinberg & Janak, 2012), this does not prove that the directly stimulated substrate (and underlying neural computations) responsible for eICSS is identical to that supporting oICSS. In fact, the stage of reward processing recruited by electrical and optical stimulation, and perhaps the underlying neural computations (and psychological processes) as well, likely differ. The rewarding effect of eICSS of the MFB continues to grow over a range of stimulation frequencies that far exceeds the maximum firing frequency of midbrain DA neurons (Anderson, Fatigati, & Rompré, 1996; Bielajew, Lapointe, Kiss, & Shizgal, 1982; Cossette, Conover, & Shizgal, 2016; Gallistel et al., 1981; Murray & Shizgal, 1996b; Rompré & Miliaressis, 1987; Rompré & Shizgal, 1986; Shizgal, Bielajew, & Rompre, 1988; Solomon, Trujillo-Pisanty, Conover, & Shizgal, 2015; Yeomans, 1979; Yeomans, Maidment, & Bunney, 1988). The threshold for direct extracellular stimulation of DA axons (which are unmyelinated) is considerably higher than the threshold implied by the stimulation parameters required to produce rewarding stimulation (Shizgal et al., 1980; Yeomans et al., 1988). At least some of the reward-relevant MFB fibers project rostro-caudally whereas midbrain DA neurons send their projections caudal-rostrally (Bielajew & Shizgal, 1986). Finally, the conduction velocities of midbrain DA neurons ranges between 0.3-0.9 m/s while the conduction velocities of the reward-relevant fibers recruited by eICSS is much faster: 2.2-7.2 m/s (Bielajew et al., 1982; Bielajew & Shizgal, 1982; Murray & Shizgal, 1994; 1996a; 1996b). Overall, these findings strongly suggest that at least some of the reward-relevant axons in eICSS are non-dopaminergic, myelinated fibers that arise from rostral MFB nuclei projecting to the Ventral Tegmental Area (VTA).

The subjective intensity of the electrical reward is determined by spatio-temporal summation of the post-synaptic effects produced by the action potentials triggered in the directly stimulated substrate (Gallistel, 1978; Gallistel et al., 1981). The number of reward-relevant fibers recruited by electrical stimulation pulses of a given duration is dependent on the current (which determines the radius of excitation), whereas the number of action potentials in a given fiber that are triggered by a stimulation train of

given duration depends on the pulse frequency (Gallistel, 1978; Gallistel et al., 1981). Similar behavioral outputs can be obtained by stimulating a small set of reward-relevant axons at high frequencies or a large number of axons at low frequencies. This suggests that the number of action potentials produced by the electrical stimulation is integrated spatio-temporally to yield a representation of subjective reward intensity (Figure 24.1 and 24.2). The rewarding effect increases rapidly as a function of train duration, pulse-frequency, and current, but eventually saturates (Gallistel & Leon, 1991; Leon & Gallistel, 1992; Simmons & Gallistel, 1994; Solomon et al., 2015; Sonnenschein, Conover, & Shizgal, 2003). At later stages of processing, the subjective reward intensity is weighed against the costs entailed in procuring a stimulation train (Figure 24.4) in order to compute the net *payoff* provided by the electrical stimulation (Figure 24.5). The payoff from eICSS is compared against the payoff from other activities the animal could perform in the operant chamber (such as grooming, resting, or exploring) to ultimately determine how much time should be invested in pursuing the electrical reward (Figure 24.6; Arvanitogiannis & Shizgal, 2008; Breton, Conover, & Shizgal, 2014; Hernandez et al., 2010; Shizgal, 2012).

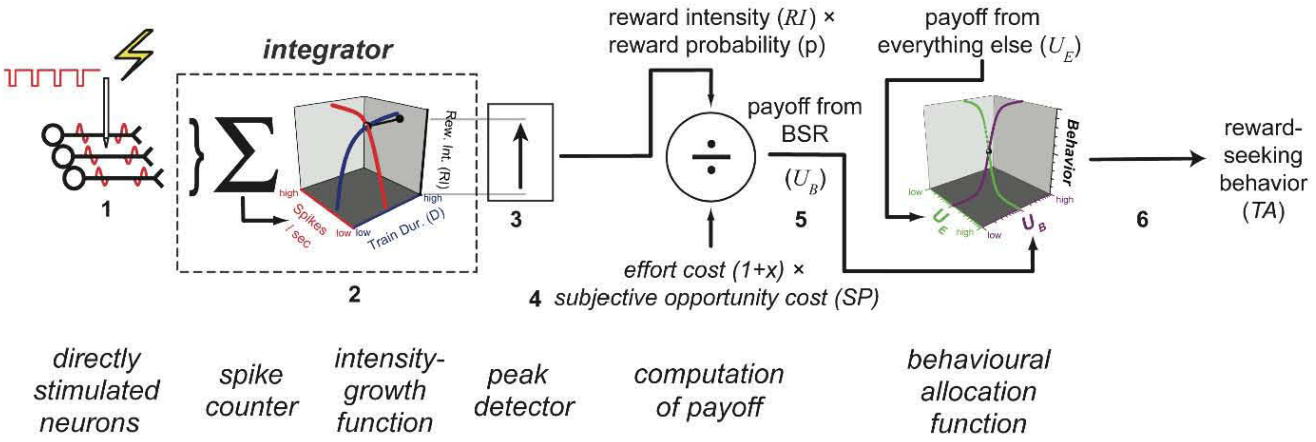

1: $$FF = F_{bend} \times \left[\mathrm{Ln}\left(1+e^{\frac{F_{NearMax}}{F_{bend}}}\right) - \mathrm{Ln}\left(1+e^{\frac{F_{NearMax}-F}{F_{bend}}}\right) \right]$$

2: $$RI(D,FF) = RI_{\max} \times \frac{FF^{g}}{FF^{g} + \left[FF_{hm_R}\left(1+\frac{C}{D}\right) \right]^{g}}$$

3: $$RI_{peak} = RI_{max} \times RI(t, FF_{sat})_{t=D}$$

4: $$SP = SP_{\min} + SP_{bend} \times \mathrm{Ln}\left(1+e^{\frac{P-SP_{\min}}{SP_{bend}}}\right)$$

5: $$U_{BSR} = \frac{RI_{peak}}{SP \times (1+\xi)}$$

6: $$TA = \left[(TA_{\max} - TA_{\min}) \times \frac{U_{bsr}{}^{a}}{U_{bsr}{}^{a} + U_{e}{}^{a}} \right] - TA_{\min}$$

Figure 24. An overview of the factors that determine reward seeking according to the reward-mountain model, as formalized by Breton et al. (Breton et al., 2013). **1.** Frequency following: The pulse frequency delivered through the electrode tip is translated into a firing frequency (*FF*) in the directly stimulated substrate for eICSS, as described by (Solomon et al., 2015). **2.** Reward growth: Subjective reward intensity (*RI*) is determined by *FF*, the induced firing frequency and the train duration, as described by (Sonnenschein et al., 2003) **3.** Reward gain: the maximal reward intensity at a given train duration is achieved when the directly stimulated neurons are driven at their maximal firing frequency (FF_{sat}). The reward-intensity signal peaks at the end of the train and is scaled by RI_{max}. **4.** Subjective price: Objective prices are translated into their subjective equivalents, as described by (Solomon, 2014). **5.** Payoff: The payoff from the rewarding stimulation (U_{BSR}) is computed by scalar combination of the peak subjective reward intensity and the subjective opportunity and effort costs of the reward. **6.** Time allocation: The proportion of trial time spent working for the reward (TA) is determined by the behavioral-allocation function. This function compares the payoff from the electrical

or optical reward (U_{BSR}) to the payoff from competing activities such as resting, grooming, or exploring (U_e). See Breton et al. (2013) for further details.

In the curve-shift paradigm, changes in subjective reward intensity (Figure 24.2) produce horizontal displacements of the psychometric curves. However, other variables such as reward probability and cost (Figure 24.4) can produce similar curve shifts (Figure 25). This makes the results from the curve-shift paradigm ambiguous: if a given experimental manipulation produces horizontal displacements of the psychometric curves, these shifts could be due to changes in subjective reward intensity, reward probability or cost. Strictly speaking, the curve-shift method yields global information about the *effectiveness* of a reward (as reflected by the amount of stimulation required to produce a given level of behavioral output) rather than specific information about the subjective reward intensity produced by the electrical stimulation.

The firing of DA neurons in response to electrical stimulation is correlated with the reward effectiveness of the stimulation (Moisan & Rompré, 1998). In accordance with the counter model, the pulse frequency required to obtain a similar behavioral output differed between two different electrical currents. However, midbrain DA neurons fired as if they were coding for the behavioral effectiveness of the stimulation rather than the objective current or pulse frequency delivered through the electrode tip (Moisan & Rompré, 1998). This correlational evidence suggests that midbrain DA neurons may constitute a stage of neural processing downstream from the directly stimulated neurons. Neural activity in this downstream stage closely matches the integrated signal that contributes to the overall effectiveness of the electrical reward. Indeed, the stimulation of descending reward-relevant MFB fibers (Bielajew & Shizgal, 1986) recruits midbrain DA neurons transynaptically (Cossette et al., 2016; Kita, Kile, Parker, & Wightman, 2009), and eICSS of the MFB is modulated by the activity of DA neurons in the VTA (Wise, 1996). In addition, we have provided causal evidence that DA modulation of eICSS occurs at a stage downstream from the initial integration of reward intensity. Different pharmacological manipulations affecting the DA system consistently

affect the opportunity cost at which rats will work at a given level for a fixed reward without changing the subjective reward intensity (Figures 24.1 and 24.2) (Hernandez et al., 2010; 2012; Trujillo-Pisanty et al., 2011; Trujillo-Pisanty, Conover, & Shizgal, 2013). This suggests that DA signaling affects eICSS by altering the maximal attainable reward value (i.e. reward gain) (Figure 24.3) (Hernandez et al., 2010), the subjective price of the reward (i.e. effort, or opportunity costs, Figure 24.4), and/or the value of alternate activities (Figure 24.5). One of the objectives of the present chapter is to test the causal role of DA neurons in computing reward intensity by means of optogenetics and a behavioral paradigm that can differentiate between subjective reward intensity and other variables affecting reward seeking.

The selectivity and temporal resolution offered by in-vivo optogenetic manipulations provide unparalleled advantages for establishing causal relationships between midbrain DA neurons and reward pursuit (Steinberg & Janak, 2012). The success of this endeavor depends on the power and validity of the behavioral paradigms employed and on the computational framework linking independent and dependent variables. Shizgal's reward mountain model is a neuroeconomic formalization that was first developed to predict eICSS performance as a function of reward intensity and cost (Arvanitogiannis & Shizgal, 2008; Breton, Mullett, Conover, & Shizgal, 2013; Hernandez et al., 2010; Shizgal, 2012). This approach overcomes the limitations of the curve-shift paradigm in differentiating changes in subjective reward intensity (Figure 24.2) from changes in other variables affecting reward seeking (Figure 24.4).

The reward-mountain model and the associated testing paradigm relate the proportion of trial-time rats spend working for eICSS (Time Allocation, TA) to two independent variables: the strength of the reward (i.e. electrical or optical pulse-frequency) and its opportunity cost (i.e. the "price", the cumulative amount of time the animal must work to harvest a reward). Fitting the mountain model to such data generates a surface that predicts how much the rat will work for any combination of reward strength and price. The location of the fitted structure along the pulse-frequency axis (Figures 24.1 and 25) is determined by the subjective reward intensity, which, in turn, arises from spatio-temporal integration of the output of the directly stimulated neurons subserving the

rewarding effect (Figure 24.2). Any experimental variables affecting reward seeking by actions prior to the output of the reward-intensity-growth function shift the 3D structure along the pulse-frequency axis, changing the pulse frequency required to attain a half-maximal reward intensity (the F_{hm} parameter) (Figure 25A and 25B). Several variables can affect the location of the structure along the price axis. These variables change the price at which a reward of maximal strength supports half-maximal time allocation, the location parameter P_e (Figure 25A and 25C). The variables that alter P_e include the reward-intensity scaling constant, RI_{max}, which determines reward gain, and the subjective values of effort cost, opportunity cost, reward probability, and alternate activities. In later stages of processing, the probability-weighted value of reward intensity is discounted by reward costs to compute the payoff from brain stimulation (Figure 24.4), which is compared with the payoff from competing activities (Figure 24.5) to determine how much time should be invested in the pursuit of brain stimulation reward (Figure 24.6). Importantly, this three-dimensional approach allows for the behavioral dissection of variables affecting motivated behavior upstream and downstream from the output of the reward-intensity-growth function.

Optogenetic stimulation of midbrain DA neurons is not only selective to those cell types, but it also stimulates them directly, bypassing the MFB input to the VTA which is traditionally recruited by eICSS of the MFB. Because the firing of DA neurons in response to eICSS does not correspond to the objective stimulation parameters (Cossette et al., 2016; Moisan & Rompré, 1998) and pharmacological challenges of the DA system fail to alter the initial computation of reward intensity in eICSS of the MFB (Hernandez et al., 2010; 2012; Trujillo-Pisanty et al., 2011; 2013), oICSS likely targets the system at a stage downstream from the output of the reward intensity-growth function in eICSS of the MFB (Figures 24.3-24.6). Detailed quantitative behavioral testing of oICSS can yield important information in understating the psychological and computational role of midbrain DA neurons in reward seeking. In the present chapter, I used oICSS of midbrain DA neurons, pharmacological DA reuptake blockade, and the reward mountain model (Arvanitogiannis & Shizgal, 2008; Breton et al., 2013; Hernandez et al., 2010; Shizgal, 2012) to causally test wether eICSS of the MFB and

oICSS of midbrain DA neurons indeed target different neural substrates responsible for different computational and psychological processes in reward-seeking. My experiments also have implications on the role of DA neurons in computing reward intensity, payoff, and costs.

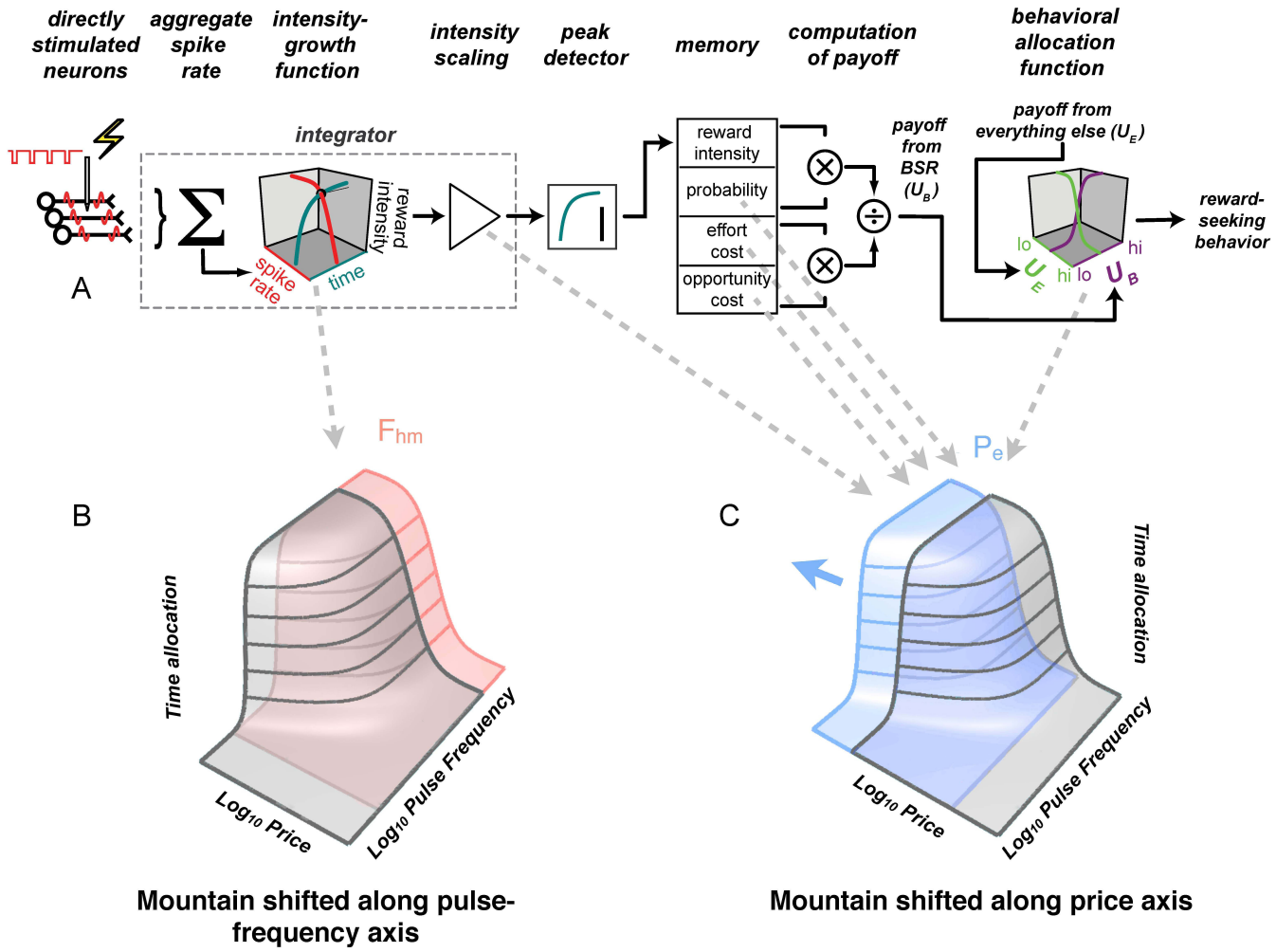

Figure 25. Changes in the location parameters of the mountain model reflect changes at different stages of reward processing. **A** graphical summary of the mountain model as explained in Figure 24. **B** Interventions acting prior to the output of the reward-growth function shift the mountain along the frequency axis as measured by a change in the F_{hm} parameter, that locates the structure along this axis. **C**

Interventions acting at or beyond the output of the integrator shift the 3D structure along the price axis, as measured by a change in the parameter of the reward-mountain model, P_e, that locates the structure along this axis. Modified from (Trujillo-Pisanty et al., 2011).

Dissecting the differences between eICSS of the MFB and oICSS of midbrain DA neurons.

In chapter 1, we showed that DA reuptake blockade increases the opportunity cost at which rats will work for eICSS of the MFB without affecting the subjective reward intensity (i.e. increases in P_e without changes in F_{hm}) (Hernandez et al., 2010; 2012). Conversely, in chapter 2 we showed that in the case of eICSS of the MFB, DA receptor blockade causes a decrease in P_e without affecting subjective reward intensity (Trujillo-Pisanty et al., 2013). These findings suggest that DA signaling affects eICSS beyond the point at which subjective reward intensity is computed. These findings also provide support for the transsynaptic activation of DA midbrain neurons by rewarding MFB stimulation: if the rewarding effects had been due to direct stimulation of DA neurons, than enhancing their output by means of DA reuptake blockade should have decreased the frequency required to attain a half-maximal reward intensity (i.e., the drug should have decreased F_{hm}). In this chapter, I report the effects of DA reuptake blockade on oICSS of midbrain DA neurons (which stimulates these cells directly). If eICSS of the MFB and oICSS of midbrain DA neurons recruit different stages of reward processing, then a given pharmacological manipulation (i.e. DA reuptake blockade) may affect the location parameters of the reward mountain model differentially in the two paradigms. The direct activation of DA neurons in the oICSS paradigm predicts that GBR12909 will decrease F_{hm} in oICSS, in contrast to the failure of this drug to do so in the eICSS paradigm.

Testing the role of DA neurons in reward intensity.

Compelling evidence from the eICSS paradigm implies that DA signaling influences reward-seeking beyond the initial integration of reward intensity. Nonetheless, midbrain DA neurons could still influence the subjective reward-intensity signal. For example, these neurons may transform an already-computed reward-intensity signal by rescaling it (multiplying the signal by a scalar, an effect to which we refer as a change in gain). In the case of a DA reuptake blocker (which boosts DAergic neurotransmission), the scalar would be greater than unity; all subjective reward-intensity values would be increased by the same proportion. If DA neurons comprise a transsynaptic stage of the circuitry subserving eICSS of the MFB, a stage positioned downstream from the point where subjective reward intensity is computed, we would expect DA reuptake blockade to increase P_e. In contrast, boosting the output of midbrain DA neurons that have been activated directly by optical stimulation in the oICSS paradigm should decrease the pulse frequency required to attain a half-maximal reward intensity (i.e., F_{hm} should decrease). The optically generated reward signal is also expected to undergo spatio-temporal integration (Ilango et al., 2014), in which case a given rewarding effect should be produced by high-frequency optical stimulation at low optical power, and by lower-frequency stimulation at higher optical powers. This chapter reports tests of these predictions, carried out by application of the mountain model in the oICSS paradigm and by power-frequency trade off experiments.

Testing the role of DA neurons in computing payoff.

Electrophysiological evidence from primates has been interpreted to argue that midbrain dopamine (DA) neurons are responsible for computing payoff. When primates chose between different rewards that varied in magnitude and likelihood, DA neurons fired as if they were coding the subjective economic value of each action (Lak, Stauffer, & Schultz, 2014). Moreover, DA prediction error signals match the non-linear utility functions representing subjective payoff (Stauffer, Lak, & Schultz, 2014). However, in rats facing choices between different reward magnitudes and different reward costs, phasic DA release in the nucleus accumbens in response to reward-predicting cues did not

incorporate behaviorally effective information about reward costs (Hollon, Arnold, Gan, Walton, & Phillips, 2014). This finding represents an important challenge to the idea that DA neurons encode payoff and ultimately determine choice. Nonetheless, the available evidence for and against the role of DA neurons in computing payoff comes from electrophysiological and neurochemical detection methods, which are strictly correlational. One of the aims of the work described in the present chapter is to test the role of midbrain DA neurons in computing payoff. The oICSS paradigm can establish casual relationships between specific neural manipulations and behavior. The computation of payoff requires the prior computation of subjective reward intensity (Figure 24.2) and subjective reward costs (Figure 24.4). If DA neurons encode subjective payoff, then their direct optogenetic stimulation would bypass signals representing reward intensity and cost, which would already be factored into the payoff signal represented by their induced activity. If so, the performance of the rats working for oICSS should not decrease as the opportunity costs increase. This would prevent us from fitting the mountain-model in its current formulation as the surface would fail to decline along the price axis (i.e. rats working for oICSS would be insensitive to increments in the price of the reward). Conversely, if performance for oICSS is affected by increments in the price of the reward, then the computation of payoff must occur downstream from midbrain DA output. If so, the mountain model should accurately predict changes in oICSS as a function of pulse-frequency and reward cost. Thus, if the mountain model can be used to predict changes in performance for oICSS from variations on reward cost, DA neurons cannot compose the final common path for the computation of payoff but rather constitute one of many neural populations that contribute to this process

Testing the role of DA neurons in computing reward cost.

As mentioned in the introduction to this thesis and demonstrated in chapters 1 and 2, one of the main advantages of the mountain model is that it can differentiate between pharmacological effects on the initial computation of reward intensity and effects on reward costs. These differential effects are reflected by the orthogonal location parameters of the mountain (F_{hm} and P_e). Thus, if midbrain DA neurons play a role in

computing the price of the reward, boosting their output by means of GBR12909 should increase the half-maximal price the rats are willing to work to obtain a maximal rewarding stimulation (i.e. an increase in P_e), regardless on whether they are stimulated directly (by means of oICSS) or indirectly (by means of eICSS). This effect is independent of potential drug-induced changes on F_{hm}. It is possible that in the oICSS paradigm midbrain DA neurons may be involved in computing reward intensity (reflected by changes in F_{hm}) as well as in computing reward cost (reflected by changes in P_e), perhaps through the differential involvement of phasic and tonic DA signaling (Schultz, 2002). The dual role of midbrain DA neurons in computing reward intensity and cost would be confirmed if GBR12909 produces changes in F_{hm} and P_e in rats working for optical stimulation of midbrain DA neurons.

METHODS

SUBJECTS: Seven TH::Cre, male, Long-Evans rats weighing 350 g at the time of surgery, served as subjects. Animals were obtained from the Shizgal-lab TH::Cre rat colony, established from three original TH::Cre sires generously donated by Drs. Karl Deisseroth and Ilana Witten. Upon reaching sexual maturity, animals were housed in pairs in a 12 h -12 h reverse light-cycle room (lights off at 8:00 AM). The rats were single housed following surgery.

SURGERY: Midbrain DA neurons were transfected with the light-sensitive cation channel *channel rhodopsin 2* (ChR2) fused to the reporter protein, *enhanced yellow fluorescent protein*. The construct was delivered by means of a Cre-dependent Adeno-Associated Viral vector (AAV5-DIO-ChR2-EYFP, University of North Carolina Viral Vector Core, Chapel Hill, NC). The virus was injected bilaterally (± 0.7 mm ML), at a volume of 0.5 μl, at three different DV coordinates (-8.2, -7.7 and -7.2 mm) and two different AP coordinates (-5.4 and -6.2 mm), to yield a total volume of 3.0 μl per hemisphere. Optical-fiber implants, 300 μm in core dimeter, were bilaterally aimed at the VTA at a 10° angle (AP: -5.8, DV: 8.02 or 8.12, ML: ± 0.7 mm). Anesthesia was induced

by an IP injection of Ketamine-xylaxine mix (87 mg/kg-13 mg/kg, Bionicle, Bellville, Ontario and Bayer Inc., Toronto, Ontario, respectably). Atropine sulfate (0.02-0.05 mg/kg, 1 mL/kg, Sandoz Canada Inc., Quebec) was injected s.c. to reduce bronchial secretions, and 0.3 mL of penicillin procaine G (300 000 IU/ml, Bimeda-MTC Animal Health Inc., Cambridge, Ontario) were administered SC, as a preventive antibiotic. "Tear gel" (1% w/v, 'HypoTears' Novartis) was applied to the eyes to prevent damage from dryness of the cornea. Anesthesia was maintained throughout surgery by means of isoflurane (1-2.5% + O2). The head of the rat was fixed to the sterotaxic frame (David Kopf instruments, Tujunga, CA) by means of ear bars inserted into the auditory canal and by hooking the incisors over the tooth bar. Bregma and the lambdoidal suture were exposed by a scalpel incision of the scalp. Three blur holes were drilled in the skull over each hemisphere (AP: -5.4, -5.8, and -6.2 mm; ML: ± 0.7, ± 2.08, ± 0.7, respectively). A 28 gauge injector was loaded with the viral vector. Six 0.5 µl boli of the virus-containing suspension were infused into each brain hemisphere at the following coordinates: AP: –5.4 and -6.2 mm; ML: +/- 0.7 mm; DV: -8.2, -7.7 and -7.2 mm. Infusions were performed at a rate of 0.1 µl per minute using a precision pump (Harvard Instruments) and a 10 µl hamilton syringe (Hamilton Labaoratory prodcuts, Reno, NV). To allow for diffusion, the injector was left in place for ten minutes following each infusion. Optical-fiber implants with a 300 µm core were constructed following the methods described by Sparta (Sparta et al., 2011). Optical fibers were aimed bilaterally at the VTA at a 10° angle. The implants were placed at two different DV coordinates to increase the chances of placing the tip of at least one of the optical fibers directly over the neurons that support optical self-stimulation (AP –5.8 mm; ML +/- 0.7 mm; DV –8.02 and -8.12 mm). The optical implants were anchored to the skull by means of stainless steel screws and dental acrylic. Gelfoam™ (Upjohn Company of Canada, Don Mills, Ontario) was used to fill the holes in the skull and promote healing. Buprenorphine (0.05 mg/kg SC, 1 mL/kg, RB Pharmaceuticals Ltd., Berkshire, UK) was used as a post-surgery analgesic. The rats were singly housed in the animal care facility for over five weeks to allow for surgical recovery and to achieve appropriate expression and distribution of the ChR2-EYFP construct.

APPARATUS: Three plastic operant boxes (30 21 51 cm) with a mesh floor and a clear Plexiglas front equipped with a flashing light located 10 cm above the floor mesh, and a retractable lever (ENV–112B, MED Associates) mounted on a side wall. A 1 cm light was located 2 cm above the lever and was activated when the rat depressed the lever. A blue laser (Shanghai Lasers and Optics Century Co. or Laserglow Technologies, Toronto, ON) was placed on the roof of each box. The laser was connected to a 1 x 1 FC/M3 optical rotary joint (Doric lenses, Quebec, Canada) by means of a laser coupler (Oz Optics Limitted, Ottawa, ON, or Thorlabs, Inc., Newton, New Jersey, USA) and fiber-optic cables. Robust, custom-built, optical-fiber patch cords designed for rats (Trujillo Pisanty, Sanio, Chaudhri, & Shizgal, 2015) were used to attach the implants in the animal's head to the 1 x 1 FC/M3 optical swivel so as to allow the rat to move without tangling the cable. Experimental control and data acquisition were handled by a personal computer running a custom-written program ("PREF") developed by Steve Cabilio (Concordia University, Montreal, QC, Canada). The temporal parameters of the electrical stimulation were set by a computer-controlled, digital pulse generator. Stimulation consisted of 1 s trains of blue (473 nm) light pulses, 5 msec in duration.

DRUG: GBR12909 was obtained from a generous donation by the NIMH Chemical Synthesis and Drug Supply Program. It was dissolved in 0.9% saline at a volume of 10 mg per ml. The pH of the solution was adjusted to 5 ± 0.1 with 0.1M NaOH.

SELF-STIMULATION SCREENING AND TRAINING: Each animal underwent two to three screening sessions in which only one of the optical implants was attached to the light source at a time. Optical power was measured by means of an optical power meter (PM100D, Thorlabs Inc., Newton, New Jersey, USA) and adjusted through trial and error for each rat to elicit robust oICSS behavior (30-60 mW, measured at the tip of the patch-cord with the laser operating in continuous-wave mode). Animals were trained by means of the successive approximation procedure to depress the lever to receive optical stimulation (a 1 sec train of 5 ms optical pulses at 80 Hz was delivered every time the rat performed the adjusting criterion required to earn a reward). After the rats had learned to lever press, they were allowed to work for the optical reward, on a

Continous Reinforcement (CRF) schedule, during two 15 min trials. The total number of presses was recorded. Both of the implants were tested under these conditions; the implant that yield the larger number of presses was used for the rest of the experiment.

REWARD-MOUNTAIN PARADIGM FOR oICSS: Figure 26 shows an overview of the behavioral procedure. Animals were trained to hold down a lever for a cumulative time (i.e. opportunity cost: price) to obtain optical stimulation of midbrain DA neurons by one of the implanted fibers. The mountain model requires systematic testing of self-stimulation across different pulse frequencies and opportunity costs (prices). One way to sample the space defined by the independent variables (pulse frequency, price) is to conduct frequency, price, and radial sweeps (Hernandez et al., 2010; Trujillo-Pisanty et al., 2011) along which pulse frequency, and/or price are systematically varied across trials. Initially, the rats were trained to keep the lever depressed for a cumulative time of 1-2 s to receive a 1 sec train of 5 ms pulses of blue light. The dependent variable was the proportion of trial time spent working for the reward (time allocation, TA(Breton, Marcus, & Shizgal, 2009)). Frequency sweeps (Hernandez et al., 2010) consisted of 10 to 12 trials during which the rat had the opportunity to harvest as many as 60 rewards (except for rat BeChr19, who was allowed to harvest a maximum of 30 rewards per trial due to the unusual effectiveness of optical stimulation in this subject). Each reward was followed by a 2 s Black Out Delay (BOD) during which the lever was disarmed and retracted, and timing of the trial-duration was paused. The pulse frequency during the first two trials was set to yield maximal TA. The first trial was considered a warm-up trial and was excluded from analysis. From the second trial onwards, the rewarding stimulation was decreased systematically from trial to trial by decreasing the pulse frequency in equal proportional steps. The range of tested pulse frequencies was selected as to drive TA from its maximal to its minimal value in a sigmoidal fashion (Figures 26B and 27). Every trial was preceded by a 10 s Inter-Trial Interval (ITI) signaled by a flashing light. During the last 2 s of this period rats received priming stimulation consisting of a non-contingent, 1 s stimulation train, delivered at the maximally rewarding pulse frequency. Rats performed one frequency sweep per

session, consisting of ten trials (except for subject BeChr19 who was tested on 12 trials per frequency sweep).

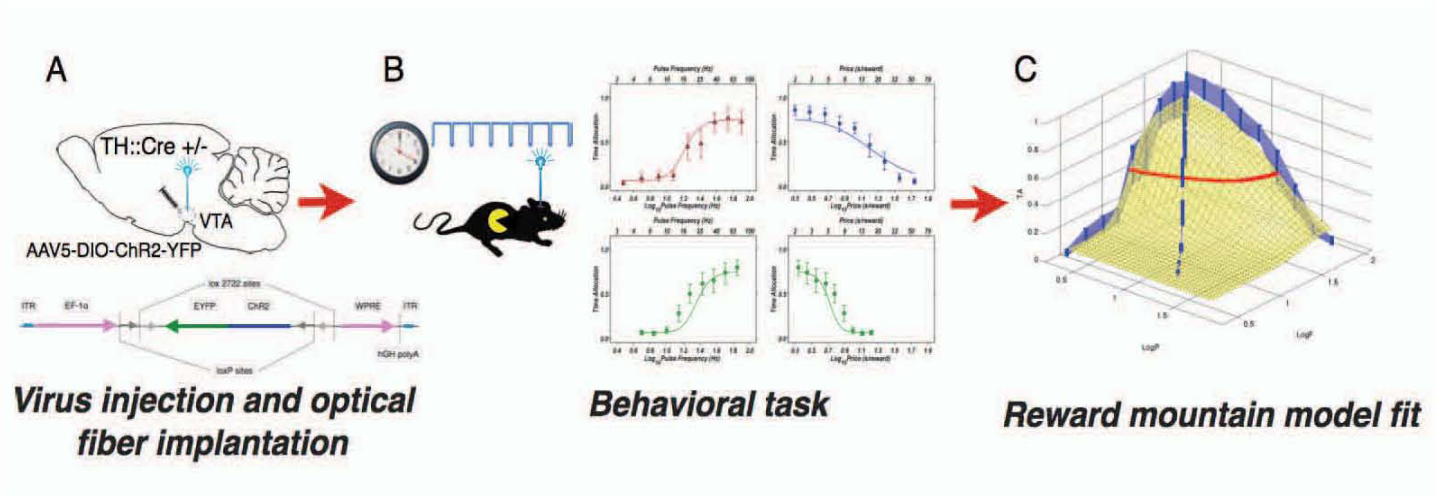

Figure 26. Graphical summary of the experimental procedure. **A** TH::Cre +/- rats received bilateral VTA injections of an AAV5 virus bearing a Cre-dependent, ChR2-YFP transcript. Optical fibers were bilaterally aimed at the VTA. **B** Rats were trained to hold down a lever for a specified cumulative amount of time to deliver trains of optical stimulation to the VTA. The red curve represents the proportion of trial time the rat spent working for the optical reward as the optical pulse frequency (the reward-strength variable) was systematically manipulated. The blue curve shows the proportion of trial time the rat spent working for a maximal optical reward as the cumulative amount of time required to harvest the reward (reward price) was systematically manipulated. The green curves show proportion of trial time the rat spent working for the optical reward as the strength and price of the reward were simultaneously manipulated. **C** The reward-mountain model was fit independently to the data from each rat following injection of GBR12909 or vehicle. Within subject comparisons were performed.

When the rats showed consistent performance across trials and sessions in the frequency-sweep condition, we incorporated “price sweeps” into the training sessions.

In the price-sweep condition, the pulse frequency was kept constant at the maximal value for each rat, but the cumulative work time required to harvest the reward (i.e. the price of the reward) was increased systematically across trials. The price was the same on the first two trials of each sweep. As in the frequency sweep condition, the first trial was considered a warm-up trial and was excluded from analysis. Starting at the second trial of the sweep, prices were increased by equal proportional steps across trials. The prices were set by trial and error so as to yield a sigmoidal transition between maximal and minimal TA as a function of price (Fig 26B and Fig 27). Trial duration was set so as to allow the rats to harvest a maximum of 60 rewards per trial (30 in the case of BeChr19). The BOD, ITI, and priming were the same as in the frequency sweep. During price-sweep training sessions, the rats also performed a frequency sweep. The order of the sweeps was randomized across sessions.

Radial sweeps were incorporated when the curve relating TA to price was sigmoidal in form and consistent in its position along the price axis. Along radial sweeps, the pulse-frequency was decreased and the price was increased simultaneously across trials. The radial sweeps were composed of ten trials; the first trial served as a warm-up and was identical to the second trial. From the second trial onwards, both pulse frequency and price were varied systematically in equal proportional changes so as to yield a sigmoidal decrease in TA over the course of the sweep (Fig 26B and Fig 27). The trajectory of the vector defined by the tested pulse frequencies and prices was aimed to pass as close as possible to the point defined by the estimated values of the F_{hm} and P_e location parameters (see model fitting section). This required fitting the mountain model to preliminary data from each rat and adjusting the pulse frequencies and prices tested along the radial sweep accordingly for the following session. Pulse-frequency and price sweeps were also performed in each session during this phase of testing. The order of presentation of the three different sweeps was random across sessions, and the BOD, ITI, and priming parameters were the same on all trials. Rats were considered ready for drug-test sessions when TA declined sigmoidally and consistently along all three sweeps and the trajectory of the radial sweep in the independent-variable space passed close to the point defined by the estimated values of F_{hm} and P_e.

EFFECTS OF GBR12909 ON oICSS IN THE REWARD-MOUNTAIN PARADIGM: Rats received i.p. injections 90 min prior to behavioral testing. Vehicle (2.0 ml/Kg) was administered on Mondays and Thursdays and GBR12909 (20 mg/Kg) on Tuesdays and Fridays. In each session, rats performed a frequency, a price, and a radial sweep in random order. Each sweep consisted of ten trials each (except for the frequency sweep for rat BeChr19, which consisted of 12 trials). The duration of each trial was set so as to allow rats to harvest a maximum of sixty rewards per trial (except for rat BeChr19, who was allowed to harvest a maximum of 30 rewards per trial due to his unusual proclivity to work for very high opportunity costs). Wednesdays and weekends were used as drug elimination days: no testing was conducted on these days, and the rats remained in the animal care facility. Ten vehicle and ten drug sessions were conducted with each rat.

MODEL FITTING AND COMPARISONS: The mountain model and the fitting approach have been described in detail elsewhere (Hernandez et al., 2010; 2012; Trujillo-Pisanty et al., 2011). Briefly, the six- and seven-parameter versions of the mountain model (Hernandez et al., 2010; 2012; Trujillo-Pisanty et al., 2011) were fit to the data from each rat independently (Figures 26C and 28). Both models include parameters that specify the location of the fitted surface along the frequency and price axes (F_{hm} and P_e respectively), its steepness (g and a), and the maximal and minimal TA (Figure 24). The seven-parameter version includes an additional term that estimates the contribution of conditioned reward (Hernandez et al. 2010). It allows for a more accurate fit if the lever and/or the act of depressing it become secondary reinforcers. The fits were carried out through a procedure developed by Kent Conover, based on the nonlinear least-squares routine in the MATLAB optimization toolbox (the MathWorks, Natick,MA) and on resampling methods (Efron & Tibshirani, 1994). The TA data from each rat were resampled with replacement 1,000 times by reward encounter (i.e. the time spent working for a given reward in each trial). Mean values for each parameter were obtained by averaging the 1,000 estimates. Confidence intervals were estimated by excluding the lowest and the highest 25 values of the 1,000 estimates. This yields unbiased estimates of the location and slope parameters and their dispersions for each subject. The Akaike

information criterion (Akaike, 1974) was used to select the model that offers the best balance between achieving a good fit and minimizing the number of parameters required to do so. Drug-induced shifts in the location of the 3D structure were considered significant when the 95% confidence interval around the difference between the 1000 resampled estimates of the location parameters across drug and vehicle conditions excluded zero (i.e. no difference between conditions).

POWER-FREQUENCY TRADE-OFF: Following the pharmacological experiment, we explored the effects of systematic changes in optical laser-power and pulse frequency on the number of rewards obtained by each rat. The same subjects were trained to press the lever on a CRF schedule to trigger optical stimulation of midbrain DA neurons through the same optical implant used in the reward-mountain experiment. We quantified the number of rewards each rat harvested in each of a series of nine or ten trials lasting two minutes each. The pulse frequency was decreased systematically across trials: the highest pulse frequency was in effect during the first trial of the series (the “warm-up”) and also on the second trial, and data from the first trial was excluded from analysis. Subsequently, the pulse-frequency decreased in equal logarithmic steps from trial to trial. A single pulse-frequency sweep was run in each of five to six sessions per day. In each session, the optical power (measured at the tip of the patch-cord with the laser operating in continuous-wave mode) was set to one of five values (1.87, 3.75, 7.5, 15 or 30 mW for rat Bechr14; 3.75, 7.5, 15, 30, or 60 mW for rats Bechr21, Bechr28 and Bechr29; and 2.5, 5, 10, 20, and 40 mW for rats Bechr19, Bechr26, and Bechr27). The rats were tested under these conditions for five days. The order of presentation of optical powers was determined pseudorandomly for each rat. Each power was presented in a different sequential order across each testing day (i.e. each power was used 1st, 2nd, 3rd, 4th, or 5th at least once across days, but the preceding and/or subsequent tested powers may have been different across test days). To control for carry-over effects across test sessions, rats were given 30-minute breaks between each session: following completion of each of the five to six daily sessions, they were taken out of the operant chambers, brought back to their home cage in the animal care facility, and had free access to food and water for 30 minutes before resuming with the

following test session. During this 30 minute break, the lasers were set to continuous operation mode to minimize potential power-output instability resulting from the cooling of the laser.

HISTOLOGY: Rats were sacrificed by means of a lethal injection of pentobarbital i.p. After deep anesthesia had been induced, the rats underwent intracardiac perfusion with phosphate-buffered saline and 4% paraformaldehyde chilled to 4 °C. Upon extraction, the brains were stored in a solution of 4% paraformaldehyde and 30% sucrose for forty eight hours at 4 °C and transferred to a -20 °C freezer thereafter. The brains were sliced coronally in 40 µm sections by means of a cryostat, and mounted in electrostatically adhesive slides (Fisherbrand™ Superfrost™ Plus slides, Fisher Scientific,Pittsburgh, PA). Immunocytochemistry was performed on slide-mounted sections for Tyrosine hydroxylase and YFP with the following antibodies and concentrations: mouse anti-GFP, 1:1000 (Invitrogen, Life Technologies, Burlington, ON); Rabbit anti-TH, 1:100 (Fischer Scientific, Pittsburgh, PA); Alexa fluor 488 donkey anti-mouse, 1:200 (Jackson ImmunoResearch, Laboratories, Inc. West Grove, PA); Alexa fluor 594 donkey anti-rabbit, 1:200 (Jackson ImmunoResearch, Laboratories, Inc. West Grove, PA). Sections were coverslipped using Vectashield with DAPI (Vector Laboratories Inc. Burlington, Ontario, Canada) as mounting medium. Low- and high-magnification images were obtained by means of confocal microscopy (Nikon Eclipse TiE inverted C2). High-magnification 3D reconstruction was achieved by means of the 3D view, image snapshot, and animation tools in Imaris scientific software (Bitplane. Concord, MA). Non-linear gamma adjustments were made to reveal detail in high-magnification images and video.

RESULTS

Figure 26 shows a graphical summary of the behavioral strategy; more details are provided in the methods section.

In all of the rats included in this study, TA varied as a function of optical pulse-frequency and reward price. Rats spent more time working for the optical stimulation when the rewards were strong and cheap: performance decreased in a sigmoidal fashion as a function of proportional decrements in optical pulse frequency and proportional increments in the price of the optical stimulation (Figure 27). The mountain model provides an accurate 3D fit of the data from each subject under drug and vehicle conditions (Figure 28): adjusted r^2 values range from 0.99860 to 0.99958.

Within-subject comparisons between vehicle and GBR12909 conditions reveal a drug-induced decrease in the pulse frequency required to produce a half-maximal reward intensity (F_{hm}) and an increase in the price at which animals spent half the trial time working for a maximal reward (P_e). These effects are illustrated in Figure 29 by data from one subject and are shown for the entire group in Figure 30A. In one respect, these results resemble those obtained in our earlier study of the effects of GBR12909 on eICSS of the MFB, but in another respect, they contrast sharply. In the eICSS study, GBR12909 also produced consistent increases in P_e, but it failed to produce significant changes in the F_{hm} parameter (Figure 30B).

In the power-frequency trade-off experiment, the number of rewards earned in a two minute trial varied systematically as a function of pulse frequency and optical power. The pulse frequency required to produce half-maximal behavior decreased at higher powers, and the maximal number of rewards obtained decreased as optical power was lowered (Figure 31).

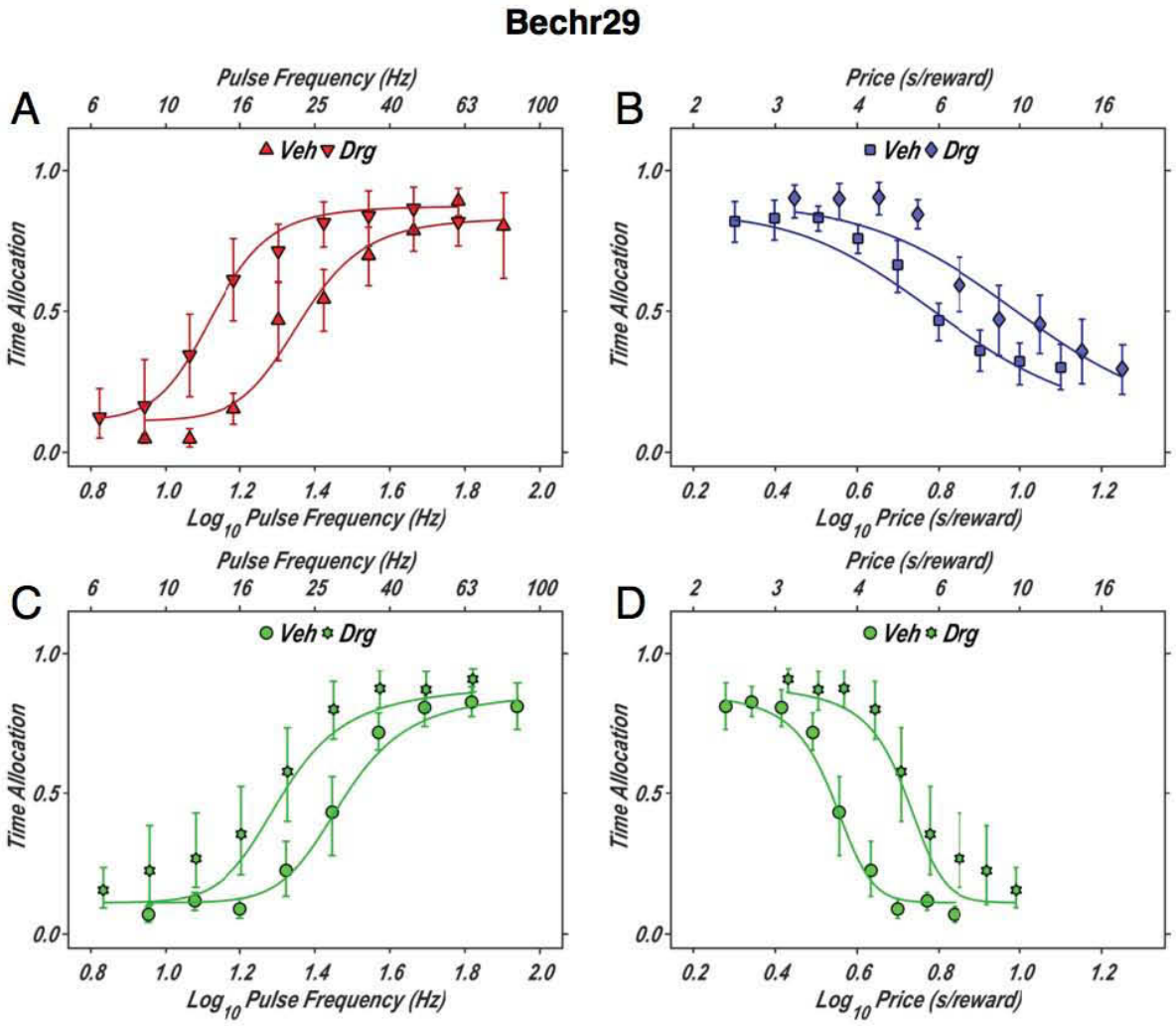

Figure 27. Time-allocation (TA) data from a representative subject (Bechr29), under vehicle and GBR12909 conditions. Data shown are means and 95 % confidence intervals. Solid lines represent the silhouette of the surface generated by fitting the mountain model. **A** During frequency sweeps the pulse frequency varied across trials, and the price was held constant. **B** During price sweeps the price varied across trials, and the frequency was kept at a value that yielded maximal reward. **C** During radial sweeps frequency and price varied conjointly across trials. The same radial-sweep data are plotted twice, once along the pulse-frequency axis and once along the price axis. Note the sigmoidal relationship between TA and the independent variables.

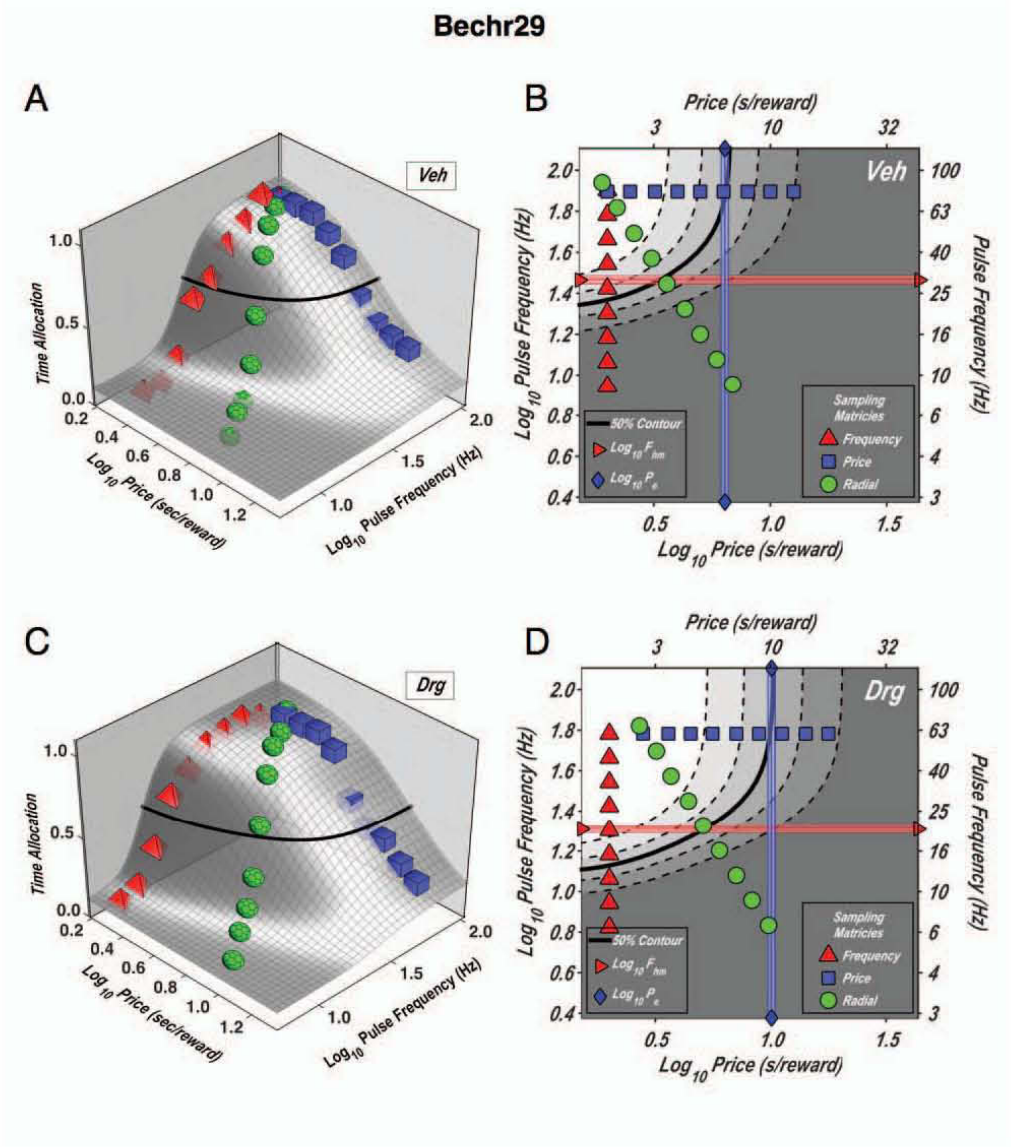

Figure 28. Mean time allocation, fitted surfaces, and contour maps. The data are from rat Bechr29. **A** and **B** show the fitted surface, data points, and contour map for the vehicle condition. **C** and **D** show the fitted surface, data points, and contour map for the drug condition. In the 3D graphs (**A** and **C**), the fitted surfaces are shown in gray, frequency-sweep data are designated by red pyramids, price-sweep data are designated by blue cubes, and radial-sweep data are designated by green polyhedrons. In the contour graphs of the fitted surfaces (**B** and **D**) the points along the frequency sweep are designated by red triangles, the points along the price sweeps by blue squares, and the points along the radial sweeps by green circles. The values of F_{hm}, P_e, are indicated by horizontal lines with right-facing triangular end points and vertical lines with diamond end points, respectively. The shaded regions surrounding the lines denote 95 % confidence intervals.

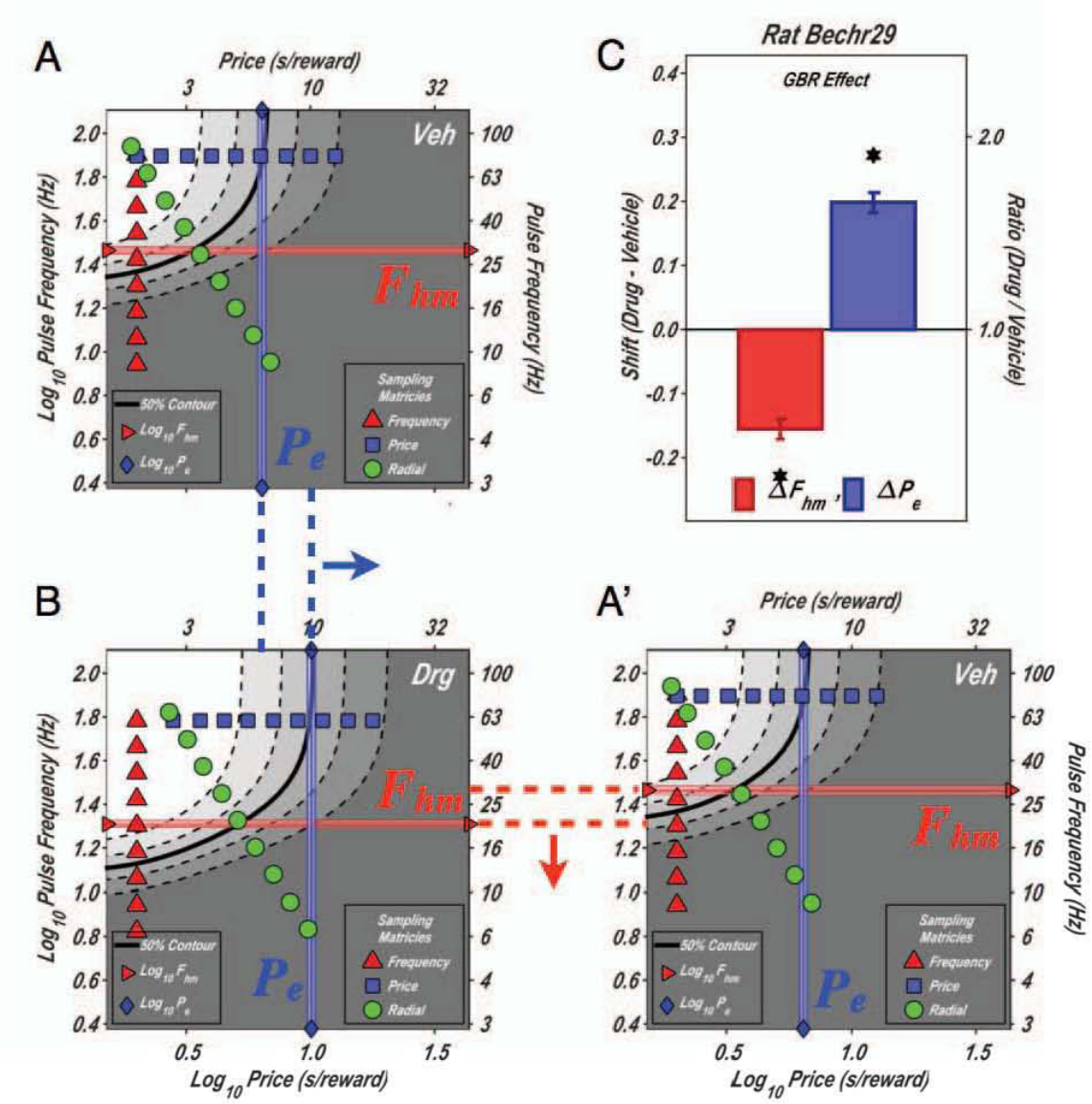

Figure 29. Contour-graph representation of the effect of GBR12909 in rat Bechr29. **A** and **A'** The contour map for the vehicle condition is shown twice to facilitate across-condition comparison of location-parameter values ($Log10F_{hm}$, $Log10P_e$) along the frequency and price axes. **B** Contour map for the drug condition. **C** The bar graph shows the size of the drug-induced change in the values of the location parameters. GBR12909 produced a leftwards shift of the reward mountain along the frequency axis (decreasing the value of F_{hm}) and displaced the mountain rightwards along the price axis (increasing the value of P_e).

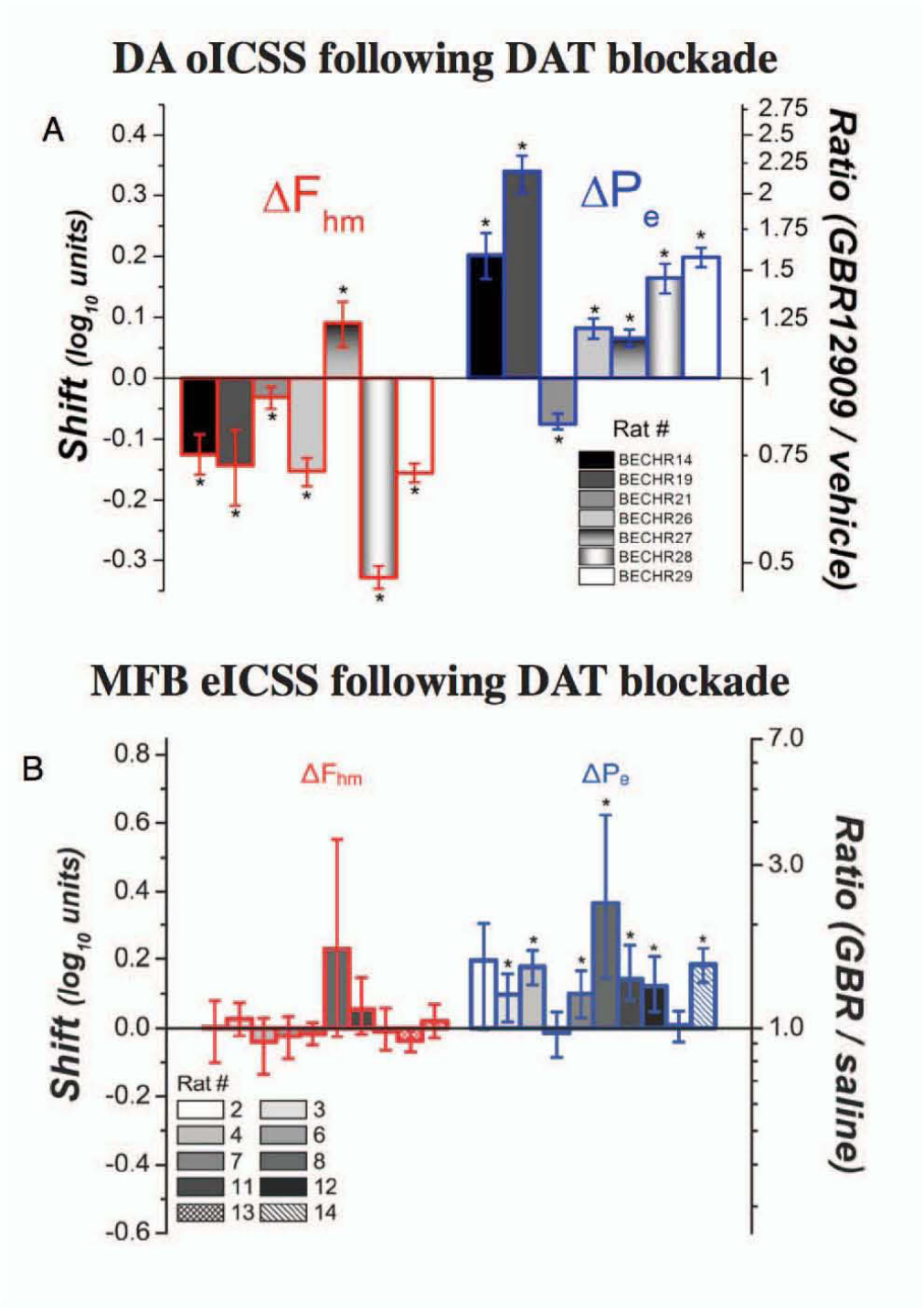

Figure 30. **A** GBR12909-induced shifts for all subjects in the oICSS mountain paradigm. Error bars denote 95% confidence intervals. The drug reliably decreased F_{hm}, and increased P_e in 6/7 subjects. **B** The effects of GBR12909 on eICSS, as reported in Chapter 1 (Hernandez et al., 2012). GBR12909 failed to produce any reliable changes in F_{hm}, *but* it reliably increased P_e in 7/10 subjects. Thus, GBR12909 produces contrasting effects on the location of the mountains along the frequency axis in oICSS and in eICSS.

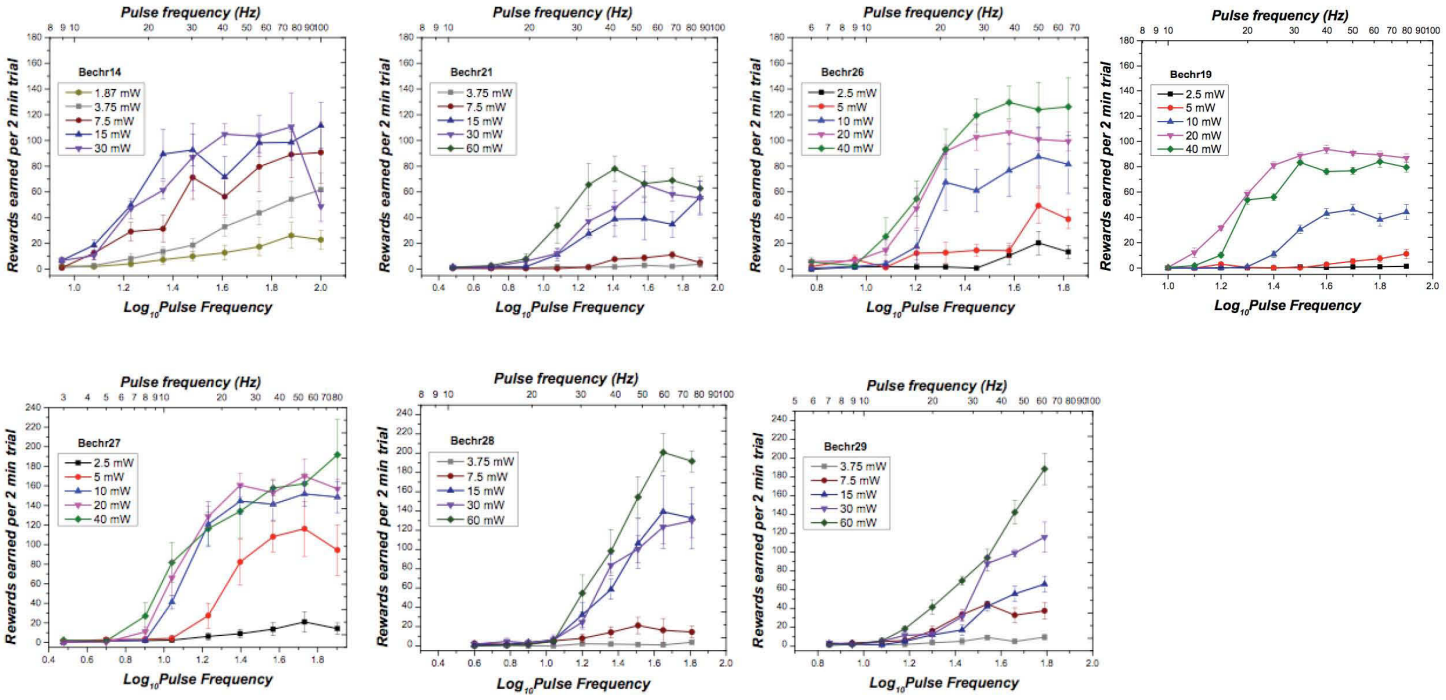

Figure 31. Optical power-frequency tradeoff. The number of rewards earned in an FR1 schedule of reinforcement varied as a function of optical intensity and optical pulse-frequency in all rats. At lower optical intensities, higher pulse frequencies were required to attain a given behavioral output.

Immunohistology and confocal microscopy confirmed that the tips of all optical-fiber implants were located close to transfected DA midbrain-neurons and that ChR2 was selectively expressed on TH+ neurons (Figure 32).

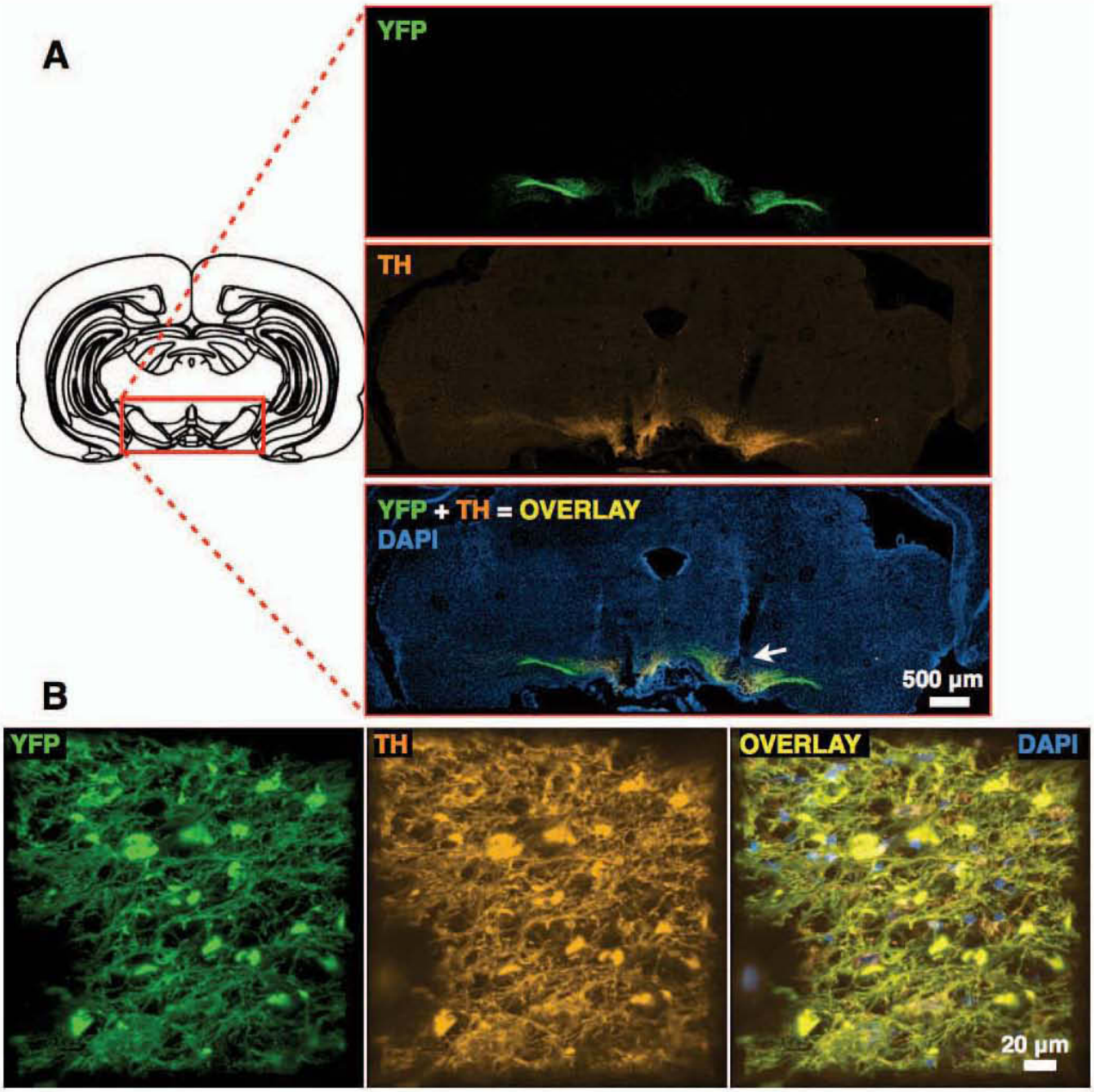

Figure 32. Viral construct expression from rat BeChr29. **A** Left: Schematic representation of a coronal section at the approximate location of the optical-implant tip (modified from (Paxinos & Watson, 2007)). Right: Representative immunohistochemical images. YFP and TH staining is shown in the top and middle panels respectively. The bottom panel shows the co-expression of YFP and TH (overlay) along with DAPI for anatomical reference. The arrow indicates the approximate location of the tip of the optical implant used for oICSS. **B** High magnification 3D reconstruction of the area below the optical-fiber track. Left: YFP-

positive neurons; Middle: TH-positive neurons; Right: Overlay of YFP, TH and DAPI staining. Note that YFP is expressed in TH positive neurons.

DISCUSSION

In rats working for optical stimulation of midbrain DA neurons, GBR12909 produced decreases in the value of F_{hm} and increases in P_e in 6/7 rats. This is in sharp contrast with the effects of GBR12909 on eICSS (i.e. increase in P_e but no change in F_{hm} (Hernandez et al., 2012)). Whereas in eICSS of the MFB, GBR12909 modulates reward seeking by affecting computations that occur downstream from the reward-growth function, the shifts in F_{hm} reported here indicate that in oICSS, GBR12909 affected the integration of the reward signal from the directly stimulated DA neurons. This provides conclusive evidence that eICSS and oICSS target different stages of reward processing.

In the case of eICSS of the MFB, the anatomical and neurochemical properties of the directly stimulated substrate have remained elusive, but substantial evidence suggests that the MFB reward-relevant axons targeted by eICSS are mostly non-dopaminergic and that midbrain DA neurons are recruited transynaptically by the electrical stimulation (Bielajew et al., 1982; Bielajew & Shizgal, 1982; 1986; Gallistel, 1986; Moisan & Rompré, 1998; Shizgal et al., 1980; Yeomans, 1989; Yeomans et al., 1988); disinhibition of VTA DA neurons (Jennings et al., 2013; Stuber & Wise, 2016) may be involved in this process. In contrast, in oICSS of midbrain DA neurons, the DA cells are directly and selectively stimulated. Thus, the different effects produced by DA reuptake blockade in the eICSS and oICSS paradigms can be explained by the stage of neural processing that is directly recruited. On this view, GBR12909 boosts the output of the directly stimulated neurons in oICSS (thus decreasing F_{hm}), but it affects the output of transynaptically activated DA neurons in eICSS. Because the DA neurons are activated after spatiotemporal integration of the outputs of directly stimulated MFB fibers, blocking DA reuptake increases P_e in the eICSS paradigm.

DOPAMINE AND THE SPATIO-TEMPORAL INTEGRATION OF REWARD SIGNALS

Higher optical intensities deliver light deeper into the tissue, potentially recruiting more DA transfected neurons, whereas higher pulse-frequencies trigger more action potentials in a given transfected DA neuron. Here we show that a given behavioral output in rats pursuing oICSS can be attained with low optical powers and high pulse-frequencies, or with high optical powers and low pulse-frequencies. This suggests that as in the case of eICSS, the output of the neurons that are activated directly by the optical stimulation is integrated spatially and temporally to determine reward-intensity. We have previously suggested that in the case of eICSS, the lack of GBR-induced changes in F_{hm} and the drug-induced increases in P_e implies that DA neurons are recruited downstream from the output of the reward-growth function. In contrast, the drug-induced decrease in F_{hm} observed here confirms that oICSS of DA neurons bypasses the eICSS reward-growth function. Nonetheless, the strength of the optical reward is also determined by spatio-temporal integration of the output from the DA neurons. Thus, the reward system seems to rely on at least two different reward-growth integrators: an upstream integrator of non-DA signals and a downstream integrator of DA output. The simplest arrangement of these two integrators is achieved by placing them in series. However, further mathematical modeling is required to assess whether the in-series dual-integrator model is sufficient to account for our existing eICSS and oICSS DA-reuptake data. These two integrators could represent different components of the reward processing and decision-making systems and could be responsible for different psychological variables that affect reward-seeking.

THE ROLE OF DOPAMINE IN COMPUTING REWARD COSTS

GBR12909 increased P_e in both eICSS and oICSS. This suggest that dopamine may play two roles in reward seeking: as part of a secondary integrator of reward intensity, and as a signal that influences gain and/or subjective costs. GBR12909 increases both phasic and tonic midbrain-DA signaling (Blaha & Phillips, 1990; Reith, Li, & Yan, 1997). The dual role of midbrain-DA neurons in coding for reward intensity and cost may be carried out by differential involvement of phasic vs tonic DA signaling (Schultz, 2002).

Overall, the present study illustrates the advantages of combining optogenetics, behavioral pharmacology, psychophysical measurement and computational modeling: using all these approaches in tandem was critical to the functional dissection of reward processing. The distinction between upstream and downstream integrators and the positioning of the DA neurons with respect to them is a consequence of combining these approaches and would not likely have been conceived and investigated otherwise. This approach could proof useful in future studies aiming to pinpoint the computational role of other neural circuits in reward-seeking. The selectivity and temporal control attainable with optogenetics and the more precise behavioral inferences that can be made using the reward-mountain model may be adopted in future studies to further refine the role of DA in reward and decision-making. To dissect the specific functions of DA signaling (as an input to a secondary reward-growth integrator and as a potential cost signal), formal explanations will be critical. Moreover, future experiments on how reward signals and their corresponding integrators interact will require the use of powerful behavioral and computational methods.

GENERAL CONCLUSIONS AND FUTURE DIRECTIONS

Dopamine signaling is necessary for the pursuit of natural and artificial rewards (Wise & Rompré, 1989). However, the precise computational and psychological contribution of DA to motivated behavior has remained elusive. Earlier accounts advocated a role of DA in computing the hedonic value of reinforcers (Wise, 1978). More recent hypotheses postulate DA as a signal that encodes the proclivity to invest effort in working for a reward (Salamone, Correa, Mingote, & Weber, 2005), incentive salience (Flagel et al., 2011; Niv et al., 2006; T. E. Robinson & Berridge, 2003), reward payoff (Lak et al., 2014; Stauffer et al., 2014), reward approach (Ikemoto, 2010), flexible approach behavior (Hoffmann & Nicola, 2014; McGinty, Lardeux, Taha, Kim, & Nicola, 2013; Morrison & Nicola, 2014), or reward-prediction errors (Montague, Dayan, et al., 1996; Schultz, Dayan, & Montague, 1997). The striking diversity of these views suggests that DA plays multiple roles and that the task of determining what they are is not an easy one.

In this thesis, I have used a novel behavioral and computational approach to better understand the role of DA in reward seeking. The mountain model is a step forward in the behavioral study of reward because it is able to differentiate between different stages of reward processing in animals engaged in electrical or optical self-stimulation.

In chapters 1 and 2 we used the reward mountain model to narrow down the stage of neural processing at which DA affects the pursuit of eICSS. We found that DA signaling modulates reward-seeking at a stage beyond the initial computation of reward intensity (Hernandez et al., 2010; 2012; Trujillo-Pisanty et al., 2013). This is reflected in the consistent drug-induced shifts of the mountain along the price axis and the lack of consistent changes along the frequency axis. The contrast between effects on F_{hm} and P_e strongly suggests that DA modulates eICSS downstream from the output of the reward-growth function. However, the drug-induced changes in P_e described in chapters 1 and 2 can be the result of a number of factors. Dopamine signaling may modulate eICSS by rescaling the output of the reward-growth function (i.e. multiplying it by a constant, affecting reward gain) or by altering reward costs, or the value of competing

activities (Hernandez et al., 2010). Nonetheless, these findings challenge the initial view of the role of DA as a purely hedonic signal (Fouriezos, Hansson, & Wise, 1978; Wise, Spindler, deWit, & Gerberg, 1978). The results are in line with the overwhelming evidence suggesting that midbrain DA neurons are activated transsynaptically in eICSS of the MFB (Bielajew & Shizgal, 1982; 1986; Gallistel et al., 1981; Hernandez et al., 2010; Moisan & Rompré, 1998; Shizgal, 1997; Shizgal et al., 1980; Yeomans, 1989; 1979; Yeomans et al., 1988).

In chapter 4, I used optogenetics to selectively stimulate midbrain DA neurons directly. This allowed me to bypass the neural substrate that is directly stimulated in eICSS. In oICSS, DA reuptake blockade produced consistent shifts of the mountain along the frequency axis. This is exactly what would be expected from the direct, specific activation of DA neurons that the optogenetic approach provides. To hold reward intensity constant in the face of potentiated DA neurotransmission, the rate at which the DA neurons are fired must be reduced in compensatory fashion, thus decreasing F_{hm}. This implies that the intensity of the rewarding effect produced by the optical stimulation is determined by a spatiotemporal integration process operating downstream of the DA neurons. This spatiotemporal integration process is manifested in the power-frequency tradeoff: as optical power is increased, the number of activated DA neurons grows, and in order to hold reward intensity constant, the rate at which the DA neurons are fired must be reduced.

In sharp contrast to the downstream integration of the effects of optical stimulation described in Chapter 4, the rewarding intensity produced by electrical stimulation of the MFB arises from a spatiotemporal integration process upstream of the DA neurons, as described in Chapters 1 and 2. In the case of eICSS, manipulation of DA neurotransmission shifts P_e but has no effect on F_{hm} (Hernandez et al., 2012; Trujillo-Pisanty et al., 2013).

In addition to decreasing F_{hm} in the present optogenetic experiment, dopamine reuptake blockade also shifted the optical mountains along the price axis. This suggests that DA

signaling also affects oICSS at a stage downstream from the reward-growth function, perhaps by computing reward costs or by rescaling the reward-intensity signal (Hernandez et al., 2010). Tonic and phasic DA signaling are thought to be involved in different aspects of motivated behavior (Schultz, 2007). These signals may play a differential role in computing reward intensity and reward cost. Phasic DA release in response to electrical simulation of the MFB is quantifiable by means of Fast Scan Cyclic Voltametry (Garris et al., 1999; Wightman & Robinson, 2002). Tonic DA signaling during eICSS can be quantified by means of microdialysis and High Precision Liquid Chromatography (Hamid et al., 2016; Hernandez & Shizgal, 2009; Hernandez, Rajabi, Stewart, Arvanitogiannis, & Shizgal, 2008; Trujillo-Pisanty et al., 2011). Incorporating these neurochemical detection strategies into the mountain-model paradigm could differentiate the contribution of tonic and phasic DA signaling in reward-seeking. Furthermore, interpretation of the data presented in this thesis will benefit from further computational modeling aimed at understanding the implications of spatiotemporal integration occurring upstream and downstream of the DA neurons. This should also provide a valuable perspective on the hypothesis that DA signaling plays differential roles in computing reward intensity on the one hand and reward costs or reward-intensity scaling on the other hand.

Overall, the contrasting effects of DA-reuptake blockade on eICSS and oICSS demonstrate that eICSS and oICSS target the reward system at two different stages of neural processing. Moreover, increasing prices devalued reward-seeking in rats engaged in oICSS of DA neurons. This shows that contrary to a current formulation (Lak et al., 2014; Stauffer et al., 2014), the activity of DA neurons does not represent payoff and that this critical variable is instead computed downstream from the output of the DA neurons. To my knowledge, this is the first time this hypothesis has been challenged using methods that can establish causality.

The results presented in this thesis demonstrate that the computational and psychological underpinnings of oICSS and eICSS differ, in contrast to a current formulation (Steinberg & Janak, 2012) and despite the similarity of the two phenomena

at the behavioral level. Although the eventual computational modeling of the current data should provide more information on the specific computations underlying eICSS and oICSS, further empirical evidence will be necessary to ascertain how these stages interact. Reward summation and reward competition experiments between eICSS, oICSS, and natural rewards could prove valuable for this purpose. If eICSS and oICSS summate and/or compete with each other, a common *reward currency* for both types of stimulation must be computed in the brain. This common currency could be critical when computing payoff. The competition and summation between eICSS and natural reinforcement has been established (Conover & Shizgal, 1994a; 1994b; Conover, Woodside, & Shizgal, 1994), but whether oICSS is also susceptible to these effects remains unknown. This is of importance as it would complement recent findings on the involvement of DA signaling in the computation of natural rewards (Tellez et al., 2016).

Do animals working for eICSS and oICSS experience the same subjective internal state? According to the view presented here, both types of stimulation target the system at different stages, but they do so prior to the final computation of payoff. However, the subjective internal states induced by optical and electrical stimulation may be different: Not only do both types of stimulation target the reward system at different stages, but optical stimulation activates only a subset of the neurons that are activated by electrical stimulation. Stimulus discrimination and stimulus generalization paradigms could help us address this problem (Druhan, Fibiger, & Phillips, 1990; Druhan, Martin-Iverson, Wilkie, Fibiger, & Philips, 1987). Animals could be trained to press levers under an FR10 schedule to obtain a natural reinforcer such as sucrose. The rats would be presented with two operanda, only one of which would be active on a given trial. A high pulse-frequency and a low pulse-frequency train of MFB electrical stimulation would serve as a discriminative stimuli to signal which lever will result in reinforcement if the response requirement is satisfied. Once the rats show reliable discrimination between the two pulse frequencies, test trials would be presented. In test trials, the animals would be primed with different pulse frequencies of midbrain optical stimulation. In a second group of rats optical stimulation would serve as the discriminative stimulus during training and electrical stimulation would be substituted during test trials. If the optical

and electrical stimulation induce similar states, then the rats should readily generalize from one form of stimulation to the other. If both groups generalize to the test stimulation, the argument for a rewarding-state signal that converges on a common state detector could be made. However, if the animals fail to generalize between the two forms of stimulation, we could conclude that the rewarding states they induce differ. These data could be important in further understanding the information that is computed (and shared) by both stages of neural processing.

In the introduction to this thesis, I identified two main questions about eICSS that have remain elusive: 1) which neuronal subtypes constitute the directly stimulated substrate for eICSS of the MFB? and 2) what is the precise role of DA in eICSS? The results from Chapters 1, 2, and 4 shed light on the second question, and lay the groundwork for addressing this issue in an unprecedented and revealing way. Although question 1 was not addressed in this thesis, the methodological and conceptual developments presented here may prove useful in studies aimed at identifying the directly stimulated substrate in eICSS. Indeed, we have validated the potential of the mountain model to answer this question. In eICSS, a small electrical lesion to the MFB produced consistent shifts along the frequency axis (Solomon, 2014). We have also taken the first steps to locate the cell bodies of the directly stimulated axons by performing excitotoxic lesions in rats trained on the mountain-model task. Incorporating novel strategies to selectively inhibit specific neural populations (Berndt, Lee, Ramakrishnan, & Deisseroth, 2014; Chow et al., 2010; Dong, Allen, Farrell, & Roth, 2010; Gradinaru, Thompson, & Deisseroth, 2008; Han & Boyden, 2007; Mahn, Prigge, Ron, Levy, & Yizhar, 2016; Wietek et al., 2014; Zhao et al., 2008) into the mountain paradigm could prove critical in solving question 1.

The functional dissection of the reward system is an ongoing challenge. The novel technologies for selectively stimulating or silencing specific neurons based on their genetics, connectivity, and/or location promise to address this problem. To fully understand how the reward system functions, anatomical and physiological evidence must be complemented with computational and psychological explanations. These

explanations are attainable through meticulous and quantitative behavioral testing. The conceptual and methodological framework presented in this thesis represents a sound approach to understand the specific contribution of at least some subcomponents of the reward system in motivated behavior.

REFERENCES

Adamantidis, A. R., Tsai, H.-C., Boutrel, B., Zhang, F., Stuber, G. D., Budygin, E. A., et al. (2011). Optogenetic Interrogation of Dopaminergic Modulation of the Multiple Phases of Reward-Seeking Behavior. *Journal of Neuroscience*, *31*(30), 10829–10835. http://doi.org/10.1523/JNEUROSCI.2246-11.2011

Airan, R. D., Thompson, K. R., Fenno, L. E., Bernstein, H., & Deisseroth, K. (2009). Temporally precise in vivo control of intracellular signalling. *Nature*, *458*(7241), 1025–1029. http://doi.org/10.1038/nature07926

Akaike, H. (1974). A new look at the statistical model identification. *IEEE Transactions on Automatic Control*, *19*(6), 716–723. http://doi.org/10.1109/TAC.1974.1100705

Andersen, P. H. (1989). The dopamine inhibitor GBR 12909: selectivity and molecular mechanism of action. *European Journal of Pharmacology*, *166*(3), 493–504.

Anderson, R. M., Fatigati, M. D., & Rompré, P. P. (1996). Estimates of the axonal refractory period of midbrain dopamine neurons: their relevance to brain stimulation reward. *Brain Research*, *718*(1-2), 83–88.

Anlezark, G. M., Arbuthnott, G. W., Christie, J. E., Crow, T. J., & Spear, P. J. (1974). Electrical self-stimulation in relation to cells of origin of catecholamine-containing neural systems ascending from the brain stem. *The Journal of Physiology*, *237*(2), 31P–32P.

Arbuthnott, G. W., Crow, T. J., Fuxe, K., Olson, L., & Ungerstedt, U. (1970). Depletion of catecholamines in vivo induced by electrical stimulation of central monoamine pathways. *Brain Research*, *24*(3), 471–483.

Arvanitogiannis, A., & Shizgal, P. (2008). The reinforcement mountain: allocation of behavior as a function of the rate and intensity of rewarding brain stimulation. *Behavioral Neuroscience*.

Aston-Jones, G., Smith, R. J., Moorman, D. E., & Richardson, K. A. (2009). Role of lateral hypothalamic orexin neurons in reward processing and addiction. *Neuropharmacology*, *56 Suppl 1*, 112–121. http://doi.org/10.1016/j.neuropharm.2008.06.060

Aston-Jones, G., Smith, R. J., Sartor, G. C., Moorman, D. E., Massi, L., Tahsili-Fahadan, P., & Richardson, K. A. (2010). Lateral hypothalamic orexin/hypocretin neurons: A role in reward-seeking and addiction. *Brain Research*, *1314*, 74–90. http://doi.org/10.1016/j.brainres.2009.09.106

Atalay, J., & Wise, R. (1983). Time course of pimozide effects on brain stimulation reward. *Pharmacology Biochemistry and Behavior*, *18*(4), 655–658.

Atasoy, D., Aponte, Y., Su, H. H., & Sternson, S. M. (2008). A FLEX switch targets Channelrhodopsin-2 to multiple cell types for imaging and long-range circuit mapping. *Journal of Neuroscience*, *28*(28), 7025–7030. http://doi.org/10.1523/JNEUROSCI.1954-08.2008

Bauco, P., & Wise, R. A. (1997). Synergistic effects of cocaine with lateral hypothalamic brain stimulation reward: lack of tolerance or sensitization. *The Journal of Pharmacology and Experimental Therapeutics*, *283*(3), 1160–1167.

Bauco, P., Wang, Y., & Wise, R. A. (1993). Lack of sensitization or tolerance to the facilitating effect of ventral tegmental area morphine on lateral hypothalamic brain stimulation reward. *Brain Research*, *617*(2), 303–308.

Baum, W. M., & Rachlin, H. C. (1969). Choice as time allocation. *Journal of the Experimental Analysis of Behavior*, *12*(6), 861–874.

Beier, K. T., Steinberg, E. E., DeLoach, K. E., Xie, S., Miyamichi, K., Schwarz, L., et al. (2015). Circuit Architecture of VTA Dopamine Neurons Revealed by Systematic Input-Output Mapping. *Cell*, *162*(3), 622–634. http://doi.org/10.1016/j.cell.2015.07.015

Berndt, A., Lee, S. Y., Ramakrishnan, C., & Deisseroth, K. (2014). Structure-guided transformation of channelrhodopsin into a light-activated chloride channel. *Science (New York, NY)*, *344*(6182), 420–424. http://doi.org/10.1126/science.1252367

Berndt, A., Lee, S. Y., Wietek, J., Ramakrishnan, C., Steinberg, E. E., Rashid, A. J., et al. (2016). Structural foundations of optogenetics: Determinants of channelrhodopsin ion selectivity. *Proceedings of the National Academy of Sciences of the United States of America*, *113*(4), 822–829. http://doi.org/10.1073/pnas.1523341113

Berndt, A., Schoenenberger, P., Mattis, J., Tye, K. M., Deisseroth, K., Hegemann, P., & Oertner, T. G. (2011). High-efficiency channelrhodopsins for fast neuronal stimulation at low light levels. *Proceedings of the National Academy of Sciences of the United States of America*, *108*(18), 7595–7600. http://doi.org/10.1073/pnas.1017210108

Berndt, A., Yizhar, O., Gunaydin, L. A., Hegemann, P., & Deisseroth, K. (2009). *Bi-stable neural state switches. Nature neuroscience* (Vol. 12, pp. 229–234).

Berridge, K. C., & Kringelbach, M. L. (2008). Affective neuroscience of pleasure: reward in humans and animals. *Psychopharmacology*, *199*(3), 457–480. http://doi.org/10.1007/s00213-008-1099-6

Bielajew, C., & Shizgal, P. (1982). Behaviorally derived measures of conduction velocity in the substrate for rewarding medial forebrain bundle stimulation. *Brain Research*, *237*(1), 107–119.

Bielajew, C., & Shizgal, P. (1986). Evidence implicating descending fibers in self-stimulation of the medial forebrain bundle. *The Journal of Neuroscience : the Official Journal of the Society for Neuroscience*, *6*(4), 919–929.

Bielajew, C., Lapointe, M., Kiss, I., & Shizgal, P. (1982). Absolute and relative refractory periods of the substrates for lateral hypothalamic and ventral midbrain self-stimulation. *Physiology & Behavior*, *28*(1), 125–132.

Blaha, C. D., & Phillips, A. G. (1990). Application of in vivo electrochemistry to the measurement of changes in dopamine release during intracranial self-stimulation. *Journal of Neuroscience Methods*, *34*(1-3), 125–133.

Bonnavion, P., & de Lecea, L. (2010). Hypocretins in the control of sleep and wakefulness. *Current Neurology and Neuroscience Reports*, *10*(3), 174–179. http://doi.org/10.1007/s11910-010-0101-y

Boyden, E. S., Zhang, F., Bamberg, E., Nagel, G., & Deisseroth, K. (2005). Millisecond-timescale, genetically targeted optical control of neural activity. *Nature Neuroscience*, *8*(9), 1263–1268. http://doi.org/10.1038/nn1525

Breton, Y.-A., Conover, K., & Shizgal, P. (2014). The effect of probability discounting on reward seeking: a three-dimensional perspective. *Frontiers in Behavioral Neuroscience*, *8*, 284. http://doi.org/10.3389/fnbeh.2014.00284

Breton, Y.-A., Marcus, J. C., & Shizgal, P. (2009). Rattus Psychologicus: construction of preferences by self-stimulating rats. *Behavioural Brain Research*, *202*(1), 77–91. http://doi.org/10.1016/j.bbr.2009.03.019

Breton, Y.-A., Mullett, A., Conover, K., & Shizgal, P. (2013). Validation and extension of the reward-mountain model. *Frontiers in Behavioral Neuroscience*, *7*. http://doi.org/10.3389/fnbeh.2013.00125

Britt, J. P., Benaliouad, F., McDevitt, R. A., Stuber, G. D., Wise, R. A., & Bonci, A. (2012). Synaptic and Behavioral Profile of Multiple Glutamatergic Inputs to the Nucleus Accumbens. *Neuron*, *76*(4), 790–803. http://doi.org/10.1016/j.neuron.2012.09.040

Brown, M. T. C., Bellone, C., Mameli, M., Labouèbe, G., Bocklisch, C., Balland, B., et al. (2010). Drug-driven AMPA receptor redistribution mimicked by selective dopamine neuron stimulation. *PLoS ONE*, *5*(12), e15870. http://doi.org/10.1371/journal.pone.0015870

Budygin, E. A., Kilpatrick, M. R., Gainetdinov, R. R., & Wightman, R. M. (2000). Correlation between behavior and extracellular dopamine levels in rat striatum: comparison of microdialysis and fast-scan cyclic voltammetry. *Neuroscience Letters*, *281*(1), 9–12.

Campbell, K. A., Evans, G., & Gallistel, C. R. (1985). A microcomputer-based method for physiologically interpretable measurement of the rewarding efficacy of brain stimulation. *Physiology & Behavior*, *35*(3), 395–403.

Carlezon, W. A., & Chartoff, E. H. (2007). Intracranial self-stimulation (ICSS) in rodents to study the neurobiology of motivation. *Nature Protocols*, *2*(11), 2987–2995. http://doi.org/10.1038/nprot.2007.441

Carlezon, W. A., & Thomas, M. J. (2009). Biological substrates of reward and aversion: a nucleus accumbens activity hypothesis. *Neuropharmacology*, *56 Suppl 1*, 122–132. http://doi.org/10.1016/j.neuropharm.2008.06.075

Chow, B. Y., Han, X., Dobry, A. S., Qian, X., Chuong, A. S., Li, M., et al. (2010). High-performance genetically targetable optical neural silencing by light-driven proton pumps. *Nature*, *463*(7277), 98–102. http://doi.org/10.1038/nature08652

Chuong, A. S., Miri, M. L., Busskamp, V., Matthews, G. A. C., Acker, L. C., Sørensen, A. T., et al. (2014). *Noninvasive optical inhibition with a red-shifted microbial rhodopsin. Nature neuroscience* (Vol. 17, pp. 1123–1129).

Colle, L. M., & Wise, R. A. (1988). Effects of nucleus accumbens amphetamine on lateral hypothalamic brain stimulation reward. *Brain Research*, *459*(2), 361–368.

Conover, K. L., & Shizgal, P. (1994a). Competition and summation between rewarding effects of sucrose and lateral hypothalamic stimulation in the rat. *Behavioral Neuroscience*, *108*(3), 537–548.

Conover, K. L., & Shizgal, P. (1994b). Differential effects of postingestive feedback on the reward value of sucrose and lateral hypothalamic stimulation in rats. *Behavioral Neuroscience*, *108*(3), 559–572.

Conover, K. L., Woodside, B., & Shizgal, P. (1994). Effects of sodium depletion on competition and summation between rewarding effects of salt and lateral hypothalamic stimulation in the rat. *Behavioral Neuroscience*, *108*(3), 549–558.

Corbett, D., & Wise, R. A. (1980). Intracranial self-stimulation in relation to the ascending dopaminergic systems of the midbrain: a moveable electrode mapping study. *Brain Research*, *185*(1), 1–15.

Cossette, M.-P., Conover, K., & Shizgal, P. (2016). The neural substrates for the rewarding and dopamine-releasing effects of medial forebrain bundle stimulation have partially discrepant frequency responses. *Behavioural Brain Research*, *297*, 345–358. http://doi.org/10.1016/j.bbr.2015.10.029

Crow, T. J. (1970). Enhancement of coaine of intra-cranial self-stimulation in the rat. *Life Sciences*, *9*(7), 375–381.

Crow, T. J. (1972). A map of the rat mesencephalon for electrical self-stimulation. *Brain Research*, *36*(2), 265–273.

Davis, W. M., & Smith, S. G. (1975). Effect of haloperidol on (+)-amphetamine self-administration. *The Journal of Pharmacy and Pharmacology*, *27*(7), 540–542.

Deisseroth, K. (2010). Controlling the Brain with Light. *Scientific American*, *303*(5), 48–55. http://doi.org/10.1038/scientificamerican1110-48

Deisseroth, K. (2011). Optogenetics. *Nature Methods*, *8*(1), 26–29. http://doi.org/doi: 10.1038/nmeth.f.324

Deisseroth, K., Feng, G., Majewska, A. K., Miesenböck, G., Ting, A., & Schnitzer, M. J. (2006). Next-generation optical technologies for illuminating genetically targeted brain circuits. *Journal of Neuroscience*, *26*(41), 10380–10386. http://doi.org/10.1523/JNEUROSCI.3863-06.2006

Dietrich, M. O., & Horvath, T. L. (2009). Feeding signals and brain circuitry. *The European Journal of Neuroscience*, *30*(9), 1688–1696. http://doi.org/10.1111/j.1460-9568.2009.06963.x

Dong, S., Allen, J. A., Farrell, M., & Roth, B. L. (2010). A chemical-genetic approach for precise spatio-temporal control of cellular signaling. *Molecular bioSystems*, *6*(8), 1376–1380. http://doi.org/10.1039/c002568m

Druhan, J. P., Fibiger, H. C., & Phillips, A. G. (1990). Amphetamine-like stimulus properties produced by electrical stimulation of reward sites in the ventral tegmental area. *Behavioural Brain Research*, *38*(2), 175–184.

Druhan, J. P., Martin-Iverson, M. T., Wilkie, D. M., Fibiger, H. C., & Philips, A. G. (1987, October 1). Differential effects of physostigmine on cues produced by electrical stimulation of the ventral tegmental area using two discrimination procedures. http://doi.org/10.1016/0091-3057(87)90223-1

Edmonds, D. E., & Gallistel, C. R. (1974). Parametric analysis of brain stimulation reward in the rat: III. Effect of performance variables on the reward summation function. *Journal of Comparative and Physiological Psychology*, *87*(5), 876–883.

Edmonds, D. E., & Gallistel, C. R. (1977). Reward versus performance in self-stimulation: electrode-specific effects of alpha-methyl-p-tyrosine on reward in the rat. *Journal of Comparative and Physiological Psychology*, *91*(5), 962–974.

Efron, B., & Tibshirani, R. (1994). An introduction to the bootstrap. *(15 May 1994).* http://www.citeulike.org/group/108/article/161811

Esposito, R. U., Motola, A. H., & Kornetsky, C. (1978). Cocaine: acute effects on reinforcement thresholds for self-stimulation behavior to the medial forebrain bundle. *Pharmacology Biochemistry and Behavior*, *8*(4), 437–439.

Fiala, A., Suska, A., & Schlüter, O. M. (2010). Optogenetic approaches in neuroscience. *Current Biology : CB*, *20*(20), R897–903. http://doi.org/10.1016/j.cub.2010.08.053

Fibiger, H. C., LePiane, F. G., Jakubovic, A., & Phillips, A. G. (1987). The role of dopamine in intracranial self-stimulation of the ventral tegmental area. *The Journal of Neuroscience : the Official Journal of the Society for Neuroscience*, *7*(12), 3888–3896.

Fields, H. L., Hjelmstad, G. O., Margolis, E. B., & Nicola, S. M. (2007). Ventral tegmental area neurons in learned appetitive behavior and positive reinforcement. *Annual Review of Neuroscience*, *30*, 289–316. http://doi.org/10.1146/annurev.neuro.30.051606.094341

Figlewicz, D. P., & Sipols, A. J. (2010). Energy regulatory signals and food reward. *Pharmacology Biochemistry and Behavior*, *97*(1), 15–24. http://doi.org/10.1016/j.pbb.2010.03.002

Flagel, S. B., Clark, J. J., Robinson, T. E., Mayo, L., Czuj, A., Willuhn, I., et al. (2011). A selective role for dopamine in stimulus-reward learning. *Nature*, *469*(7328), 53–57. http://doi.org/10.1038/nature09588

Fouriezos, G., Bielajew, C., & Pagotto, W. (1990). Task difficulty increases thresholds of rewarding brain stimulation. *Behavioural Brain Research*, *37*(1), 1–7.

Fouriezos, G., Hansson, P., & Wise, R. A. (1978). Neuroleptic-induced attenuation of brain stimulation reward in rats. *Journal of Comparative and Physiological Psychology*, *92*(4), 661. http://doi.org/10.1037/h0077500

Frank, R. A., & Williams, H. P. (1985). Both response effort and current intensity affect self-stimulation train duration thresholds. *Pharmacology Biochemistry and Behavior*, *22*(4), 527–530.

Franklin, K. B. (1978). Catecholamines and self-stimulation: reward and performances effects dissociated. *Pharmacology Biochemistry and Behavior*, *9*(6), 813–820.

Gagnaire, F., & Micillino, J.-C. (2006). Effects of triadimefon on extracellular dopamine, DOPAC, HVA and 5-HIAA in adult rat striatum. *Toxicology*, *217*(2-3), 91–104. http://doi.org/10.1016/j.tox.2005.08.021

Gallistel, C. (1986). The role of the dopaminergic projections in MFB self-stimulation. *Behavioural Brain Research*, *20*(3), 313–321.

Gallistel, C. R. (1978). Self-stimulation in the rat: quantitative characteristics of the reward pathway. *Journal of Comparative and Physiological Psychology*, *92*(6), 977–998.

Gallistel, C. R., & Davis, A. J. (1983). Affinity for the dopamine D2 receptor predicts neuroleptic potency in blocking the reinforcing effect of MFB stimulation. *Pharmacology Biochemistry and Behavior*, *19*(5), 867–872.

Gallistel, C. R., & Freyd, G. (1987). Quantitative determination of the effects of catecholaminergic agonists and antagonists on the rewarding efficacy of brain stimulation. *Pharmacology Biochemistry and Behavior*, *26*(4), 731–741.

Gallistel, C. R., & Leon, M. (1991). Measuring the subjective magnitude of brain stimulation reward by titration with rate of reward. *Behavioral Neuroscience*, *105*(6), 913–925.

Gallistel, C. R., Leon, M., Waraczynski, M., & Hanau, M. S. (1991). Effect of current on the maximum possible reward. *Behavioral Neuroscience*, *105*(6), 901–912.

Gallistel, C. R., Shizgal, P., & Yeomans, J. S. (1981). A portrait of the substrate for self-stimulation. *Psychological Review*, *88*(3), 228–273.

Gallistel, C., & Karras, D. (1984). Pimozide and amphetamine have opposing effects on the reward summation function. *Pharmacology Biochemistry and Behavior*, *20*(1), 73–77.

Garris, P. A., Kilpatrick, M., Bunin, M. A., Michael, D., Walker, Q. D., & Wightman, R. M. (1999). Dissociation of dopamine release in the nucleus accumbens from intracranial self-stimulation. *Nature*, *398*(6722), 67–69. http://doi.org/10.1038/18019

Geisler, S., Derst, C., Veh, R., & Zahm, D. (2007). Glutamatergic afferents of the ventral tegmental area in the rat. *Journal of Neuroscience*, *27*(21), 5730.

Gilliss, B., C, M., Pieper, J., & Carlezon, W. (2002). Cocaine and SKF-82958 potentiate brain stimulation reward in Swiss-Webster mice. *Psychopharmacology*, *163*(2), 238–248. http://doi.org/10.1007/s00213-002-1153-8

Gomita, Y., & Gallistel, C. (1982). Effects of reinforcement-blocking doses of pimozide on neural system driven by rewarding stimulation of the MFB: A 14C-2-

deoxyglucose analysis. *Pharmacology Biochemistry and Behavior*, *17*(4), 841–845.

Gong, S., Doughty, M., Harbaugh, C. R., Cummins, A., Hatten, M. E., Heintz, N., & Gerfen, C. R. (2007). Targeting Cre recombinase to specific neuron populations with bacterial artificial chromosome constructs. *Journal of Neuroscience*, *27*(37), 9817–9823. http://doi.org/10.1523/JNEUROSCI.2707-07.2007

Govorunova, E. G., Spudich, E. N., Lane, C. E., Sineshchekov, O. A., & Spudich, J. L. (2011). New Channelrhodopsin with a Red-Shifted Spectrum and Rapid Kinetics from Mesostigma viride. *mBio*, *2*(3), e00115–11–e00115–11. http://doi.org/10.1128/mBio.00115-11

Gradinaru, V., Thompson, K. R., & Deisseroth, K. (2008). eNpHR: a Natronomonas halorhodopsin enhanced for optogenetic applications. *Brain Cell Biology*, *36*(1-4), 129–139. http://doi.org/10.1007/s11068-008-9027-6

Gradinaru, V., Zhang, F., Ramakrishnan, C., Mattis, J., Prakash, R., Diester, I., et al. (2010). Molecular and cellular approaches for diversifying and extending optogenetics. *Cell*, *141*(1), 154–165. http://doi.org/10.1016/j.cell.2010.02.037

Gratton, A., & Wise, R. A. (1988a). Comparisons of connectivity and conduction velocities for medial forebrain bundle fibers subserving stimulation-induced feeding and brain stimulation reward. *Brain Research*, *438*(1-2), 264–270.

Gratton, A., & Wise, R. A. (1988b). Comparisons of refractory periods for medial forebrain bundle fibers subserving stimulation-induced feeding and brain stimulation reward: a psychophysical study. *Brain Research*, *438*(1-2), 256–263.

Grenhoff, J., Nisell, M., Ferré, S., Aston-Jones, G., & Svensson, T. H. (1993). Noradrenergic modulation of midbrain dopamine cell firing elicited by stimulation of the locus coeruleus in the rat. *Journal of Neural Transmission. General Section*, *93*(1), 11–25.

Gunaydin, L. A., Yizhar, O., Berndt, A., Sohal, V. S., Deisseroth, K., & Hegemann, P. (2010). Ultrafast optogenetic control. *Nature Neuroscience*, *13*(3), 387–392. http://doi.org/10.1038/nn.2495

Gutierrez, R., Lobo, M. K., Zhang, F., & de Lecea, L. (2011). Neural integration of reward, arousal, and feeding: recruitment of VTA, lateral hypothalamus, and

ventral striatal neurons. *IUBMB Life*, *63*(10), 824–830. http://doi.org/10.1002/iub.539

Hamid, A. A., Pettibone, J. R., Mabrouk, O. S., Hetrick, V. L., Schmidt, R., Vander Weele, C. M., et al. (2016). Mesolimbic dopamine signals the value of work. *Nature Neuroscience*, *19*(1), 117–126. http://doi.org/10.1038/nn.4173

Han, X., & Boyden, E. S. (2007). Multiple-color optical activation, silencing, and desynchronization of neural activity, with single-spike temporal resolution. *PLoS ONE*, *2*(3), e299. http://doi.org/10.1371/journal.pone.0000299

Harrison, A. A., & Markou, A. (2001). Serotonergic manipulations both potentiate and reduce brain stimulation reward in rats: involvement of serotonin-1A receptors. *The Journal of Pharmacology and Experimental Therapeutics*, *297*(1), 316–325.

Hayes, D. J., & Greenshaw, A. J. (2011). Neuroscience and Biobehavioral Reviews. *Neuroscience & Biobehavioral Reviews*, *35*(6), 1419–1449. http://doi.org/10.1016/j.neubiorev.2011.03.005

Henny, P., Brischoux, F., Mainville, L., Stroh, T., & Jones, B. E. (2010). Immunohistochemical evidence for synaptic release of glutamate from orexin terminals in the locus coeruleus. *Neuroscience*, *169*(3), 1150–1157. http://doi.org/10.1016/j.neuroscience.2010.06.003

Hernandez, G., & Shizgal, P. (2009). Dynamic changes in dopamine tone during self-stimulation of the ventral tegmental area in rats. *Behavioural Brain Research*, *198*(1), 91–97. http://doi.org/10.1016/j.bbr.2008.10.017

Hernandez, G., Breton, Y.-A., Conover, K., & Shizgal, P. (2010). At what stage of neural processing does cocaine act to boost pursuit of rewards? *PLoS ONE*, *5*(11), e15081. http://doi.org/10.1371/journal.pone.0015081

Hernandez, G., Haines, E., & Shizgal, P. (2008a). Potentiation of intracranial self-stimulation during prolonged subcutaneous infusion of cocaine. *Journal of Neuroscience Methods*, *175*(1), 79–87. http://doi.org/10.1016/j.jneumeth.2008.08.005

Hernandez, G., Haines, E., Rajabi, H., Stewart, J., Arvanitogiannis, A., & Shizgal, P. (2007). Predictable and unpredictable rewards produce similar changes in

dopamine tone. *Behavioral Neuroscience*, *121*(5), 887–895. http://doi.org/10.1037/0735-7044.121.5.887

Hernandez, G., Hamdani, S., Rajabi, H., Conover, K., Stewart, J., Arvanitogiannis, A., & Shizgal, P. (2006). Prolonged rewarding stimulation of the rat medial forebrain bundle: neurochemical and behavioral consequences. *Behavioral Neuroscience*, *120*(4), 888–904. http://doi.org/10.1037/0735-7044.120.4.888

Hernandez, G., Rajabi, H., Stewart, J., Arvanitogiannis, A., & Shizgal, P. (2008b). Dopamine tone increases similarly during predictable and unpredictable administration of rewarding brain stimulation at short inter-train intervals. *Behavioural Brain Research*, *188*(1), 227–232. http://doi.org/10.1016/j.bbr.2007.10.035

Hernandez, G., Trujillo Pisanty, I., Cossette, M.-P., Conover, K., & Shizgal, P. (2012). Role of dopamine tone in the pursuit of brain stimulation reward. *Journal of Neuroscience*, *32*(32), 11032–11041. http://doi.org/10.1523/JNEUROSCI.1051-12.2012

Herrnstein, R. J. (1970). On the law of effect. *Journal of the Experimental Analysis of Behavior*, *13*(2), 243–266. http://doi.org/10.1901/jeab.1970.13-243

Herrnstein, R. J. (1974). Formal properties of the matching law. *Journal of the Experimental Analysis of Behavior*, *21*(1), 159–164.

Heyman, G. M., & Beer, B. (1987). A new approach for evaluating the behavioral effects of antipsychotic drugs. *Trends in Pharmacological Sciences*, *8*(10), 388–393.

Hodos, W. (1961). Progressive ratio as a measure of reward strength. *Science (New York, NY)*, *134*, 943–944.

Hoebel, B. G., & Teitelbaum, P. (1962). Hypothalamic control of feeding and self-stimulation. *Science (New York, NY)*, *135*(3501), 375–377.

Hoffmann, du, J., & Nicola, S. M. (2014). Dopamine invigorates reward seeking by promoting cue-evoked excitation in the nucleus accumbens. *Journal of Neuroscience*, *34*(43), 14349–14364. http://doi.org/10.1523/JNEUROSCI.3492-14.2014

Hollon, N. G., Arnold, M. M., Gan, J. O., Walton, M. E., & Phillips, P. E. M. (2014). Dopamine-associated cached values are not sufficient as the basis for action

selection. *Proceedings of the National Academy of Sciences of the United States of America*, *111*(51), 18357–18362. http://doi.org/10.1073/pnas.1419770111

Ikemoto, S. (2007). Dopamine reward circuitry: two projection systems from the ventral midbrain to the nucleus accumbens-olfactory tubercle complex. *Brain Research Reviews*, *56*(1), 27–78.

Ikemoto, S. (2010). Brain reward circuitry beyond the mesolimbic dopamine system: A neurobiological theory. *Neuroscience & Biobehavioral Reviews*, *35*(2), 129–150. http://doi.org/10.1016/j.neubiorev.2010.02.001

Ilango, A., Kesner, A. J., Keller, K. L., Stuber, G. D., Bonci, A., & Ikemoto, S. (2014). Similar Roles of Substantia Nigra and Ventral Tegmental Dopamine Neurons in Reward and Aversion. *Journal of Neuroscience*, *34*(3), 817–822. http://doi.org/10.1523/JNEUROSCI.1703-13.2014

Iversen, L. (2000). Neurotransmitter transporters: fruitful targets for CNS drug discovery. *Molecular Psychiatry*, *5*(4), 357–362.

Iversen, S. D., & Iversen, L. L. (2007). Dopamine: 50 years in perspective. *Trends in Neurosciences*, *30*(5), 188–193. http://doi.org/10.1016/j.tins.2007.03.002

Jennings, J. H., Rizzi, G., Stamatakis, A. M., Ung, R. L., & Stuber, G. D. (2013a). The Inhibitory Circuit Architecture of the Lateral Hypothalamus Orchestrates Feeding. *Science (New York, NY)*, *341*(6153), 1517–1521. http://doi.org/10.1126/science.1241812

Jennings, J. H., Sparta, D. R., Stamatakis, A. M., Ung, R. L., Pleil, K. E., Kash, T. L., & Stuber, G. D. (2013b). Distinct extended amygdala circuits for divergent motivational states. *Nature*, 1–7. http://doi.org/10.1038/nature12041

Jennings, J. H., Ung, R. L., Resendez, S. L., Stamatakis, A. M., Taylor, J. G., Huang, J., et al. (2015). Visualizing Hypothalamic Network Dynamics for Appetitive and Consummatory Behaviors. *Cell*, *160*(3), 516–527. http://doi.org/10.1016/j.cell.2014.12.026

Jhou, T. C., Fields, H. L., Baxter, M. G., Saper, C. B., & Holland, P. C. (2009). The rostromedial tegmental nucleus (RMTg), a GABAergic afferent to midbrain dopamine neurons, encodes aversive stimuli and inhibits motor responses. *Neuron*, *61*(5), 786–800. http://doi.org/10.1016/j.neuron.2009.02.001

Kempadoo, K. A., Tourino, C., Cho, S. L., Magnani, F., Leinninger, G. M., Stuber, G. D., et al. (2013). Hypothalamic Neurotensin Projections Promote Reward by Enhancing Glutamate Transmission in the VTA. *Journal of Neuroscience*, *33*(18), 7618–7626. http://doi.org/10.1523/JNEUROSCI.2588-12.2013

Killeen, P. (1972). The matching law. *Journal of the Experimental Analysis of Behavior*, *17*(3), 489–495.

Killeen, P. (2001). The four causes of behavior. *Current Directions in Psychological Science*, *10*(4), 136.

Kim, K. M., Baratta, M. V., Yang, A., Lee, D., Boyden, E. S., & Fiorillo, C. D. (2012). Optogenetic mimicry of the transient activation of dopamine neurons by natural reward is sufficient for operant reinforcement. *PLoS ONE*, *7*(4), e33612. http://doi.org/10.1371/journal.pone.0033612

Kita, J. M., Kile, B. M., Parker, L. E., & Wightman, R. M. (2009). In vivo measurement of somatodendritic release of dopamine in the ventral tegmental area. *Synapse (New York, N.Y.)*, *63*(11), 951–960. http://doi.org/10.1002/syn.20676

Klapoetke, N. C., Murata, Y., Kim, S. S., Pulver, S. R., Birdsey-Benson, A., Cho, Y. K., et al. (2014). Independent optical excitation of distinct neural populations. *Nature Methods*, *11*(3), 338–346. http://doi.org/10.1038/nmeth.2836

Kuhlman, S. J., & Huang, Z. J. (2008). High-resolution labeling and functional manipulation of specific neuron types in mouse brain by Cre-activated viral gene expression. *PLoS ONE*, *3*(4), e2005. http://doi.org/10.1371/journal.pone.0002005

Lak, A., Stauffer, W. R., & Schultz, W. (2014). Dopamine prediction error responses integrate subjective value from different reward dimensions. *Proceedings of the National Academy of Sciences of the United States of America*, *111*(6), 2343–2348. http://doi.org/10.1073/pnas.1321596111

Lammel, S., Lim, B. K., Ran, C., Huang, K. W., Betley, M. J., Tye, K. M., et al. (2012). Input-specific control of reward and aversion in the ventral tegmental area. *Nature*, 1–8. http://doi.org/10.1038/nature11527

Leon, M., & Gallistel, C. (1992). The function relating the subjective magnitude of brain stimulation reward to stimulation strength varies with site of stimulation. *Behavioural Brain Research*, *52*(2), 183–193.

Liebman, J. M., & Butcher, L. L. (1973). Effects on self-stimulation behavior of drugs influencing dopaminergic neurotransmission mechanisms. *Naunyn-Schmiedeberg's Archives of Pharmacology*, *277*(3), 305–318. http://doi.org/10.1007/BF00505669

Lin, Y., de Vaca, S. C., Carr, K. D., & Stone, E. A. (2007). Role of alpha(1)-adrenoceptors of the locus coeruleus in self-stimulation of the medial forebrain bundle. *Neuropsychopharmacology : Official Publication of the American College of Neuropsychopharmacology*, *32*(4), 835–841. http://doi.org/10.1038/sj.npp.1301145

Liu, X., & Tonegawa, S. (2010). Optogenetics 3.0. *Cell*, *141*(1), 22–24. http://doi.org/10.1016/j.cell.2010.03.019

Liu, Z., Zhou, J., Li, Y., Hu, F., Lu, Y., Ma, M., et al. (2014). Dorsal Raphe Neurons Signal Reward through 5-HT and Glutamate. *Neuron*, *81*(6), 1360–1374. http://doi.org/10.1016/j.neuron.2014.02.010

Lüscher, C., & Malenka, R. C. (2011). Drug-Evoked Synaptic Plasticity in Addiction: From Molecular Changes to Circuit Remodeling. *Neuron*, *69*(4), 650–663. http://doi.org/10.1016/j.neuron.2011.01.017

Mahn, M., Prigge, M., Ron, S., Levy, R., & Yizhar, O. (2016). Biophysical constraints of optogenetic inhibition at presynaptic terminals. *Nature Neuroscience*, 1–5. http://doi.org/10.1038/nn.4266

Maldonado-Irizarry, C. S., Stellar, J. R., & Kelley, A. E. (1994). Effects of cocaine and GBR-12909 on brain stimulation reward. *Pharmacology Biochemistry and Behavior*, *48*(4), 915–920.

Margules, D. L., & Olds, J. (1962). Identical "feeding" and “rewarding” systems in the lateral hypothalamus of rats. *Science (New York, NY)*, *135*(3501), 374–375.

Marshall, V. M., Allison, J., Templeton, T., & Foote, S. J. (2004). Generation of BAC transgenic mice. *Methods in Molecular Biology (Clifton, NJ)*, *256*, 159–182. http://doi.org/10.1385/1-59259-753-X:159

McDevitt, R. A., Tiran-Cappello, A., Shen, H., Balderas, I., Britt, J. P., Marino, R. A. M., et al. (2014). Serotonergic versus nonserotonergic dorsal raphe projection

neurons: differential participation in reward circuitry. *Cell Reports*, *8*(6), 1857–1869. http://doi.org/10.1016/j.celrep.2014.08.037

McGinty, V. B., Lardeux, S., Taha, S. A., Kim, J. J., & Nicola, S. M. (2013). Invigoration of reward seeking by cue and proximity encoding in the nucleus accumbens. *Neuron*, *78*(5), 910–922. http://doi.org/10.1016/j.neuron.2013.04.010

McSweeney, F. K., & Roll, J. M. (1993). Responding changes systematically within sessions during conditioning procedures. *Journal of the Experimental Analysis of Behavior*, *60*(3), 621–640. http://doi.org/10.1901/jeab.1993.60-621

Melnick, S. M., Maldonado-Vlaar, C. S., Stellar, J. R., & Trzcińska, M. (2001). Effects of repeated GBR 12909 administration on brain stimulation reward. *European Journal of Pharmacology*, *419*(2-3), 199–205.

Menacherry, S. D., & Justice, J. B. (1990). In vivo microdialysis and thermospray tandem mass spectrometry of the dopamine uptake blocker 1-[2-[bis(4-fluorophenyl)methoxy]ethyl]-4-(3-phenylpropyl)-piper azine (GBR-12909). *Analytical Chemistry*, *62*(6), 597–601.

Miliaressis, E., Malette, J., & Coulombe, D. (1986a). The effects of pimozide on the reinforcing efficacy of central grey stimulation in the rat. *Behavioural Brain Research*, *21*(2), 95–100.

Miliaressis, E., Rompre, P.-P., Laviolette, P., Philippe, L., & Coulombe, D. (1986b). The curve-shift paradigm in self-stimulation. *Physiology & Behavior*, *37*(1), 85–91. http://doi.org/10.1016/0031-9384(86)90388-4

Miyoshi, G., & Fishell, G. (2006). Directing neuron-specific transgene expression in the mouse CNS. *Current Opinion in Neurobiology*, *16*(5), 577–584. http://doi.org/10.1016/j.conb.2006.08.013

Moisan, J., & Rompré, P. P. (1998). Electrophysiological evidence that a subset of midbrain dopamine neurons integrate the reward signal induced by electrical stimulation of the posterior mesencephalon. *Brain Research*, *786*(1-2), 143–152.

Montague, P. R., Dayan, P., & al, E. (1996). A framework for mesencephalic dopamine systems based on predictive Hebbian learning. *The Journal of ….*

Morales, M., & Root, D. H. (2014). Glutamate neurons within the midbrain dopamine regions. *Neuroscience*, *282C*, 60–68. http://doi.org/10.1016/j.neuroscience.2014.05.032

Morrison, S. E., & Nicola, S. M. (2014). Neurons in the nucleus accumbens promote selection bias for nearer objects. *Journal of Neuroscience*, *34*(42), 14147–14162. http://doi.org/10.1523/JNEUROSCI.2197-14.2014

Mundl, W. J. (1980). A constant-current stimulator. *Physiology & Behavior*, *24*(5), 991–993.

Murray, B., & Shizgal, P. (1994). Evidence implicating both slow- and fast-conducting fibers in the rewarding effect of medial forebrain bundle stimulation. *Behavioural Brain Research*, *63*(1), 47–60.

Murray, B., & Shizgal, P. (1996a). Behavioral measures of conduction velocity and refractory period for reward-relevant axons in the anterior LH and VTA. *Physiology & Behavior*, *59*(4-5), 643–652.

Murray, B., & Shizgal, P. (1996b). Physiological measures of conduction velocity and refractory period for putative reward-relevant MFB axons arising in the rostral MFB. *Physiology & Behavior*, *59*(3), 427–437.

Nagel, G., Szellas, T., Huhn, W., Kateriya, S., Adeishvili, N., Berthold, P., et al. (2003). Channelrhodopsin-2, a directly light-gated cation-selective membrane channel. *Proceedings of the National Academy of Sciences of the United States of America*, *100*(24), 13940–13945. http://doi.org/10.1073/pnas.1936192100

Nieh, E. H., Matthews, G. A., Allsop, S. A., Presbrey, K. N., Leppla, C. A., Wichmann, R., et al. (2015). Decoding neural circuits that control compulsive sucrose seeking. *Cell*, *160*(3), 528–541. http://doi.org/10.1016/j.cell.2015.01.003

Niv, Y., Daw, N. D., Joel, D., & Dayan, P. (2006). Tonic dopamine: opportunity costs and the control of response vigor. *Psychopharmacology*, *191*(3), 507–520. http://doi.org/10.1007/s00213-006-0502-4

Nugent, F. S., Hwong, A. R., Udaka, Y., & Kauer, J. A. (2008). High-frequency afferent stimulation induces long-term potentiation of field potentials in the ventral tegmental area. *Neuropsychopharmacology : Official Publication of the American*

College of Neuropsychopharmacology, *33*(7), 1704–1712. http://doi.org/10.1038/sj.npp.1301561

Oakman, S. A., Faris, P. L., Kerr, P. E., Cozzari, C., & Hartman, B. K. (1995). Distribution of pontomesencephalic cholinergic neurons projecting to substantia nigra differs significantly from those projecting to ventral tegmental area. *The Journal of Neuroscience : the Official Journal of the Society for Neuroscience*, *15*(9), 5859–5869.

Olds, J. (1958). Satiation effects in self-stimulation of the brain. *Journal of Comparative and Physiological Psychology*, *51*(6), 675–678.

Olds, J., & Milner, P. (1954). Positive reinforcement produced by electrical stimulation of septal area and other regions of rat brain. *Journal of Comparative and Physiological Psychology*, *47*(6), 419–427.

Paxinos, G., & Watson, C. (2007). The Rat Brain in Stereotaxic Coordinates (6 ed.). Academic Press.

Petry, N. M., & Heyman, G. M. (1997). Rat toys, reinforcers, and response strength: An examination of the R e parameter in Herrnstein's equation. *Behavioural Processes*, *39*(1), 39–52.

Rachlin, H. (1971). On the tautology of the matching law. *Journal of the Experimental Analysis of Behavior*, *15*(2), 249–251.

Rada, P. V., Mark, G. P., Yeomans, J. J., & Hoebel, B. G. (2000). Acetylcholine release in ventral tegmental area by hypothalamic self-stimulation, eating, and drinking. *Pharmacology Biochemistry and Behavior*, *65*(3), 375–379.

Ramirez, S., Liu, X., Lin, P.-A., Suh, J., Pignatelli, M., Redondo, R. L., et al. (2013). Creating a false memory in the hippocampus. *Science (New York, NY)*, *341*(6144), 387–391. http://doi.org/10.1126/science.1239073

Ranaldi, R., Bauco, P., & Wise, R. A. (1997). Synergistic effects of cocaine and dizocilpine (MK-801) on brain stimulation reward. *Brain Research*, *760*(1-2), 231–237. http://doi.org/10.1016/S0006-8993(97)00288-6

Reith, M. E., Li, M. Y., & Yan, Q. S. (1997). Extracellular dopamine, norepinephrine, and serotonin in the ventral tegmental area and nucleus accumbens of freely moving

rats during intracerebral dialysis following systemic administration of cocaine and other uptake blockers. *Psychopharmacology*, *134*(3), 309–317.

Robinson, T. E., & Berridge, K. C. (2003). Addiction. *Annual Review of Psychology*, *54*, 25–53. http://doi.org/10.1146/annurev.psych.54.101601.145237

Rompré, P. P., & Miliaressis, E. (1987). Behavioral determination of refractory periods of the brainstem substrates of self-stimulation. *Behavioural Brain Research*, *23*(3), 205–219.

Rompré, P. P., & Shizgal, P. (1986). Electrophysiological characteristics of neurons in forebrain regions implicated in self-stimulation of the medial forebrain bundle in the rat. *Brain Research*, *364*(2), 338–349.

Rompré, P. P., & Wise, R. A. (1989). Behavioral evidence for midbrain dopamine depolarization inactivation. *Brain Research*, *477*(1-2), 152–156.

Root, D. H., Mejias-Aponte, C. A., Zhang, S., Wang, H.-L., Hoffman, A. F., Lupica, C. R., & Morales, M. (2014). Single rodent mesohabenular axons release glutamate and GABA. *Nature Neuroscience*, *17*(11), 1543–1551. http://doi.org/10.1038/nn.3823

Rothman, R. B., Mele, A., Reid, A. A., Akunne, H. C., Greig, N., Thurkauf, A., et al. (1991). GBR12909 antagonizes the ability of cocaine to elevate extracellular levels of dopamine. *Pharmacology Biochemistry and Behavior*, *40*(2), 387–397.

Salamone, J. D. (2002). Functional significance of nucleus accumbens dopamine: behavior, pharmacology and neurochemistry. *Behavioural Brain Research*, *137*(1-2), 1.

Salamone, J. D., Correa, M., Farrar, A. M., Nunes, E. J., & Pardo, M. (2009). Dopamine, behavioral economics, and effort. *Frontiers in Behavioral Neuroscience*, *3*, 13. http://doi.org/10.3389/neuro.08.013.2009

Salamone, J. D., Correa, M., Farrar, A., & Mingote, S. M. (2007). Effort-related functions of nucleus accumbens dopamine and associated forebrain circuits. *Psychopharmacology*, *191*(3), 461–482. http://doi.org/10.1007/s00213-006-0668-9

Salamone, J. D., Correa, M., Mingote, S. M., & Weber, S. M. (2005). Beyond the reward hypothesis: alternative functions of nucleus accumbens dopamine. *Current Opinion in Pharmacology*, *5*(1), 34–41. http://doi.org/10.1016/j.coph.2004.09.004

Salamone, J. D., Correa, M., Mingote, S., & Weber, S. M. (2003). Nucleus accumbens dopamine and the regulation of effort in food-seeking behavior: implications for studies of natural motivation, psychiatry, and drug abuse. *The Journal of Pharmacology and Experimental Therapeutics*, *305*(1), 1–8. http://doi.org/10.1124/jpet.102.035063

Salamone, J. D., Cousins, M. S., & Snyder, B. J. (1997). Behavioral functions of nucleus accumbens dopamine: Empirical and conceptual problems with the anhedonia hypothesis. *Neuroscience & Biobehavioral Reviews*, *21*(3), 341–359. http://doi.org/10.1016/S0149-7634(96)00017-6

Schultz, W. (1997). Dopamine neurons and their role in reward mechanisms. *Current Opinion in Neurobiology*, *7*(2), 191–197. http://doi.org/10.1016/S0959-4388(97)80007-4

Schultz, W. (2002). Getting formal with dopamine and reward. *Neuron*, *36*(2), 241–263.

Schultz, W. (2007). Behavioral dopamine signals. *Trends in Neurosciences*, *30*(5), 203–210. http://doi.org/10.1016/j.tins.2007.03.007

Schultz, W., Dayan, P., & Montague, P. R. (1997). A neural substrate of prediction and reward. *Science (New York, NY)*, *275*(5306), 1593–1599.

Shimano, T., Fyk-Kolodziej, B., Mirza, N., Asako, M., Tomoda, K., Bledsoe, S., et al. (2012). Assessment of the AAV-mediated expression of channelrhodopsin-2 and halorhodopsin in brainstem neurons mediating auditory signaling. *Brain Research*. http://doi.org/10.1016/j.brainres.2012.10.030

Shizgal, P. (1997). Neural basis of utility estimation. *Current Opinion in Neurobiology*, *7*(2), 198–208.

Shizgal, P. (2012). Scarce means with alternative uses: Robbins' definition of economics and its extension to the behavioral and neurobiological study of animal decision making. *Frontiers in Neuroscience*, *6*. http://doi.org/10.3389/fnins.2012.00020

Shizgal, P., & Hernandez, G. (2015). Intracranial Self-Stimulation. In *Encyclopedia of Psychopharmacology* (pp. 838–845). Berlin, Heidelberg: Springer Berlin Heidelberg. http://doi.org/10.1007/978-3-642-36172-2_66

Shizgal, P., Bielajew, C., & Rompre, P.-P. (1988). Quantitative characteristics of the directly stimulated neurons subserving self-stimulation of the medial forebrain bundle: Psychophysical inference and electrophysiological measurement. Lawrence Erlbaum Associates, Inc.

Shizgal, P., Bielajew, C., Corbett, D., Skelton, R., & Yeomans, J. (1980). Behavioral methods for inferring anatomical linkage between rewarding brain stimulation sites. *Journal of Comparative and Physiological Psychology*, *94*(2), 227–237.

Shizgal, P., Fulton, S., & Woodside, B. (2001). Brain reward circuitry and the regulation of energy balance. *International Journal of Obesity and Related Metabolic Disorders : Journal of the International Association for the Study of Obesity*, *25 Suppl 5*, S17–21. http://doi.org/10.1038/sj.ijo.0801906

Simmons, J. M., & Gallistel, C. R. (1994). Saturation of subjective reward magnitude as a function of current and pulse frequency. *Behavioral Neuroscience*, *108*(1), 151–160.

Solinas, M., Goldberg, S. R., & Piomelli, D. (2008). The endocannabinoid system in brain reward processes. *British Journal of Pharmacology*, *154*(2), 369–383. http://doi.org/10.1038/bjp.2008.130

Solomon, R. (2014, October 1). *The Psychophysics of Reward: Empirical Studies and Modeling of Performance for Medial Forebrain Electrical Stimulation in the Rat*. (P. Shizgal, Ed.). Montreal.

Solomon, R. B., Trujillo-Pisanty, I., Conover, K., & Shizgal, P. (2015). Psychophysical inference of frequency-following fidelity in the neural substrate for brain stimulation reward. *Behavioural Brain Research*, *292*, 327–341. http://doi.org/10.1016/j.bbr.2015.06.008

Sombers, L. A., Beyene, M., Carelli, R. M., & Wightman, R. M. (2009). Synaptic overflow of dopamine in the nucleus accumbens arises from neuronal activity in the ventral tegmental area. *Journal of Neuroscience*, *29*(6), 1735–1742. http://doi.org/10.1523/JNEUROSCI.5562-08.2009

Sonnenschein, B., Conover, K., & Shizgal, P. (2003). Growth of brain stimulation reward as a function of duration and stimulation strength. *Behavioral Neuroscience*, *117*(5), 978–994. http://doi.org/10.1037/0735-7044.117.5.978

Sparta, D. R., Smithuis, J., Stamatakis, A. M., Jennings, J. H., Kantak, P. A., Ung, R. L., & Stuber, G. D. (2014). Inhibition of projections from the basolateral amygdala to the entorhinal cortex disrupts the acquisition of contextual fear. *Frontiers in Behavioral Neuroscience*, *8*, 129. http://doi.org/10.3389/fnbeh.2014.00129

Sparta, D. R., Stamatakis, A. M., Phillips, J. L., Hovelsø, N., van Zessen, R., & Stuber, G. D. (2011). Construction of implantable optical fibers for long-term optogenetic manipulation of neural circuits. *Nature Protocols*, *7*(1), 12–23. http://doi.org/10.1038/nprot.2011.413

Spiller, K., Xi, Z.-X., Peng, X.-Q., Newman, A. H., Ashby, C. R., Jr., Heidbreder, C., et al. (2007). The selective dopamine D3 receptor antagonists SB-277011A and NGB 2904 and the putative partial D3 receptor agonist BP-897 attenuate methamphetamine-enhanced brain stimulation reward in rats. *Psychopharmacology*, *196*(4), 533–542. http://doi.org/10.1007/s00213-007-0986-6

Stamatakis, A. M., & Stuber, G. D. (2012). Activation of lateral habenula inputs to the ventral midbrain promotes behavioral avoidance. *Nature Neuroscience*, *15*(8), 1105–1107. http://doi.org/10.1038/nn.3145

Stamatakis, A. M., Jennings, J. H., Ung, R. L., Blair, G. A., Weinberg, R. J., Neve, R. L., et al. (2013). A unique population of ventral tegmental area neurons inhibits the lateral habenula to promote reward. *Neuron*, *80*(4), 1039–1053. http://doi.org/10.1016/j.neuron.2013.08.023

Stamatakis, A. M., Van Swieten, M., Basiri, M. L., Blair, G. A., Kantak, P., & Stuber, G. D. (2016). Lateral Hypothalamic Area Glutamatergic Neurons and Their Projections to the Lateral Habenula Regulate Feeding and Reward. *Journal of Neuroscience*, *36*(2), 302–311. http://doi.org/10.1523/JNEUROSCI.1202-15.2016

Stauffer, W. R., Lak, A., & Schultz, W. (2014). Dopamine Reward Prediction Error Responses Reflect Marginal Utility. *Current Biology : CB*. http://doi.org/10.1016/j.cub.2014.08.064

Steinberg, E. E., & Janak, P. H. (2012). Establishing causality for dopamine in neural function and behavior with optogenetics. *Brain Research*. http://doi.org/10.1016/j.brainres.2012.09.036

Stellar, J. R., Kelley, A. E., & Corbett, D. (1983). Effects of peripheral and central dopamine blockade on lateral hypothalamic self-stimulation: evidence for both reward and motor deficits. *Pharmacology Biochemistry and Behavior*, *18*(3), 433–442.

Stuber, G. D. (2010). Dissecting the neural circuitry of addiction and psychiatric disease with optogenetics. *Neuropsychopharmacology : Official Publication of the American College of Neuropsychopharmacology*, *35*(1), 341–342. http://doi.org/10.1038/npp.2009.102

Stuber, G. D., & Wise, R. A. (2016). Lateral hypothalamic circuits for feeding and reward. *Nature Neuroscience*, *19*(2), 198–205. http://doi.org/10.1038/nn.4220

Stuber, G. D., Britt, J. P., & Bonci, A. (2012). Optogenetic modulation of neural circuits that underlie reward seeking. *Biological Psychiatry*, *71*(12), 1061–1067. http://doi.org/10.1016/j.biopsych.2011.11.010

Stuber, G. D., Hnasko, T. S., Britt, J. P., Edwards, R. H., & Bonci, A. (2010). Dopaminergic terminals in the nucleus accumbens but not the dorsal striatum corelease glutamate. *Journal of Neuroscience*, *30*(24), 8229–8233. http://doi.org/10.1523/JNEUROSCI.1754-10.2010

Sutcliffe, J. G., & de Lecea, L. (2002). The hypocretins: setting the arousal threshold. *Nature Reviews Neuroscience*, *3*(5), 339–349. http://doi.org/10.1038/nrn808

Swanson, L. W. (1982). The projections of the ventral tegmental area and adjacent regions: a combined fluorescent retrograde tracer and immunofluorescence study in the rat. *Brain Research Bulletin*, *9*(1-6), 321–353.

Tan, K. R., Yvon, C., Turiault, M., Mirzabekov, J. J., Doehner, J., Labouèbe, G., et al. (2012). GABA neurons of the VTA drive conditioned place aversion. *Neuron*, *73*(6), 1173–1183. http://doi.org/10.1016/j.neuron.2012.02.015

Tecuapetla, F., Patel, J. C., Xenias, H., English, D., Tadros, I., Shah, F., et al. (2010). Glutamatergic signaling by mesolimbic dopamine neurons in the nucleus

accumbens. *Journal of Neuroscience*, *30*(20), 7105–7110. http://doi.org/10.1523/JNEUROSCI.0265-10.2010

Tellez, L. A., Han, W., Zhang, X., Ferreira, T. L., Perez, I. O., Shammah-Lagnado, S. J., et al. (2016). Separate circuitries encode the hedonic and nutritional values of sugar. *Nature Neuroscience*, *19*(3), 465–470. http://doi.org/10.1038/nn.4224

Trujillo Pisanty, I., Sanio, C., Chaudhri, N., & Shizgal, P. (2015). Robust optical. *MethodsX*, *2*, 263–271. http://doi.org/10.1016/j.mex.2015.05.003

Trujillo-Pisanty, I., Conover, K., & Shizgal, P. (2013). A new view of the effect of dopamine receptor antagonism on operant performance for rewarding brain stimulation in the rat. *Psychopharmacology*, *231*(7), 1351–1364. http://doi.org/10.1007/s00213-013-3328-x

Trujillo-Pisanty, I., Hernandez, G., Moreau-Debord, I., Cossette, M.-P., Conover, K. L., Cheer, J. F., et al. (2011). Cannabinoid receptor blockade reduces the opportunity cost at which rats maintain operant performance for rewarding brain stimulation. *Journal of Neuroscience*, *31*(14), 5426–5435.

Tsai, H.-C., Zhang, F., Adamantidis, A., Stuber, G. D., Bonci, A., de Lecea, L., & Deisseroth, K. (2009). Phasic firing in dopaminergic neurons is sufficient for behavioral conditioning. *Science (New York, NY)*, *324*(5930), 1080–1084. http://doi.org/10.1126/science.1168878

Tye, K. M., Mirzabekov, J. J., Warden, M. R., Ferenczi, E. A., Tsai, H.-C., Finkelstein, J., et al. (2013). Dopamine neurons modulate neural encoding and expression of depression-related behaviour. *Nature*, *493*(7433), 537–541. http://doi.org/10.1038/nature11740

Tye, K. M., Prakash, R., Kim, S.-Y., Fenno, L. E., Grosenick, L., Zarabi, H., et al. (2011). Amygdala circuitry mediating reversible and bidirectional control of anxiety. *Nature*, *471*(7338), 358–362. http://doi.org/10.1038/nature09820

van Zessen, R., Phillips, J. L., Budygin, E. A., & Stuber, G. D. (2012). Activation of VTA GABA Neurons Disrupts Reward Consumption. *Neuron*, *73*(6), 1184–1194. http://doi.org/10.1016/j.neuron.2012.02.016

Warden, M. R., Selimbeyoglu, A., Mirzabekov, J. J., Lo, M., Thompson, K. R., Kim, S.-Y., et al. (2012). A prefrontal cortex-brainstem neuronal projection that controls

response to behavioural challenge. *Nature*, *492*(7429), 428–432. http://doi.org/10.1038/nature11617

Wasserman, E. M., Gomita, Y., & Gallistel, C. R. (1982). Pimozide blocks reinforcement but not priming from MFB stimulation in the rat. *Pharmacology Biochemistry and Behavior*, *17*(4), 783–787.

Watabe-Uchida, M., Zhu, L., Ogawa, S. K., Vamanrao, A., & al, E. (2012). Whole-brain mapping of direct inputs to midbrain dopamine neurons. *Neuron*, *74*(5), 858–873.

Wietek, J., Wiegert, J. S., Adeishvili, N., Schneider, F., Watanabe, H., Tsunoda, S. P., et al. (2014). Conversion of channelrhodopsin into a light-gated chloride channel. *Science (New York, NY)*, *344*(6182), 409–412. http://doi.org/10.1126/science.1249375

Wightman, R. M., & Robinson, D. L. (2002). Transient changes in mesolimbic dopamine and their association with 'reward'. *Journal of Neurochemistry*, *82*(4), 721–735.

Wise, R. A. (1978). Catecholamine theories of reward: a critical review. *Brain Research*, *152*(2), 215–247.

Wise, R. A. (1980). Action of drugs of abuse on brain reward systems. *Pharmacology Biochemistry and Behavior*, *13 Suppl 1*, 213–223.

Wise, R. A. (1996). Addictive Drugs and Brain Stimulation Reward. *Annual Review of Neuroscience*, *19*(1), 319–340. http://doi.org/10.1146/annurev.ne.19.030196.001535

Wise, R. A. (1998). Drug-activation of brain reward pathways. *Drug and Alcohol Dependence*, *51*(1-2), 13–22.

Wise, R. A. (2006). Role of brain dopamine in food reward and reinforcement. *Philosophical Transactions of the Royal Society of London. Series B, Biological Sciences*, *361*(1471), 1149–1158. http://doi.org/10.1098/rstb.2006.1854

Wise, R. A. (2008). Dopamine and reward: the anhedonia hypothesis 30 years on. *Neurotoxicity Research*, *14*(2-3), 169–183. http://doi.org/10.1007/BF03033808

Wise, R. A., & Rompré, P. P. (1989). Brain Dopamine and Reward. *Annual Review of Psychology*, *40*(1), 191–225. http://doi.org/10.1146/annurev.ps.40.020189.001203

Wise, R. A., Spindler, J., deWit, H., & Gerberg, G. J. (1978). Neuroleptic-induced "anhedonia" in rats: pimozide blocks reward quality of food. *Science (New York, NY)*, *201*(4352), 262–264.

Witten, I. B., Lin, S.-C., Brodsky, M., Prakash, R., Diester, I., Anikeeva, P., et al. (2010). Cholinergic interneurons control local circuit activity and cocaine conditioning. *Science (New York, NY)*, *330*(6011), 1677–1681. http://doi.org/10.1126/science.1193771

Witten, I. B., Steinberg, E. E., Lee, S. Y., Davidson, T. J., Zalocusky, K. A., Brodsky, M., et al. (2011). Recombinase-Driver Rat Lines: Tools, Techniques, and Optogenetic Application to Dopamine-Mediated Reinforcement. *Neuron*, *72*(5), 721–733. http://doi.org/10.1016/j.neuron.2011.10.028

Yang, X. W., & Gong, S. (2005). An overview on the generation of BAC transgenic mice for neuroscience research. *Current Protocols in Neuroscience / Editorial Board, Jacqueline N. Crawley ... [Et Al.]*, *Chapter 5*, Unit 5.20. http://doi.org/10.1002/0471142301.ns0520s31

Yeomans, J. (1989). Two substrates for medial forebrain bundle self-stimulation: myelinated axons and dopamine axons. *Neuroscience & Biobehavioral Reviews*, *13*(2-3), 91–98.

Yeomans, J. S. (1975). Quantitative measurement of neural post-stimulation excitability with behavioral methods. *Physiology & Behavior*, *15*(5), 593–602. http://doi.org/10.1016/S0031-9384(75)80035-7

Yeomans, J. S. (1979). The absolute refractory periods of self-stimulation neurons. *Physiology & Behavior*, *22*(5), 911–919.

Yeomans, J. S., Maidment, N. T., & Bunney, B. S. (1988). Excitability properties of medial forebrain bundle axons of A9 and A10 dopamine cells. *Brain Research*, *450*(1-2), 86–93.

Yizhar, O., Fenno, L. E., Davidson, T. J., Mogri, M., & Deisseroth, K. (2011). Optogenetics in neural systems. *Neuron*, *71*(1), 9–34. http://doi.org/10.1016/j.neuron.2011.06.004

You, Z. B., Chen, Y. Q., & Wise, R. A. (2001). Dopamine and glutamate release in the nucleus accumbens and ventral tegmental area of rat following lateral hypothalamic self-stimulation. *Neuroscience*, *107*(4), 629–639.

Zhang, F., Aravanis, A., Adamantidis, A., de Lecea, L., & Deisseroth, K. (2007a). Circuit-breakers: optical technologies for probing neural signals and systems. *Nature Reviews Neuroscience*, *8*(8), 577–581.

Zhang, F., Gradinaru, V., Adamantidis, A. R., Durand, R., Airan, R. D., de Lecea, L., & Deisseroth, K. (2010). Optogenetic interrogation of neural circuits: technology for probing mammalian brain structures. *Nature Protocols*, *5*(3), 439–456. http://doi.org/10.1038/nprot.2009.226

Zhang, F., Wang, L.-P., Brauner, M., Liewald, J. F., Kay, K., Watzke, N., et al. (2007b). Multimodal fast optical interrogation of neural circuitry. *Nature*, *446*(7136), 633–639. http://doi.org/10.1038/nature05744

Zhao, S., Cunha, C., Zhang, F., Liu, Q., Gloss, B., Deisseroth, K., et al. (2008). Improved expression of halorhodopsin for light-induced silencing of neuronal activity. *Brain Cell Biology*, *36*(1-4), 141–154. http://doi.org/10.1007/s11068-008-9034-7

Zhao, S., Ting, J. T., Atallah, H. E., Qiu, L., Tan, J., Gloss, B., et al. (2011). Cell type–specific channelrhodopsin-2 transgenic mice for optogenetic dissection of neural circuitry function. *Nature Methods*, 1–11. http://doi.org/10.1038/nmeth.1668